Energy demand and environmental impacts of food transport refrigeration and energy reduction methods during temperature-controlled distribution

A thesis submitted for the degree of

Doctor of Philosophy

By

Ashika Rai, B.Sc., M.Sc.

Department of Mechanical and Aerospace Engineering

College of Engineering, Design and Physical Sciences

Brunel University London

July 2019

ABSTRACT

The growing demand for temperature-controlled food distribution is driving the growth of transport refrigeration units (TRUs). The majority of these TRUs are powered using auxiliary diesel engines of less than 19 kW power output. These engines are currently not covered by European regulations on emissions. The emissions from TRUs are instead regulated by the Non-Road Machinery (NRMM) standard which is considered insufficient to adequate control emissions. The reliance of most TRUs on diesel fuel which contributes to both greenhouse gas and particulate emissions has heightened the need for more energy efficient and low carbon alternatives.

In this work, a model has been developed to determine the fuel consumption and GHG emission of auxTRUs for the distribution parameters obtained from a survey study conducted as part of research to quantify the energy usage and emissions associated with auxiliary engines for transport refrigeration units in London.

Using the model, different alternative technologies have been investigated, which include, cryogenic systems using LN_2, cryogenics systems using LCO_2, all-electric TRU and hydrogen fuel cell powered TRU. Both production and operation related GHG emissions were considered for the studies. The production related emissions for electricity are lower than the emissions from the production of hydrogen and cryogenic fluids by almost 60%. For this reason, the all-electric TRU was found to be the most suitable alternative to diesel auxTRU in respect to GHG emissions and current infrastructure. The infrastructure for both hydrogen and cryogenic fluids does not exist as yet to support frequent refilling of the transport vehicles.

Infiltration of ambient air during door openings has been identified to be a major source of refrigeration load in multi-drop temperature controlled food distribution. Plastic strips curtains are inconvenient to use as they impede loading and unloading. For this reason, even when they are fitted on the vehicle they are not utilised by the drivers. Air curtains can avoid the use of a physical barrier but have not been previously investigated sufficiently for this application. For this reason, extensive experimental and numerical investigations were performed to establish the

effectiveness of air curtains to reduce air infiltration into the refrigerated space of distribution vehicles.

The air curtain discharge velocity was identified to be an important design parameter for the air curtain. Optimising the discharge velocity and angle has shown to produce an energy savings of 50% in distribution vehicles.

Publications

Published Journal Paper

Rai, A., Tassou, S.A. (2017) "Environmental impacts of vapour compression and cryogenic transport refrigeration technologies for temperature controlled food distribution", *Energy Conversion and Management*, Volume 150, pp. 914-923.

Published Conference Papers

Rai, A., Tassou, S.A. (2017) "Energy demand and environmental impacts of alternative food transport refrigeration systems", *1st International Conference on Energy Resource Use in Food Chains*, ICSEF, *Energy Procedia*, pp. 113-120.

Rai, A., Tassou, S.A. (2017) "Environmental impacts of temperature controlled food distribution", *4th Sustainable Thermal Energy Management International Conference (SusTEM2017), Alkmaar Netherlands*.

Rai, A., Sun, J., Tassou, S.A. (2018) "Numerical investigation of the protective mechanisms of air curtain in a refrigerated truck during door openings", *2nd International Conference on Energy Resource Use in Food Chains*, ICSEF, Energy *Procedia.*

Rai, A., Sun, J., Tassou, S.A. (2018) "Numerical investigation into the influence of air curtain discharge angles in refrigerated trucks", *2nd International Conference on Energy Resource Use in Food Chains*, ICSEF, Energy *Procedia, Paphos, Cyprus.*

Rai, A., Sun, J., Tassou, S.A. (2018) "Three-dimensional investigation on the positioning of air curtain on its effectiveness in refrigerated vehicles used for food distribution", *2nd International Conference on Energy Resource Use in Food Chains*, ICSEF, Energy *Procedia, Paphos, Cyprus.*

Rai, A., Sun, J., Tassou, S.A., Tsamos, K.M., (2019) "Numerical and experimental investigation on the energy efficiency of an air curtain in temperature-controlled vehicles for vehicle distribution", *4th Sustainable Thermal Energy Management International Conference (SusTEM2019), China*.

Published Collaborative Report

Cenex, Low CVP, Brunel University London (2018), "Auxiliary temperature reduction in the Greater London area", project for Transport for London (TfL), *http://content.tfl.gov.uk/auxiliary-temperature-reduction-units-in-the-greater-london-area.pd*

Dedication

To

My parents

Shaya Kumar Rai and Asha Rai

Acknowledgements

"Energy demand and environmental impacts of food transport refrigeration systems and energy reduction methods during temperature-controlled distribution" was a research project carried out in the "RCUK Centre for Sustainable Energy Use in Food Chains (CSEF)" under the "Institute of Energy Future" at Brunel University London. This project was managed by Professor Savvas Tassou and Dr Yunting Ge. This thesis is based on the research work which incorporates various investigation, modelling and experimental work.

Firstly, I would like to express my appreciation to my principle supervisor Professor Savvas Tassou for his continuous support and valuable feedbacks which helped me complete my PhD journey successfully. Researching and working under his guidance has greatly enhanced my knowledge and work abilities which will forever support me in my future endeavour. I would also like to thank Dr Jining Sun for his excellent guidance and valuable support in the area of fluid dynamics.

I would also like to thank all my colleagues at CSEF for making my PhD journey an enjoyable experience, especially Dr Konstantinos Tsamos, Dr Liang Li, Dr Samira Saravi and Mrs Maureen Senatore for their valuable support.

Lastly but most importantly, I would like to express a very special thankyou and gratitude to my parents Mr S.K. Rai and Mrs Asha Rai and my sisters for always being there to support me. This difficult journey of PhD would not have been possible without my family's continuous encouragement and support. Thank you again to my sisters for always being there to listen, and for always making time for me to talk regardless their busy schedule.

Table of Contents

CHAPTER 1

Introduction

1.1 Temperature-controlled vehicles

Temperature-controlled transportation is an integral element for both the inbound and outbound segments of the Cold Chain without which the material/physical flow that relies on temperature controlled environment is next to impossible. However, the majority of these temperature-controlled vehicles highly rely on diesel powered auxiliary engines to provide refrigeration in the chamber.

Unlike the effective mandatory standards such as Euro VI/6 on all road vehicles, these auxiliary diesel engines which are used for powering the refrigeration units are exempt of these strict regulations imposed by the EU and the UK government. The power category of the auxiliary engine is approximately 2-5 kW for vans, 5- 10 kW for small trucks, 8- 12 kW for larger trucks and 12-19 kW for articulates. The 19kW engine is the minimum limit covered by NRMM regulations [1]. Hence, at present there are no requirements for the majority of the existing diesel auxTRU (auxiliary diesel powered transport refrigeration units) to comply with emissions standard. However it is expected that the standard will be extended to cover auxTRUs in the near future.

1.2 Growing demand for temperature-controlled distribution

With over 84,000 diesel-driven refrigerated road vehicles in the road of UK (over 3 million worldwide) and a predicted growth of road freight transport by 2% annually until 2030, the growth of temperature-controlled transportation will consume increasing energy to sustain growth [2-4]. The growing energy demand also increases environmental concerns from increased emissions.

In 2013, around 90 million metric tons of food and beverages were imported into the EU with 9% of the overall transportation done by road [5]. About 80% of the total energy associated with the food life cycle (from production to disposal stage) in 2013

originated from fossil fuel [6]. The most recognised impacts of food transportation are in relation to climate change, air quality and noise [7].

Refrigeration in articulated vehicles over 33 t, which accounts for more than 80% of temperature-controlled food transportation, is invariably provided using auxTRUs. The current number of TRUs in UK alone is estimated to be around 84,000 and is predicted to reach 97,000 by 2025 [8].

1.3 Replacements for auxTRUs

Vapour compression is one of the most commonly used refrigerated systems for food transport applications The vapour compression cycle is run using a wide range of compressor drive methods which include vehicle alternator unit, direct drive unit, and auxiliary diesel unit. The choice of the design may vary depending on the duty, weight, capacity, noise level, maintenance requirements, installation cost, and fuel taxation. The vapour compression cycle system powered using auxiliary diesel engines is the most commonly used technology but is also responsible for high energy consumption, accounting for almost 30% of the final energy used in the temperature controlled food transport sector [9].

A number of technologies have currently emerged in the market as alternatives to conventional TRUs. These alternatives include TRU powered using hydrogen fuel cell, solar-powered photovoltaic (PV) TRUs, cryogenic based TRUs using liquid nitrogen and liquid carbon dioxide, TRUs using waste heat from diesel internal combustion engine and finally either hybrid plug-in or all-electric TRUs. Recent assessment conducted by Transport for London (TfL) considers electrically driven refrigeration and cryogenic gases and liquids to be the most suitable options among the emerging technologies [10].

The assessment also considers the use of phase change and eutectic materials, currently in use in small scale, as suitable alternatives which not only eliminates the need of diesel or complex refrigeration unit but also provides environmentally friendly refrigeration option. However, the limited operation time (maximum 10 hours) and heavy weight imposed by the eutectic materials made the use of this option impractical for use on its own for temperature-controlled distribution.

1.4 Methods of reducing energy consumption for current technology in use

The main purpose of a TRU is to pulldown the temperature inside the trailer by removing the heat from the chamber and releasing it to external environment. There are various factors that influence the level of refrigeration load encountered by the trailer and hence the amount of energy needed to maintain the low temperature required for safe delivery of temperature controlled food products.

The overall refrigeration load is a combination of infiltration load, precooling load, product load and transmission load. Due to the nature of distribution vehicles, door opening is inevitable. From a survey conducted on cold chain logistics, a distribution vehicle can spend the majority of its distribution time for loading and unloading of products [11]. And hence, infiltration of warm air during door opening can account for significant amount of thermal load resulting requirement of more energy to pulldown the temperature gain.

Unlike the ATP standards [12] which impose strict regulations on insulation and hence reduction of the refrigeration load due to conduction (transmission load), there exists no such regulation which can restrict the duration or frequency of door opening and hence infiltration.

1.5 Research approach

It is essential to analyse the benefits of the alternative technologies using a similar approach. For this reason, a spreadsheet based model has been created using the calculation methodology specified by ASHRAE and CIBSE. The model was validated using investigation data collected in collaboration with temperature-controlled logistics company Kuehne & Nagel. A small difference was found between the investigation-based and model-based estimations, however within reasonable boundary. There are many unforeseen factors that can occur in reality which cannot be taken into consideration in theoretical calculations, and hence a reasonable level of difference can be found between model based and real investigation based results.

This model has been used to analyse the energy consumption and environmental impacts of prominent emerging technologies taking into consideration both the

production and operation phase emissions. Previous studies have not considered in detail the impacts of infiltration and the use of air curtains to reduce it. For this reason this study also considers the performance of air curtains and their effectiveness of reducing infiltration in temperature controlled distribution vehicles.

The air curtain investigations include both experimentation in the laboratory and CFD modelling. The test results were used to validate the CFD model which was subsequently used to evaluate the effectiveness of air curtains in larger food distribution vehicles.

1.6 Aims and objectives

The main aim of this thesis is to investigate, analyse and compare energy and environmental impact reduction technologies in temperature-controlled distribution vehicles. The study included a number of objectives which include;

1. Investigation of the energy consumption and environmental impact of TRU powered using auxiliary diesel engine (auxTRU).
2. Comparison of the production and operation related energy consumption and environmental impacts of auxTRUs and other prominent alternative technologies during distribution of different temperature-sensitive food products.
3. Identification of the main sources of energy consumption in refrigerated vehicles and investigate the performance of air curtains to reduce the impacts of infiltration during door openings.
4. Development of a suitable numerical model to study the performance of the technology and generalise the results.

1.7 Outline

This thesis is organized as follows:

Following this chapter, **Chapter 2** discusses the energy demand and environmental impacts of auxTRUs. The chapter also reviews alternative transport refrigeration technologies and barriers to their wider adoption.

Chapter 3 presents the spreadsheet model developed to conduct the theoretical calculations of refrigeration loads, the energy required to overcome it and the environmental impacts as result of fossil fuel consumption. The chapter also discusses the investigation work carried out on an actual distribution truck. The collected data from the investigation work is used to validate the spreadsheet model.

Chapter 4 assesses the energy demand and environmental impacts of cryogenic based transport refrigeration technologies using LCO_2 and LN_2 during temperature-controlled distribution (chilled and frozen) of different food products. This assessment considers both the production-related and operation-related environmental impacts. These estimations are then compared with the estimations of auxTRUs to illustrate if these new technologies are indeed more suitable in terms of energy and greenhouse gas (GHG) emissions.

Similar to Chapter 4, **Chapter 5** presents a comparison of two other prominent alternative technologies to auxTRU, hydrogen fuel cell powered TRUs and all-electric TRUs. The chapter presents analysis on the energy consumption and environmental impacts of these technologies during distribution of different food products.

From the assessment conducted in Chapters 3, 4, and 5, it was identified that the infiltration load was the primary source of refrigeration load due to the requirement of frequent door openings in a distribution vehicle. After a thorough analysis, an air curtain was found to be the most suitable protective technology against infiltration. **Chapter 6** explores the experimental set-up for investigating the performance of an air curtain in a refrigerated container. The chapter also presents the CFD model developed for numerical analysis on the performance of air curtain in refrigerated vehicles. The experimental results obtained from the experimental investigations were used to validate the CFD model.

Using the CFD model discussed in Chapter 6, **Chapter 7** explores the performance of air curtains in larger trucks. This chapter also focuses on different methods of optimizing the performance of an air curtain further.

Chapter 8 presents the final conclusions of the thesis and suggestions for future work.

CHAPTER 2

Literature Review

The literature review in this chapter discusses the energy demand and environmental impacts of current transport refrigeration units (TRUs) powered using auxiliary diesel engine. The chapter also covers an analysis of alternative transport refrigeration technologies considered as possible replacements of current TRUs and of technologies aimed at reducing the energy consumption of current cooling units.

2.1 Energy demand and environmental impact of auxTRUs

Tassou et al [13, 14] in collaboration with Defra conducted an investigation to measure the fuel intensity and CO_2e (carbon dioxide equivalent) emissions of auxTRU and main engine of the truck. Table 2.1 presents the fuel consumption of auxTRU based on the refrigeration duties.

Table 2.1: Fuel consumption of auxTRU

Body Inside length/ Inside Volume/Type	Minimum refrigeration capacity long distance transport (W)		Required refrigeration capacity, multi drop distribution (W)		Fuel consumption (litre/h)	
	-20°C K=0.4 W/m^2· K	0°C K=0.7W/ m^2 ·K	-20°C K=0.4W/ m^2 ·K	0°C K=0.7W/ m^2· K	-20°C K=0.4W/ m^2 ·K	0°C K=0.7W/ m^2 ·K
6.2m/33.42m^3/Rigid	3765	3876	5630	4554	2.0	1.5
10.4m/61.15m^3/Rigid	6155	6353	9897	7920	3.0	2.5
13.4m/78.79m^3/Semi-trailer	7730	7986	13500	10078	4.0	3.0

Table 2.2 presents the fuel consumption of auxTRU and truck's main engine based on the survey conducted by Defra [13].

Table 2.2: Fuel consumption of auxTRU and truck's main engine.

Vehicle class	Main engine's fuel consumption (l/ day)	Main engine fuel efficiency (km/ l)	Refrigeration engine (l/ day)	Overall vehicle fuel efficiency (km/ l)	Refrigeration energy to motive energy (%)
Medium-rigid	111.3	3.7	21	3.09	18.09
Large-rigid	90.71	3.15	17.7	2.63	19.5
City-artic	112.33	2.98	26.1	2.42	23.2
32 t artic	140.8	2.97	34.1	2.4	24.2
38 t artic	159.62	3.04	24.9	2.52	15.6

The majority of perishable food products are arranged on wooden pallets for transportation purposes. Analysis work by Tassou et al. [14] estimated an average fuel intensity of 43.2 ml/pallet·km for medium rigid, 41.7 ml/pallet·km for large rigid, 28.0 ml/pallet·km for city artic, 25.1 ml/pallet·km for 32 t, and 23.6 ml/pallet·km for 38 t articulated vehicle. A survey conducted by Cenex estimated rigid vehicles less than 3.5 t and 3.5- 7.5 t categories to travel an average distance of 37,000 miles each year, medium-rigid a distance of 65,000 miles each year and heavy artic an average of 202,316 miles per year [10]. Given the level of fuel consumption per km by Tassou et al. [14], these vehicles can contribute to significant amount of GHG emission.

For the estimated fuel intensity of auxTRU and main engine, the GHG emissions as presented in Table 2.3 were assessed per pallet per km.

Table 2.3: GHG emission of ambient, chilled and frozen distribution

Vehicle class	Ambient (gCO_2e/pallet·km)	Chilled (single-drop) (gCO_2e/pallet·km)	Chilled (multi-drop) (gCO_2e/pallet·km)	Frozen and multi-temp (single-drop) (gCO_2e/pallet·km)	Frozen and multi-temp (multi-drop) (gCO_2e/pallet·km)
Medium-rigid	88	106	109	112	115
Large-rigid	85	102	105	108	111
City-artic	56	69	70	73	75
32 t artic	51	61	63	65	67
38 t artic	48	58	59	61	63

Analysis work carried by Rai and Tassou [15] for different distribution scenarios showed the fuel intensity of auxTRU varied depending on the length (time duration) and distribution type (ambient, chilled, or frozen). The results indicate frozen distribution to consume greater fuel in comparison to chilled distribution for same distribution time-length. Rai and Tassou [16] in follow up work estimated the diesel consumption of auxTRUs to be between 2- 4 l/h depending on the distribution type and vehicle category.

In addition, the auxTRUs is also responsible for GHG emissions from refrigerant leakage as commonly used refrigerants have significant GWP values [15]. The annual leakage can vary anywhere between 5- 25% per year. Even though the environmental impact of refrigerant leakage can be 65- 86% lower than that from fossil fuel combustion, they are still significant and need to be addressed.

2.2 Current technologies for food transport refrigeration

2.2.1 Vehicles

Trailers can range anywhere from 2.4 to 2.6 m wide, 3.7 to 4.1 m high, and 7.3 to 16.8 m long. Heavy goods vehicles (HGVs) used for temperature controlled food distribution can be categorised by their net weight in tonnes, 3.5 to 7.5 t, 7.5 to 14 t,

14 to 17 t, 17 to 25 t and finally articulated vehicles above 25 t [17]. The refrigerated vehicles, especially large-rigid and artic, have insulated roll-up door with smaller and medium vehicles having hinged doors. Some include a curb-side door in addition to rear doors. The design of the refrigerated vehicles take into consideration the extremes of exterior conditions, desired interior conditions, insulation properties, infiltration of air and moisture and trade-offs between construction cost and operating expenses.

(a) (b)

(c) (d)

Figure 2.1: Refrigerated vehicles with weight categories (a) <3.5 t, (b) 7.5 t, (c) 12 t and (d) articulated.

Table 2.4 provides average cargo dimensions of different vehicle categories;

Table 2.4: Internal dimensions of different vehicle categories.

	Vehicle categories			
	<3.5 tonnes	7.5 tonnes	12 tonnes	Artic
Internal length (m)	3.7	5	6.5	11.8
Internal width (m)	1.9	2.3	2.3	2.3
Internal height (m)	1.9	2.3	2.3	2.6

Door (m × m)	1.8 × 1.9	2.2 × 2.2	2.2 × 2.2	2.2 × 2.5
Cooling unit's volumetric airflow (m^3/h)	1075	2150	3200	5000
Insulation thickness (mm)	50	75	75	75

Primary food distribution from food factories to regional distribution centres (RDCs) and secondary distribution to supermarkets and superstores almost always takes place using articulated vehicles of 32- 44 t. Tertiary distribution to small shops and catering outlets is mainly performed using rigid vehicles (18 t being a popular choice). Smaller lorries and vans are used for last mile delivery (<3.5 t, 3.5-7.5 t).

Out of 3,500 temperature-controlled vehicles with auxTRU which enter London regularly, 15% are in the 0- 3.5 t gross vehicle weight category, 52% in 3.5- 12 t and 33% in 12 t [10]. However, in regards to global figure, articulated vehicles over 33 t are responsible for more than 80% of temperature-controlled food transportation which mainly use auxTRUs for refrigeration purpose [18].

2.2.2 Current transport refrigeration systems- the vapour compression cycle

Current transport refrigeration systems predominantly employ vapour compression cycle technology, powered either electrically or mechanically using the vehicle's main engine or an independent auxiliary engine, both which typically run on diesel. Figure 2.2 shows the schematic diagram of the vapour compression cycle driven using an auxiliary engine [16].

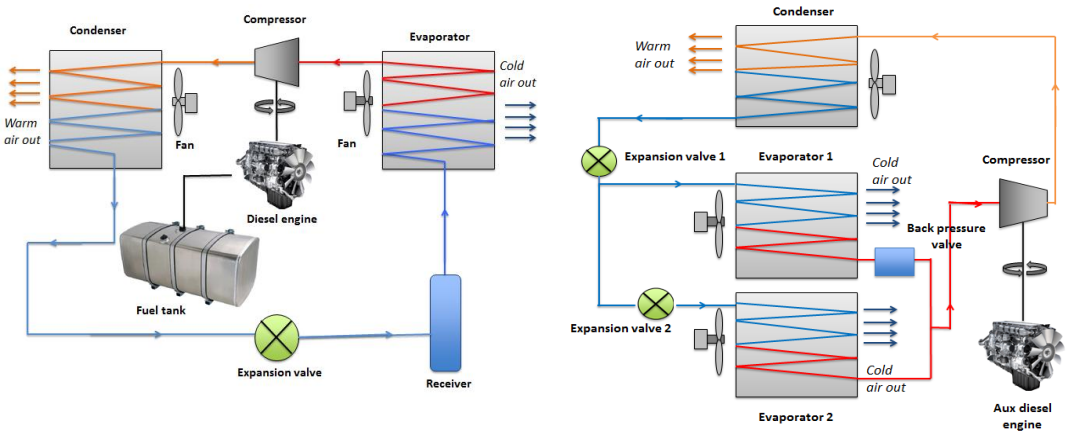

(a) (b)

Figure 2.2: Schematic diagram of vapour compression cycle driven using auxiliary engine, (a) single evaporator and (b) multi-evaporators.

Capacities of these small independent combustion engines can range anywhere between 5.9 kW to 14.6 kW and are currently governed by the Non-Road Mobile Machinery (NRMM) standard [19, 20]. However, this standard alone is insufficient to protect public health in cities [10].

Some of the main disadvantages of the auxTRU include:

- Low operating efficiency of the small combustion engine, between 20% and 25% [21].
- Use of refrigerants for the vapour compression cycle with high global warming potential (GWP) - R404A and R134a have GWP of 3922 and 1430 respectively [16].
- The COP of auxTRU is quite low, ranging around 0.5 at -20°C, to 1.5- 1.75 at +3°C and ambient temperature of 30°C [14].
- Existing transport refrigeration units powered using diesel not only consume approximately 20% of the overall fuel but can also emit six times as much NO_x and 29 times more particulate matter (PM) than a modern Euro 6 truck engine [22].
- The numerous moving parts of an internal combustion engine (ICE) require regular maintenance [20].

This auxiliary engine drives the open shaft compressor while the fans/ blowers of the compressor and evaporator are normally run using a belt-and-pulley system [17]. The mechanical energy and the cooling capacity of the refrigeration units can be controlled by switching the engine on and off and by adjusting the engine speed. An electric motor is normally integrated as an optional standby operation when the vehicle is stationary. Figure 2.3 illustrates the different v-belt arrangements [23].

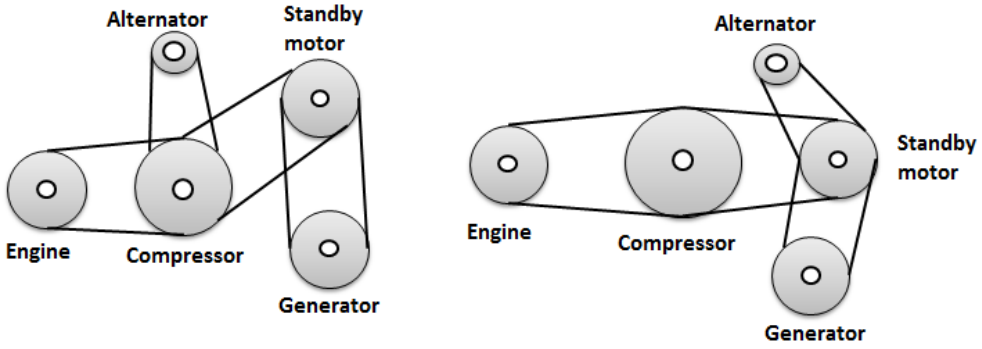

Figure 2.3: Different V-belt arrangements.

With more electric TRUs replacing mechanical ones, an on-board engine driven generator is used to electrically power the compressor and the condenser and evaporator fan/blower motors. This particular variant is the “hybrid electric TRU”. Another variant is “electric standby TRU” which includes an in-parallel electric motor and diesel engines. Many auxTRUs (auxiliary transport refrigeration units) can now be powered electrically when at the depot. This particular system eliminates losses in relation to belt transmission.

An independent fuel tank is normally used for the auxiliary engine as illustrated in Fig 2.4.

Figure 2.4: Main engine tank for white diesel and auxiliary engine tank for red diesel.

AuxTRUs traditionally used refrigerants such as R134a and R404A as working fluids. These are now being replaced with R452A in new units- offering properties similar as R404A however with 45% lower global warming potential (GWP) [16, 24]. Another new choice of working fluid is carbon dioxide (CO_2) (R744) but only few manufacturers currently offer this option.

2.2.3 Insulation

The ATP Certification 2017 (Agreement of the International Carriage of Perishable Foodstuffs) classifies the insulation with heat transfer coefficient (K) of below 0.4 $W/K \cdot m^2$ as "mechanically refrigerated normal insulated" and K value between 0.4-0.7 $W/K \cdot m^2$ as "mechanically refrigerated heavy insulated" [12]. The agreement specifies that the refrigeration plant must have heat extraction capability of atleast 1.75 times the heat flow in the insulation. The lifetime of insulation material is between 10 and 15 years with an insulation degradation rate of 3- 9% per year [4, 14].

Expanded polyurethane (PU) foam is the most popular insulation material for refrigerated vehicles [18]. The foam is normally sandwiched between plywood covered with glass-reinforced polyester sheet, fiberglass or aluminium skin. Expanded polystyrene (Styrofoam) is another common insulation material for refrigerated boxes which provides great strength and robustness at low temperature. The material's rigid structure however prevents its wider usage.

Cambridge Refrigeration Technology [25] and Lawton [26] provides a brief overview on insulation materials such as mineral wools, vacuum insulation panels (VIPs), and aerogel insulation blankets. Due to low thermal conductivity 0.002-0.004 W/(m.K),

VIPs have recently been gaining increasing popularity in the thermal insulation market [27-29]. An early study by Lawton and Marshall [26] indicated that VIPs could maintain their insulation values for well over 20 years, much longer than standard expanded foam. Modelling work by Hadawey and Tassou [30] on different thickness of VIP multi-layered with PU found that increasing the VIP thickness could provide better insulation. The effects of thermal bridging, the relatively high cost and the possibility of loss of vacuum though puncture, however, can present technical barriers for wider usage [28].

A study by Adekomaya et al. suggested that the use of lightweight polymer material or fibre-reinforced polymer composite as external skins can provide improved thermal resistance compared to metallic sheets [31]. Multilayer insulation walls using multi-foil insulation and aerogel layers were also found to be more efficient at limiting peak heat transfer during the daytime period [4].

2.2.4 Other factors contributing to environmental impacts and energy demand

Many literatures have identified the use of diesel and high GWP refrigerants to be the main contributing factors to higher environmental impacts [13-16, 32-34]. Provided the dependency of diesel and harmful working fluids can be reduced or eliminated, significant improvement in environmental impact could be achieved in the area of food transport refrigeration [14, 17, 35]. One way of reducing the dependency on diesel-powered TRUs is the acceptance and use of alternative cooling technologies [11].

Rai and Tassou [16] also suggested that the infiltration load during door openings is one of the dominant contributors to thermal load during temperature-controlled distribution. During every distribution round, several door openings (drops) take place. The door opening during each drop allows substantial amount of warm air to enter the cold chamber resulting in an increase in the internal temperature and hence greater recovery energy input to pulldown the temperature back to its set point. Reduction of the infiltration load can therefore have a significant impact on the energy consumption of transport refrigeration systems.

2.3 Protective mechanisms to reduce energy demand

2.3.1 Plastic –strip curtain and air curtain

For almost every delivery round, several delivery drops take place at every delivery point. The door opening during the multi-drop distribution allows substantial amount of warm air to enter the refrigerated chamber causing the internal temperature to rise. This would result in greater recovery energy to pulldown the temperature of the chamber to its set point. Previous modelling works estimated infiltration to be one of the dominant causes of refrigeration load in refrigerated vehicles (almost 34% of the overall refrigeration load), almost in same order of magnitude as the conduction heat gains, and even higher at times depending on distribution type [16, 36]. Refrigeration load due to infiltration can account for more than 50% of the overall share [16, 37, 38]. Tso et al. [39] assessed the heat exchange across the door to be 3.27 kW for door opening time of 2 minutes in a refrigerated truck with volume of 7.2 m^3.

The level of warm air infiltration depends on many factors such as the temperature difference between the inside and the outside of refrigerated chamber, the door opening duration, and the presence of any protective mechanisms. Currently, there are two popular protective mechanisms, PVC strip curtain and air curtain, used for controlling the rate of infiltration, as illustrated in Figure 2.5.

(a) (b)

Figure 2.5: Protective mechanisms (a) PVC strip curtain and (b) air curtain.

Though the traditional PVC strip curtains do prevent warm air from entering the refrigerated chamber, the strip curtains are generally considered to be unsafe, inefficient, unhygienic, and obstructive during loading and unloading process

requiring regular maintenance [40]. In contrast, air curtains in recent years have become more popular choice in comparison to the strip curtains.

Many investigations and studies aimed at finding ways to minimize the rate of warm air infiltration in temperature-controlled environment have suggested the use of an air curtain to be the most-effective mechanism in controlling infiltration [41-45]. Experimental work conducted by Azzouz et al. [41] estimated that an air curtain can reduce the mass of warm air entering the cold room by almost 38%. Another experimental work by Tso et al. estimated an energy saving of upto 40% using an air curtain in refrigerated trucks, this figure is similar to the 30% energy saving claims provided by manufacturers [39, 46].

Study by Foster et al. has estimated the effectiveness of an air curtain to be 0.71, where effectiveness 1 represents total elimination of warm-air infiltration [42]. In follow-up study by the author, the effectiveness of air curtain can be further improved to 0.77 through careful setting i.e. adjusting the jet velocity and angle [40].

However, majority of the studies on air curtain flow characteristics so far were conducted on cold rooms and buildings only and very less in refrigerated vehicles. There still lacks adequate number of studies aimed at the use of air curtain in refrigerated vehicle, its effectiveness in energy savings and ways of optimising its effectiveness.

2.3.3 Scopes for improvement in air curtain efficiency

Previous studies on the use of air curtains in cold rooms have shown numerical simulation using Computational Fluid Dynamics software (CFD) to be an effective way of investigating the performance of an air curtain. Foster et al. [42] suggested that even though the use of air curtain in cold rooms and commercial building doorways is becoming more common, the majority of these devices are not used at optimum design conditions. Jaramillo et al. [47] suggested that the effectiveness of an air curtain can be improved through optimisation of the positioning of the air curtain with respect to the door opening and selection of appropriate nozzle width, jet discharge velocity and jet discharge angle. Many other studies suggested the air curtain velocity to be the most important design parameter influencing air curtain performance [30, 40, 42, 43, 47, 48].

Along with discharge velocity, discharge angle can also influence the efficiency of an air curtain [30, 40, 42, 43, 47, 48]. An experimental study by Jaramillo et al. assessed the energy efficiency of the air curtain discharge angles [47]. The assessment considered four different jet discharge angles: -15°, 0°, 15° and 30° (positive direction assigned to be towards the cold room) for an air curtain inlet on the cold room side (cold air suction). The results showed that the angles of 30° and 15° led to higher energy consumption, compared to the 0° and -15° angles which were found to have similar performance.

The location of the air curtain with respect to the door opening was also found to influence its performance. An experimental study by Valkeapa et al. [43] on the application of air curtains in buildings determined that a vertical air curtain offered better protection against outdoor air infiltration compared to a horizontal air curtain. Jaramillo et al. [47], from CFD investigations of the performance of air curtains applied to cold room doorways reported that placing the air curtain on the exterior warm side of the door provided a higher efficiency for long door opening periods. Mounting the air curtain on the cold side of the door, however, provided better efficiency for short opening periods. The opening periods were not specified in the paper.

However, the studies discussed above are conducted on cold room. Unlike a cold room which has stationary environment, a delivery truck is always in motion and can have many restrictions in regards to the space and weight which can limit the number of adjustments. There still lacks a sufficient number of studies that focus on use of air curtain in refrigerated truck and ways of improving its effectiveness.

2.4 Alternative cooling technologies to reduce the dependency on auxTRUs

2.4.1 Eutectic- PCM-based transport refrigeration units

Cold plates using eutectic solutions have now been in use for transport refrigeration for over 50 years [35]. The beams and plates filled with eutectic solution, as presented in Figure 2.6, are usually mounted at the roof and sidewalls of the refrigerated chamber and are electrically charged (frozen) during night for 8 to 12 hours [14]. Once frozen,

the eutectic systems can maintain the internal temperature of the container on the range 0 °C to -30 °C [49].

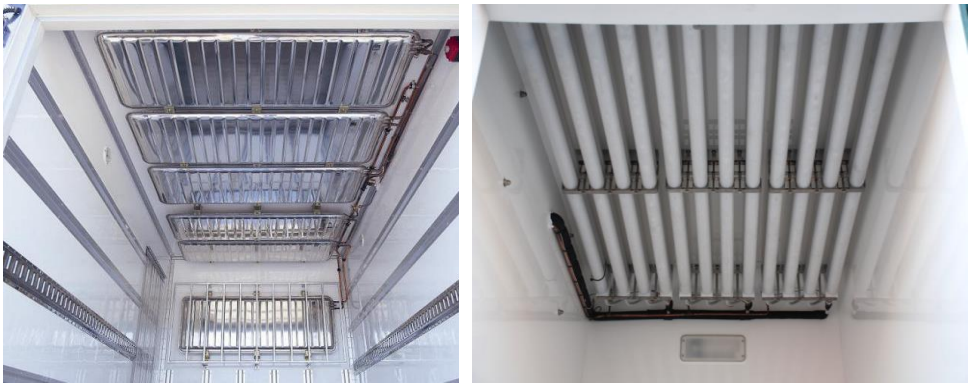

Figure 2.6: Examples of eutectic plates and eutectic beams.

Several designs of PCM based refrigeration units have been proposed over the years. Liu et al [50] proposed the idea of using encapsulated PCM plates in a storage unit and passing a secondary working fluid through it to deliver cooling from the unit to the heat exchanger inside the refrigerated chamber. For an ambient temperature of 30°C and air flow rate of 0.22 l/s, an internal temperature of -15.8°C was achieved using the design. The system was able to provide 1 kWh of cooling capacity per kWh of electric power supplied during charge. In a follow up study by the authors suggested a requirement of 280 kg of PCM for no door openings and 390 kg for door openings for chamber size of 3 m× 2 m× 1.8 m questioning the feasibility of the design for practical use [38].

Technology barriers

- The period of cooling is limited to the time required for the solution to melt reducing the operating range of the system.
- In order to increase the operating time, more eutectic solution would be required. This would however add more weight to the vehicle that would increase the energy consumption of the vehicle's main engine and reduce food load carrying capacity.

2.4.2 Hydrogen-fuel-cell powered auxiliary power unit

The hydrogen-fuel-cell powered TRUs are currently in the demonstration phase of commercialization. The current system design includes electric standby option that allows the compressor to run either on a diesel auxiliary engine or with an external 80

V or 460 V AC motor powered using hydrogen fuel cells [51]. The diesel engine is currently proposed to be left in place so it can act as a backup. Upon full commercialization, the fuel cell is expected to completely replace the diesel engine [32]. A simple configuration of the system is highlighted in Figure 2.7.

Garde et al. [52] estimated an average hydrogen requirement of 0.3 kg per 100 km for heavy-duty truck TRUs. The consumption of hydrogen to run the TRU can vary depending on different external conditions and distribution factors. For small truck with fuel cell size of 3 kW the hydrogen consumption rate can vary from 0.21 kg in January to 0.22 kg in August per 100 km, while for a HGV with fuel cell size of 5 kW the consumption rate can vary from 0.30 kg in January to 0.37 kg in August per 100 km.

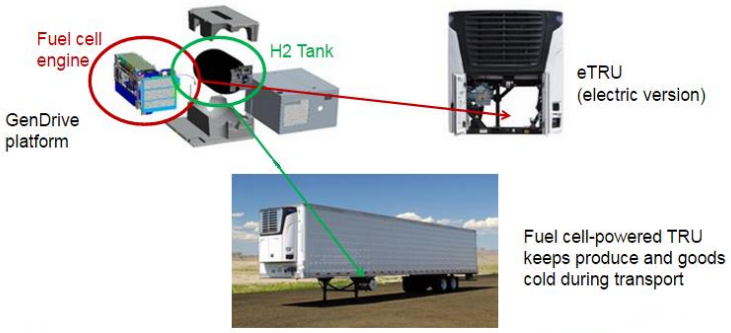

Figure 2.7: Proposed configuration of fuel cell based TRU [51].

Technology barriers

- Production of hydrogen can be an energy and cost-intensive process.
- High initial capital cost due to lack of current hydrogen refuelling infrastructure.

2.4.3 Solar-powered photovoltaic transport refrigeration systems

In such a system, silicone solar photovoltaic (PV) panels can be mounted on the trailer's roof to capture solar irradiation and convert it to direct current (DC) electricity. The DC can then be converted to alternating current (AC) using an inverter to power the refrigeration unit. An on-board battery is used to store the additional power generated from the PV for use by the refrigeration unit during hours of low or no solar radiation.

There are only a limited number of studies focus on the use of solar PV to power the TRUs. Early work by Bahaj and James [53] using a 4.4 kW PV array on a trailer roof with an area of 35 m^2 managed to generate 22 kWh of electricity during a week in November in the UK. According to the analysis, for an average ambient temperature of 12 °C, the energy requirement of a chilled delivery to a single store with delivery duration of 2 hours was estimated to be 3.2 kWh – this could be achieved using the PV panels.

A lab-scale experiment conducted by Kalbande and Deshmukh [54] on 25 litre diesel-powered vapour compression refrigeration system found an average photovoltaic conversion efficiency and exergy efficiency of 8.5% and 11%. The exergy was found to be at its highest in early morning and afternoon. Investigation by Elliston and Dennis [55], in their work on solar-assisted refrigerated transport, found the system was capable of replacing 85% of the diesel used to refrigerate the trailer down to -18°C. However, this study was conducted in Australia which has higher levels of solar insolation. Hence, at places with lower levels of solar insolation, similar results cannot be expected.

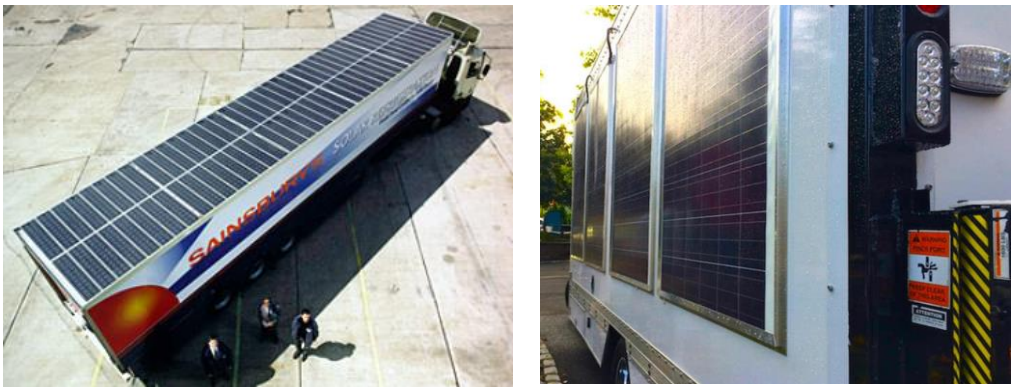

Figure 2.8: Solar-powered transport refrigeration

Technology barriers

- Dependency of PV charge collection on solar irradiation.
- High initial capital cost. Since the system requires several new components that will require replacement over the lifetime of the solar trailer, this can present an economic barrier.
- Additional components of PV-powered transport refrigeration systems (PV panels, inverter, charge controller, battery etc.) can add additional weight to the vehicle.

- The area of roof used for mounting the PV panels can be a restricting factor for the required power.

2.4.4 Cryogenic based transport refrigeration systems using liquid nitrogen (LN_2) and liquid carbon dioxide (LCO_2)

In this system, a large refillable vacuum-insulated tank with capacity ranging from 420- 700 kg mounted underneath the trailer, is used to store LN_2 or LCO_2 [16].

With direct systems, the cryogenic fluid from the tank is directly injected into the cargo space using sprayers and is released to the atmosphere during door openings. When the liquid fluid comes into contact with internal air the fluid starts expanding rapidly into gaseous state, transferring its energy to the internal space. A cool down temperature of -20°C can be achieved at ambient temperature of 30°C in less than thirty minutes [17].

Since the gas is released to the space in the refrigerated container, once it transfers all its thermal energy, it exits the space close to ambient temperature. The system provides fast and efficient cooling but also imposes safety risks from reduction in the oxygen level inside the container. In modern designs, a number of overlapping controls are incorporated to monitor the oxygen level and prevent entry into the refrigerated space in situations where low oxygen levels (below 19.5%) are detected [56].

Indirect systems, shown schematically in Figure 4.1(b), overcome the safety issues of direct systems by expanding the fluid in a heat exchanger before discharging it to the atmosphere. The cooling generated by the expansion of the cryogen is transferred to the refrigerated space by air circulating across the heat exchanger coil by a fan. A cooling capacity of approximately 0.101 kWh per kg of cryogenic fluid can be achieved using the system [57].

The temperature pulldown of indirect system is, however, not as rapid as direct systems [58]. The exit condition of the vented gas to the atmosphere is equivalent to the ambient conditions. The design of the system can vary from manufacturer to manufacturer depending on the cooling capacity, size of the cargo, and use of additional cooling units.

The hybrid system is a combination between the mechanical vapour compression system and the indirect cryogenic system. The system reduces the demand on the cryogenic fluid and thus extends the delivery time of the vehicle. It also eliminates the noise from the refrigeration system during deliveries in heavily populated areas.

Analysis carried out by Tassou et al. [59] on LCO_2-based TRUs showed the system to be more feasible for rigid and larger articulated vehicles. Rai and Tassou [16] estimated a mass requirement between 20 and 60 kg cryogenic fluid per hour depending on the thermal load encountered by the trailer. This large cryogenic fluid requirement limits the food distribution range of refrigerated vehicles before refilling is required.

The most recent innovation include LN_2 based TRU by Dearman where the fluid is first partially expanded in a heat exchanger to provide cooling to the air in the refrigerated compartment and then fully expanded in a piston engine to generate power to drive a vapour compression refrigeration system by a number of other ancillary equipment. This system is currently being trialled by a number of food retailers.

(a) (b)

Figure 2.9: Cryogenic based transport refrigeration systems (a) indirect system and (b) direct system [60, 61].

Technology barriers

- To provide similar cooling, cryogenic systems require a greater mass of cryogenic fluid compared to diesel which limits the distribution range of the vehicle.

- The production of cryogenic fluid is an energy intensive process which contributes to GHG emissions when fossil fuel is used for the energy generation.
- The lack of cryogenic fluid charging infrastructure can hinder wider adoption of cryogenic systems.

2.4.5 Refrigeration using waste heat from diesel ICE

Almost 60% of the energy is wasted from the exhaust and cooling systems of an internal combustion engine (ICE). Exhaust gas contains around 30% of the total combustion energy from the engine. Recovering the waste heat from an ICE to generate energy can help reduce the fuel consumption and can be used to run other units, for instance the TRU. Potential technologies used for waste heat recovery (WHR) include thermoelectric generators (TEG), Organic Rankine Cycles (ORC) and turbocharger technologies [62]. The working principles of WHR system is illustrated in Figure 2.10.

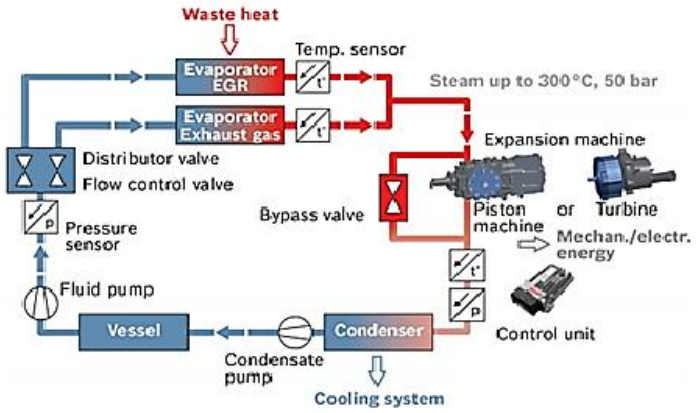

Figure 2.10: Layout of WHR system

The concept of running TRUs using exhaust heat is still at the research stage. Simulation work by Seher et al. [63] on WHR from 12 litre HGV diesel engine using an ORC system with water as the working fluid demonstrated 14 kW of delivered mechanical output power (4.3% of the main engine power). Investigations by Kalyan et al. [64] considered the exhaust heat recovery potential of a dual-fuel low-temperature combustion engine using bottoming ORC that achieved a fuel conversion efficiency of 8% and a reduction in NO_x and CO_2 emissions by 18%. A study by Zhang

et al. [65] on an ORC prototype of WHR from a diesel engine exhaust showed power output of 10.38 kW at shaft efficiency of 57.88%.

Several literatures have suggested integration of the WHR system with heat-driven refrigeration systems such as adsorption, absorption and desiccant technologies to effectively recover waste heat from an ICE for cooling purpose [20, 66, 67]. An experiment conducted by Sarma et al. [20] successfully utilised the waste heat from a two-stroke 100cc ICE to run the vapour absorption refrigeration system to produce cooling. Work by Lu et al. [66] focused on the integration of ORC and solid sorption technology to generate power and refrigeration.

Technology barriers

- Refrigerants in ORC systems require a high input power for the pump. For R245fa, the power requirement can be up to 2 kW, resulting in a high system cost and lower energy.
- Heat recovery and conversion systems can be large and complex presenting installation difficulties and requiring high maintenance cost.

2.4.6 Electric transport refrigeration systems

For all-electric transport refrigerators, the TRU is powered using an electric motor rather than a diesel engine. When stationary at depot, a plug-in option can be used to charge the battery. Convectional TRUs can also be converted to all-electric by replacing the diesel engine with an electric motor.

(a) (b)

Figure 2.11: Example of (a) all-electric refrigerated vehicle and (b) European Type 2 power plug.

A number of light delivery trucks (3.5 t and 7.5-11 t) are now opting for all-electric options, where both the TRU and truck are powered electrically [68-70]. The power required for the vehicle can range anywhere between 80 kW and 120 kW for 7.5-11 t trucks and between 133 kW and 290 kW for 14 -18 t [68, 71]. Paneltex in the UK specialises in all-electric trucks with gross weight of 5- 11 t, featuring 150 kW peak-power motors and up to 100 kWh of lithium ion phosphate battery capacity [72]. The 20 kW on-board charger provides full charge in five hours [72]. Magtec, a company that specialises in electric trucks, offers electric trucks up to 14 t which can deliver 7.33 t-mile-per-kWh. An example of TRU that can be used with an electric truck of this size is the Mitsubishi TEJ35A model, which runs on a secondary battery and can deliver cooling capacity of between 1400 W and 4300 W at ambient temperature of 35 °C [69].

Technology barriers

- Operation time is limited by the power capacity generated by the battery charge. Hence, re-charging may be required for long-range distribution.
- Charging time can vary depending on different battery types.
- High charge capacity batteries are costly but increasing demand is expected to lead to a reduction in cost.

2.5 Summary

This chapter presented a review of vapour compression transport refrigeration units (TRUs) and their environmental impacts. It has been identified that there is a need to replace diesel powered TRUs with alternative technologies to reduce particulate emissions from diesel combustion. A number of alternative technologies have been identified and briefly described together with their advantages and disadvantages and the barriers that need to overcome for wide acceptance by the industry.

A way of reducing the environmental impacts of transport refrigeration systems is to reduce the thermal load of the refrigerated container (box). This can be achieved by improving the thermal resistance of the box and also reducing air infiltration during door openings. The effectiveness of the air curtain in reducing air infiltration load and the energy consumption of the refrigeration system is investigated in the Chapters, 6 and 7, of the thesis.

Chapter 3 investigates in more detail the energy consumption and environmental impacts of conventional TRUs.

CHAPTER 3

Theoretical investigations into the energy consumption and environmental impacts of TRUs powered using auxiliary diesel engine

This chapter discusses a spreadsheet model developed to perform investigations into the refrigeration load and fuel demand to maintain the required temperature of the refrigerated box during food transportation as well as its environmental impacts. The parameters used for estimating the refrigeration load are based on real-life distribution scenarios and collected using a survey conducted in collaboration with CENEX and TfL (Transport of London) [10]. This chapter also discusses and presents the investigation work carried to validate the model. The investigations were conducted on an 18 tonne delivery truck during its normal distribution rounds in the London area.

3.1 Overview of the model

3.1.1 Model description

A spreadsheet model was developed to perform the refrigeration load calculations of refrigerated boxes during temperature controlled food transportation. The load calculations are based on the methodology proposed by ASHRAE (American Society of Heating, Refrigerating, and Air-Conditioning) [37]. The model takes into account several input parameters such as the setting temperature, ambient temperature, vehicle dimensions, insulation type and it's thermal properties, door opening duration and distribution time. The methodology used for estimating the GHG emissions are in accordance to EN16528 standard [73] and data conversion factors in accordance to Defra [16, 73, 74].

Conduction and convection									
Thermostat setting temp Tset (°C)	2								
Overall solar temp adjustment (°C)	18								
Solar radiation temp.adjustment	Nb.	Side wall (°C)							
	2	10							
		Roof (°C)							
		6							
		Rear doors (°C)							
		2							
Properties of the trailer									
Overall UA value (W/K)	20.02								
Sidewalls UA value (W/K)	8.01								
Roof UA value (W/K)	3.93								
Rear door UA value (W/K)	1.91								
Floor UA value (W/K)	2.70								
Total operating time	15								
Precooling	1								
Overall specific heat (KJ/K)	423.74								
Door width (m)	2								
Door height (m)	2								
Overall door opening time (s)	23640								

External dimensions				Internal dimensions				
Length (m)	5.15			*length (m)*	5			
Width (m)	2.45			*Width (m)*	2.3			
Height (m)	2.50			*Height (m)*	2.3			
Constitution of body								
Nose								
Material	*x(mm)*	*k(W/(m.K))*	*Ageing*	*A.Var*	*d (kg/m3)*	*x/k (km2/W)*		*U value (w/km2)*
Polyester	2.5	0.17	0.0%	0.0%	1800	0.0147	0.46%	*UA value (W/K)*
PU foam	70	0.022	4.0%	-7.0%	50	3.1818	99.08%	
Polyester	2.5	0.17	0.0%	0.0%	1800	0.0147	0.46%	
								w=
					R=	3.2112		*A=*
Floor								
Material	*x(mm)*	*k(W/(m.K))*	*Ageing*	*A.Var*	*d (kg/m3)*	*x/k (km2/W)*		*U value (w/km2)*
Aluminium alloy	4	211	0.0%	0.0%	2700	0.0000		*UA value (W/K)*
Plywood	10	0.15	0.0%	0.0%	700	0.0667		
PU foam	100	0.022	4.0%	-7.0%	50	4.5455		
Plywood	5	0.15	0.0%	0.0%	700	0.0333		
Polyester	4	0.17	0.0%	0.0%	1800	0.0235		
								w=

Figure 3.1: Screenshots of the model.

3.1.1.1 Drive method of the refrigeration unit

From a recent survey that was conducted by Cenex [10], it was identified that the majority of refrigerated vehicles use an auxiliary engine to power the refrigeration unit even vehicles down to 7.5 t [11], and hence the calculations of the environmental impacts were based on the auxTRU refrigeration system.

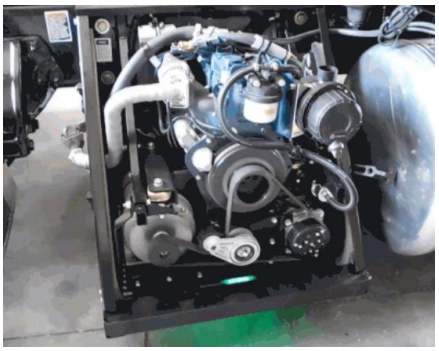

Figure 3.2: 4.0 kW auxiliary diesel engine [75].

3.1.1.2 Choice of working fluid

In recent years, the predominant refrigerant for transport refrigeration systems has been R404A. However, R404A is now being replaced by R452A, as presented in Figure 3.3, which has similar thermophysical properties as R404A (making replacement of refrigerant easier without any mechanical changes to the unit), but 45% lower GWP.

(a) (b)

Figure 3.3: (a) R404A TRU compressor replaced with (b) R452A working fluid.

3.2 Data collection

3.2.1 Distribution parameters

Table 3.1 presents the average data for three most common refrigerated vehicle categories from a survey conducted by Cenex for Transport for London (TfL) [10]. These data were used in the model to estimate the fuel consumption and GHG emissions of auxTRU by different vehicle categories.

Table 3.1: Average distribution parameters for different vehicle categories.

	Average survey-based parameters		
Parameters	Rigid 7.5 tonne	Rigid 12 tonne	Artic
Door dimension (h × w × l)	5 m × 2.3 m × 2.3 m	6.5 m × 2.3 m × 2.3m	11.8 m × 2.3 m × 2.6 m
Hours driven per day	14.5	14.1	17.5
Days per year	276	282	301
Average speed (km/h)	13.9	25.3	31.3
Deliveries per day	26	10	6
Door openings per delivery	3	4	5
Average door opening time (min)	5	8.5	15
Refrigeration time required per day (h)	10	14	24
Insulation thickness (mm)	75	75	75
Airflow in refrigerated compartment (m^3/h)	2600	3677	5600
Annual refrigerant charge (kg)	4	6	8

3.2.2 Properties of insulation material and food products

Polyurethane is the most common insulation material and thus has been chosen for this study. Table 3.2 presents the thermal properties of the insulation material.

Table 3.2: Thermal properties of the truck body.

	Conductivity (W/m·K)	Specific heat capacity (J/kg·K)	Density (kg/m^3)	Thickness (mm)
Ceiling	0.022	1470	50	75
Floor	0.022	1470	50	100
Front wall	0.022	1470	50	75
Lateral wall	0.022	1470	50	75

Table 3.3 presents the properties of food products.

Table 3.3: Properties of food products.

	Chilled	Frozen
Freezing point Tf (°C)	-0.9	0
C_p above T_f (kJ/kg·K)	3.91	4
C_p below T_f (kJ/kg)	1.93	3
Latent heat H_f (kJ/kg)	289	275
Heat of respiration (mW/kg)	12	0
Required temperature (°C)	2	-20

3.2.3 External temperature

The external temperature is not the same throughout the year and hence neither would be the refrigeration load. For this reason, the ambient temperature of an entire year of

2015 was considered for the model to analyse the difference in energy consumption throughout the year. The graph illustrated in Figure 3.4 illustrates the average daily temperature for the whole year.

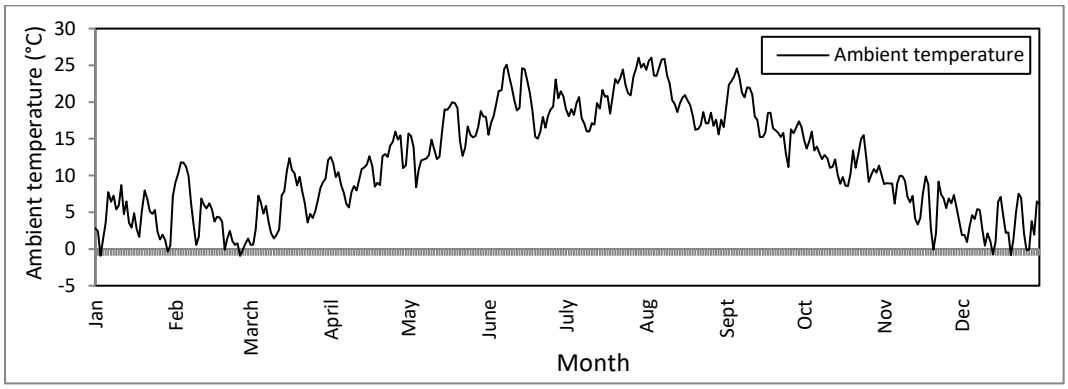

Figure 3.4: Average daily temperature of London for the year of 2015 [76].

3.3 Modelling methodology

In order to estimate the fuel intensity, it is first essential to estimate the overall refrigeration load because until it is known how much heat is likely to get in, it is hard to specify the amount of energy required to remove it [77]. The total refrigeration load of a refrigerated vehicle includes transmission load, product load, infiltration load and precooling load. Figure 3.5 illustrates different sources of refrigeration load in a refrigerated vehicle.

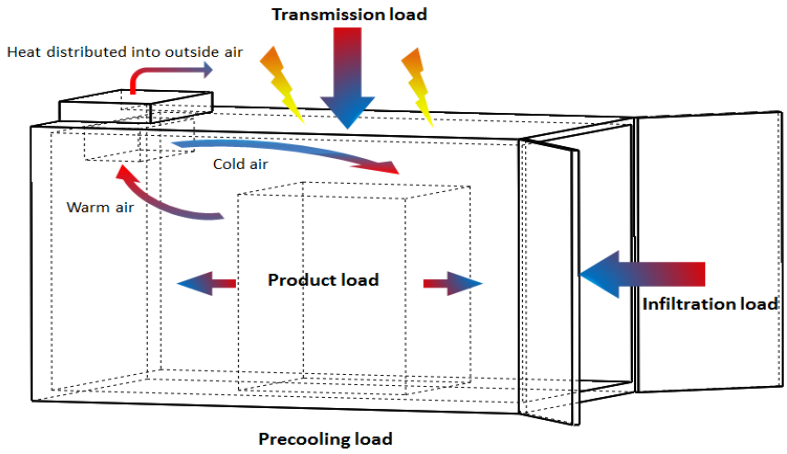

Figure 3.5: Main sources of refrigeration load in refrigerated trailer.

3.3.1 Total refrigeration load

The total refrigerated load can be estimated using,

$$Q_{ref} = Q_{trans} + Q_{pro} + Q_{pre} + Q_{inf} \quad 3.1$$

3.3.2 Transmission load

Transmission load represents the thermal load encountered as a result of the heat gain through surface of walls, floor, and ceiling and can be calculated using;

$$Q_{trans} = \sum U \cdot A \cdot (T_{amb} - T_{int}) \quad 3.2$$

Where:

U= overall heat transfer coefficient [W.m^2.K]

A =area of surface [m^2]

T_{amb}=ambient/external temperature [K]

T_{int} =represents the internal temperature [K]

The heat transfer coefficient is calculated using the following method;

$$U = \frac{1}{\sum_{i=1}^{n} \frac{x_i}{k_i}} \quad 3.3$$

Where:

x_i = thickness of material [m]

k_i=thermal conductivity of the materials [W.m^{-2}.K^{-1}]

$\frac{x_i}{k_i}$ =represents R_i or the thermal resistance of material i

ASHRAE states that the temperature difference, based on the exterior colour of the vehicle, can be adjusted to compensate the solar effect on heat load. The adjustments values are directly used in the model to compensate the solar effect. Any physical damage, moisture penetration and ageing of the insulation material can result in degradation of thermal conductivity value of the materials. For this study, we have assumed no degradation has yet taken place.

3.3.3 Product load

The food products are normally pre-chilled or pre-frozen at required temperature in cold rooms before being loaded in the vehicle (based on the investigation conducted). This eliminates the requirement of a TRU to pulldown the product temperature. Since frozen food products do not account for any heat load due to respiration like perishable/chilled food products, the product load due to heat of respiration for frozen produce is equivalent to zero. The product load of fresh produce can be estimated using;

$$Q_{pro} = \frac{h_r \cdot m}{1000} \quad 3.4$$

Where:

h_r =heat of respiration (mW/kg)

m =total mass of produce (kg)

It is however possible to chill and freeze the products in the trailer, this would however incur additional heat load. The heat that needs to be removed to cool the food products from initial temperature to temperature above freezing and/to below freezing can be calculated using;

$$Q_{above\ freezing} = m \cdot c_1 \cdot (T_1 - T_2) \quad 3.5$$

$$Q_{to\ freezing} = m \cdot c_2 \cdot (T_1 - T_f) \quad 3.6$$

Where:

c_1 = specific heat of produce to freezing [kJ/kg.K]

c_2=specific heat of produce above freezing [kJ/kg.K]

T_1 =initial temperature [K]

T_2 =lower temperature [K]

T_f=freezing temperature [K]

3.3.4 Precooling load

Precooling load represents the heat load that needs to be removed to bring the interior surface to desired temperature setting before the food products are loaded in the vehicle. Precooling load is estimated using;

$$Q_{pre} = \frac{\left(C_{pt} + V \cdot \rho_a \cdot C_{pa}\right) \cdot (T_{ini} - T_{int})}{1000} \quad 3.7$$

Where:

C_{pt}= specific heat of insulated body [kJ.kg^{-1}.K^{-1}]

V= payload volume [m^3]

ρ_a=air density [kg.m^{-3}]

C_{pa}=specific heat of air [kJ.kg^{-1}.K^{-1}]

T_{ini}= initial temperature inside the body [K]

T_{int} =thermostat setting temperature [K]

3.3.4 Infiltration load

The estimation of overall infiltration load is a complicated phenomenon and no specific equations have yet been proposed by previous studies to find the exact infiltration air load theoretically. However, it is possible to calculate the airflow through the door of a cold room as a result of air density difference between the inside and outside of the refrigerated chamber. Analytical CFD works done in the area of infiltration demonstrated the experimental conditions of cold room to be very close to that of a refrigerated transport chamber. The sensible and latent refrigeration load as a result of infiltration is estimated using the following equation [59];

$$q = 0.577 \cdot W \cdot H^{1.5} \cdot \left(\frac{Q_s}{A}\right) \cdot \left(\frac{1}{R_s}\right) \quad 3.8$$

Where:

$\frac{Q_s}{A}$= sensible heat load of infiltration air per square metre of doorway opening [kW.m^{-2}]

W =doorway width [m]

H =doorway height [m]

R_s =sensible heat ratio of the infiltration air heat gain

In the model, the door openings are calculated in hourly timeframe. For instance, we consider a T-second opening, the resulting thermal load for the hour during which the opening occurs can be calculated using [13];

$$Q_{inf} = \frac{T}{3600} \cdot q \tag{3.9}$$

3.3.5 Fuel consumption

The fuel consumption of an auxiliary diesel engine can vary depending on many factors such as the efficiency rate, use of additional cooling units, and power requirements to run the cooling units. Based on the estimated refrigeration load, the specific fuel consumption can be calculated using the efficiency rate of the auxiliary engine [16]. The energy density of diesel is approximately 11.83 kWh/kg. For the available density, only 20-25% is converted to useful energy by the engine. Out of the useful energy only the two-third is used for powering the compressor, providing cooling capacity of approximately 1.58- 2.17 kWh/kg of diesel which can be converted to kWh/litre using the conversion factor [16]. The fuel required to overcome the refrigeration load can be estimated using;

$$F_{diesel} = \frac{Q_{ref}}{cooling\ capacity_{aux}} \tag{3.10}$$

Where:

Q_{ref}= total refrigeration load [kWh]

$cooling\ capacity_{aux}$ = cooling capacity of refrigeration unit per litre of diesel [kWh/l]

3.3.6 Greenhouse gas (GHG) emissions

The model calculates the GHG emissions using the GHG conversion methodology detailed in EN16528 standard [16, 73].

Direct emission

The direct emission represents the GHG emission as a result of refrigerant leakage, which is estimated using;

$$Emission_{ref} = \frac{ref_{charge} \times GWP \times rate_{leak}}{100} \quad 3.11$$

Where:

ref_{charge}=refrigerant charge

GWP =global warming potential

$rate_{leak}$ =annual refrigerant leakage rate [%]

Indirect emission

Indirect emissions represent the emission as a result of fuel combustion process. Using the per litre GHG emission conversion factor of diesel provided by Defra [74], the carbon dioxide equivalent (CO_2e) for the fuel consumed can be estimated using;

$$Emission_{CO2e} = F_{diesel} \times EF_{diesel} \quad 3.12$$

Where:

F_{diesel}= amount of fuel [l]

EF_{diesel}= emission factor of diesel [$kgCO_2e/l$]

The current conversion factor is 2.6762 kg CO_2e per litre of diesel (which includes 2.65564 kg of CO_2, 0.0006 kg of CH_4 and 0.020906 kg of N_2O per litre of diesel).

3.4 Results

3.4.1 Total refrigeration load

Figure 3.6 represents the thermal load (kWh) values for different vehicle categories for chilled (2°C) and frozen (-20°C) operation for distribution parameters provided in Table 3.1.

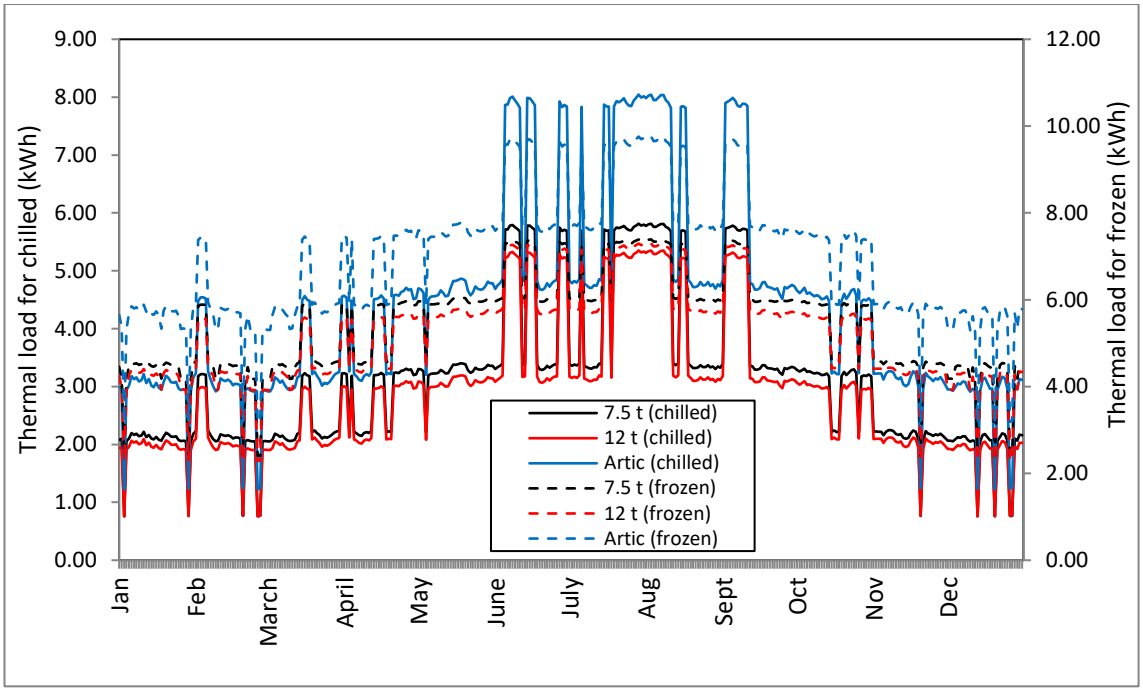

Figure 3.6: Hourly thermal load for chilled (2°C) and deep frozen (-20°C) distribution for different vehicle categories.

As can be seen in the figure, the frozen operation accounts for higher thermal load than the chilled operation due to frozen operation having greater temperature difference between the inside and outside of the refrigerated chamber, chilled set to 2°C and frozen set to -20°C.

The months between October and March have lower thermal load in comparison to other months. This is mainly due to lower ambient temperature during these months resulting in smaller temperature difference. In contrast, the months from June to September accounts for greater thermal load due to higher ambient temperature during these months.

Almost similar thermal load values have been estimated for vehicle categories 7.5 t and 12 t, with the thermal load of 7.5 t slightly higher than that of 12 t. If we observe the distribution parameters for the vehicle categories, the internal size of both the refrigerated chambers are fairly similar. However, the distribution scenario for 7.5 t category has more deliveries per day requiring more door openings and door opening duration in comparison to 12 t category leading to higher thermal load estimations.

Figure 3.7 illustrates the share of each thermal load towards the overall refrigeration load.

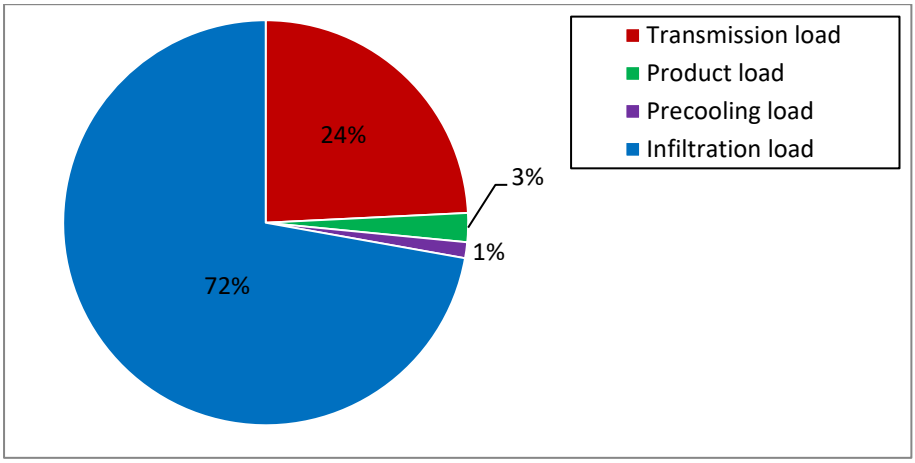

Figure 3.7: Share of each load towards overall refrigeration load for 100% of the door opening period.

As can be seen in the chart, infiltration load accounts for the highest share of total refrigeration load followed by transmission load, product load and pre-cooling load. The differences in the share of thermal load are mainly due to the distribution parameters (survey-based) used in the model. If we observe Table 3.1, we can see that the number of deliveries varies between 6 and 26 deliveries per day, the number of drops between 3 and 5 drops per delivery (each drop requiring door opening), and the door opening time between 5 and 15 minutes per door opening. Considering, the overall operation time of the vehicle during the day, a dominant part of the time is spend with door open allowing significant amount of warm air to infiltrate the space. Even investigation conducted by Foster et al. previously estimated the air infiltration to account for more than half of the total refrigeration load in cold rooms [40].

The thermal load in relation to pre-cooling only takes into account the heat that needs to be removed from the chamber at the beginning of journey to bring the internal temperature to set temperature. The thermal load encountered during the one-time temperature pulldown is much less in comparison to the thermal load that would be encountered for the overall door opening period throughout the day.

Similarly, the product load accounts for only 2% of the overall share. Since, the products are pre-chilled to required temperature before being loaded in the vehicle, the model only takes into account the heat load produced by the food products during

distribution period. In addition, the 'heat of respiration' of the products is very small producing very less heat during the process. Similarly, when the food products are densely stacked on pallets in the chamber, the overall thermal mass of the products would be high resulting temperature change to be much slower (please refer Chapter 6).

3.4.1.1 Refrigeration load for 50% less door opening time and for no door openings

It could be seen in Figure 3.8 that a significant contribution of thermal load was due to infiltration. In order to analyse the impact of infiltration in thermal load further, the door opening time was reduced by 50%. Upon 50% reduction of door opening time, the share of infiltration load dropped by 13% and the overall refrigeration load reduced by almost 35%.

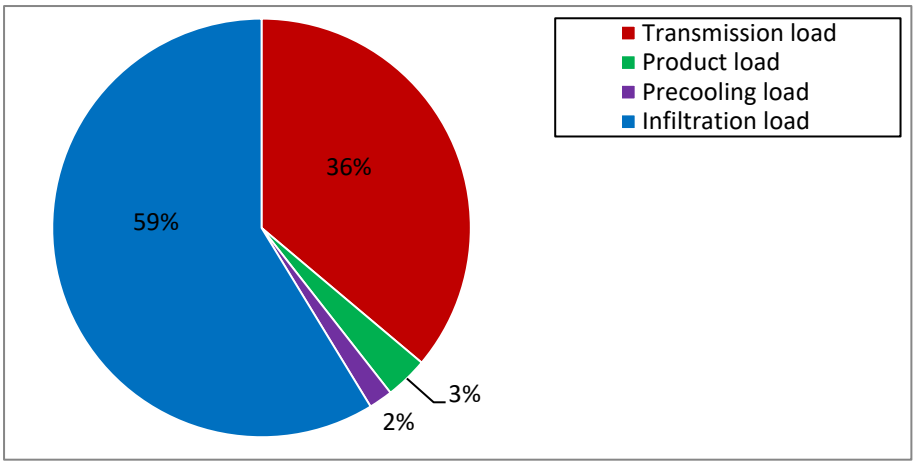

Figure 3.8: Share of each load towards overall refrigeration load for 50% of the door opening period.

Figure 3.9 presents the share of each thermal load for 75% less door opening.

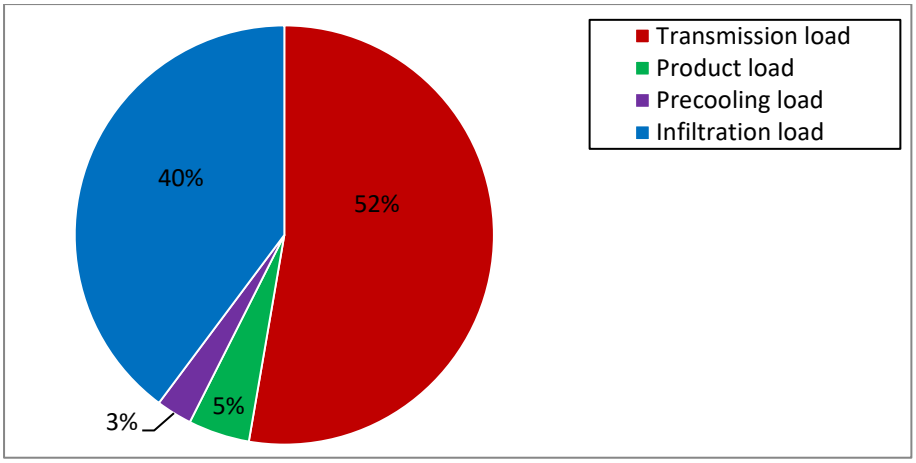

Figure 3.9: Share of each load towards overall refrigeration load for 75% less door opening period.

When the door opening time was reduced by 75%, the share of infiltration load decreased significantly resulting transmission load to be the most dominant source of the overall refrigeration load.

Please note, the shares of thermal load sources are only in consideration to this particular set of distribution parameters used for the model. The shares and values of refrigeration load can vary depending on different distribution schedules.

3.4.2 Energy consumption- Fuel consumption

Figure 3.10 presents the hourly fuel consumption of auxTRU for distribution parameters provided in Table 3.1 for different vehicle categories.

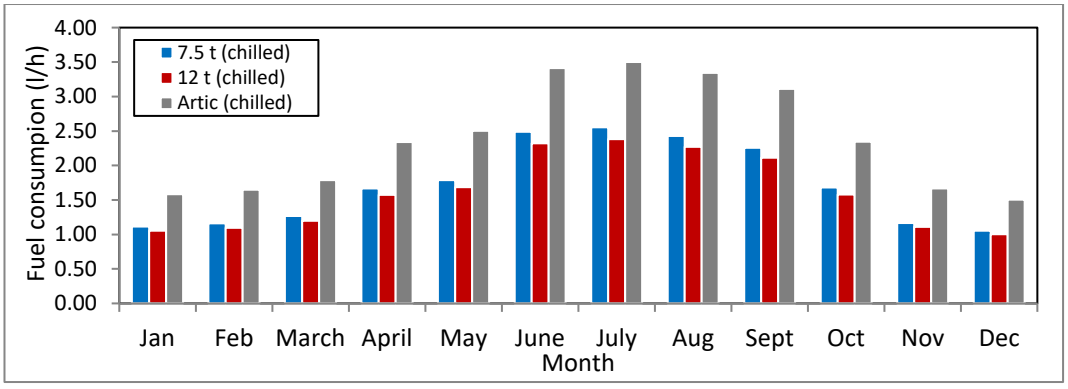

(a)

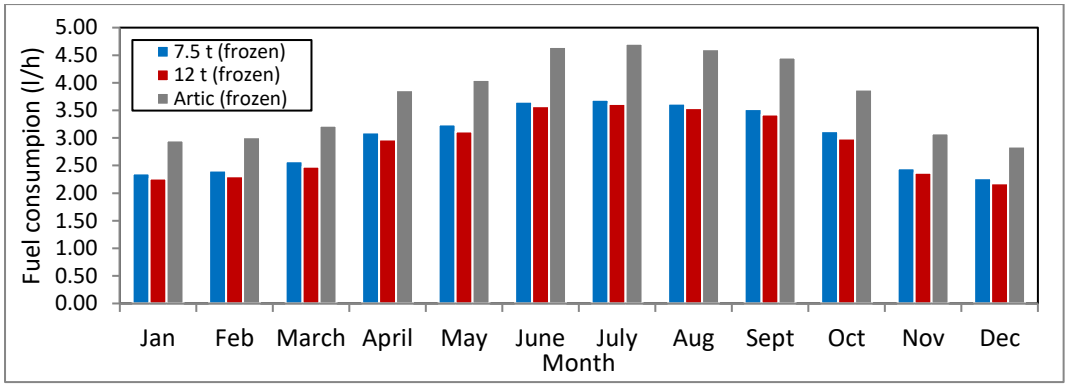

(b)

Figure 3.10: Hourly fuel consumption for (a) chilled distribution (l/h) and (b) frozen operation (l/h).

For the chilled operation (2°C), the fuel consumption of 7.5 t and 12 t varies between and 1.00 l/h to 2.38 l/h and of artic between 1.51 l/h and 3.50 l/h. For the frozen operation (-20°C), the fuel consumption of 7.5 t and 12 t varies between 2.18 l/h and 3.69 l/h while the artic vehicle between 2.85 l/h and 4.71 l/h. The fuel consumption of frozen is higher than that of chilled distribution mainly due to frozen distribution accounting for higher thermal load due to greater temperature difference between the inside and outside of refrigerated chamber.

Previous assessment estimated the fuel consumption of refrigerated chamber with volume 33.42 m^3, 61.15 m^3, 78.79 m^3 to be 1.5 l/h, 2.5 l/h and 3.0 l/h for chilled operation and 2.0 l/h, 3.0 l/h and 4.0 l/h for frozen operation respectively [14]. These estimates are very similar to the values estimated for this work providing rough verification of the results.

As predicted, the warmest months of the year (June-Sept) accounts for the highest fuel consumption due to higher thermal load during the months as illustrated in Figure 3.6.

The artic vehicle has higher fuel consumption in comparison to 7.5 t and 12 t. This is due to larger door area and internal space of the refrigerated chamber resulting more warm air to flow in (cold air to flow out) during door openings and larger surface for heat to penetrate through during operation.

If we observe the results for 7.5 t and 12 t, it can be seen that the 7.5 t accounts for higher fuel consumption than the 12 t. This is mainly due to the distribution parameters

of 7.5 t and 12 t being very similar to each other except the total door opening time. The total door opening time for the distribution of 7.5 t is more than 12 t by almost an hour.

3.4.2.1 Fuel consumption for 50% less door opening time

Figure 3.11 presents the hourly fuel consumption of auxTRU for 50% of the door opening time.

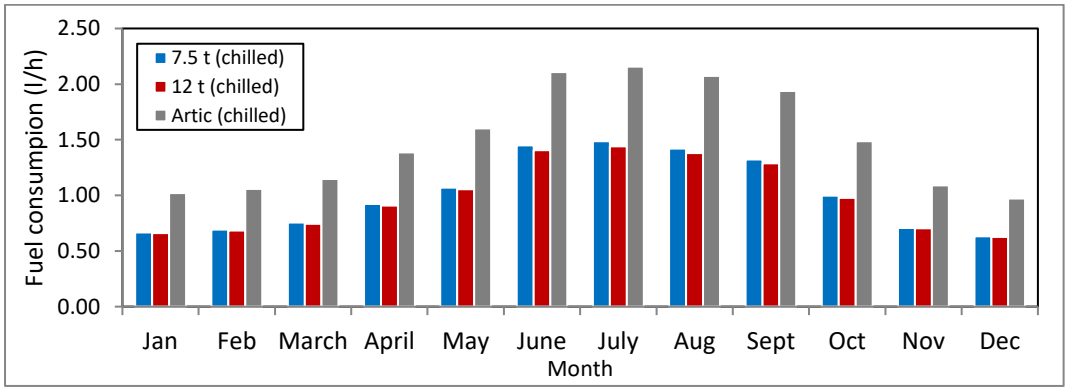

(a)

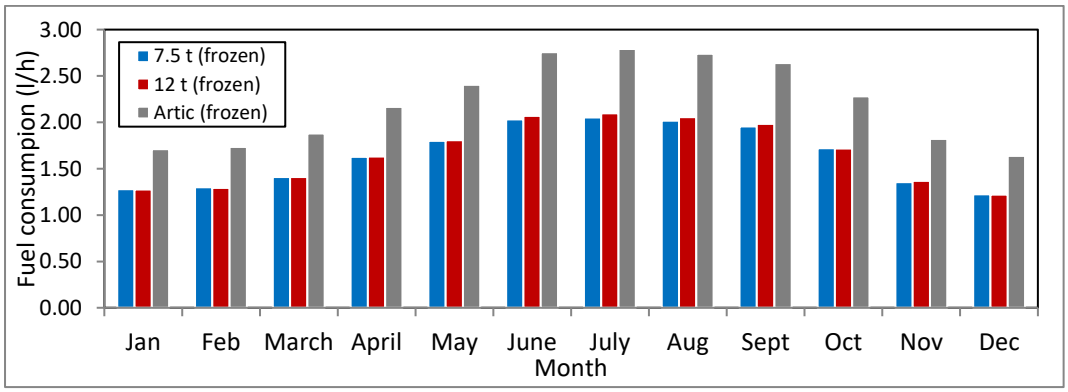

(b)

Figure 3.11: Hourly fuel consumption for (a) chilled distribution (l/h) and (b) frozen operation (l/h).

For chilled operation, the fuel consumption of 7.5 t and 12 t varies between 0.63 l/h and 1.49 l/h while artic between 0.97 l/h and 2.16 l/h. For frozen operation, the fuel consumption of 7.5 t and 12 t varies between 1.22 l/h and 2.10 l/h while artic between 1.64 l/h and 2.79 l/h.

A significant reduction in fuel consumption can be seen in Figure 3.11 in comparison to Figure 3.10. Provided the infiltration rate can be controlled, a substantial improvement in energy consumption could be achieved (Refer Chapter 6).

One difference that can be observed in Figure 3.10 and Figure 3.11 is the fuel consumption of 7.5 t and 12 t in Figure (b). Unlike other graphs, the fuel consumption of 12 t in this particular graph is slightly higher than 7.5 t. As discussed before, infiltration is the dominant cause of refrigeration load for these particular distribution scenarios. Provided the infiltration can be reduced by reducing the door opening time, the overall energy requirement can also be reduced. However, the second dominant thermal load 'transmission' still takes into account the temperature difference and surface area. And since the frozen operation of 12 t accounts for greater temperature difference and slightly larger surface area, more fuel consumption has been estimated.

3.4.3 Indirect environmental impact- GHG emissions from fuel combustion process

Figure 3.12 presents the CO_2e for the fuel consumption presented in Figure 3.10.

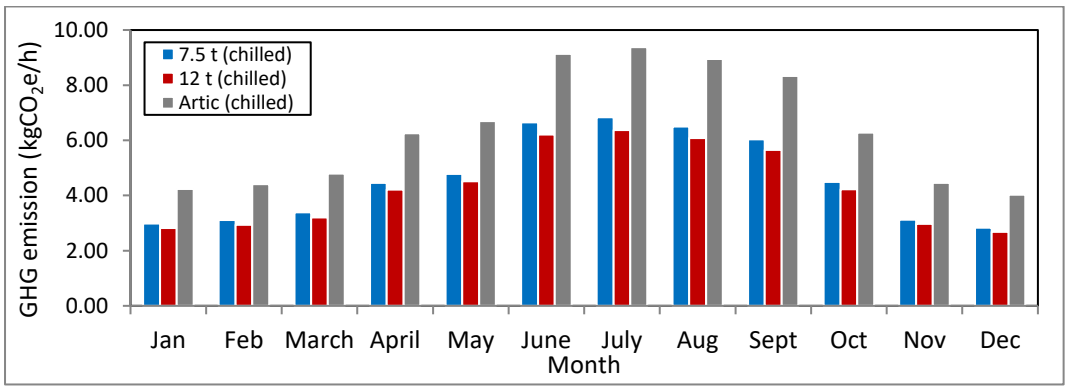

(a)

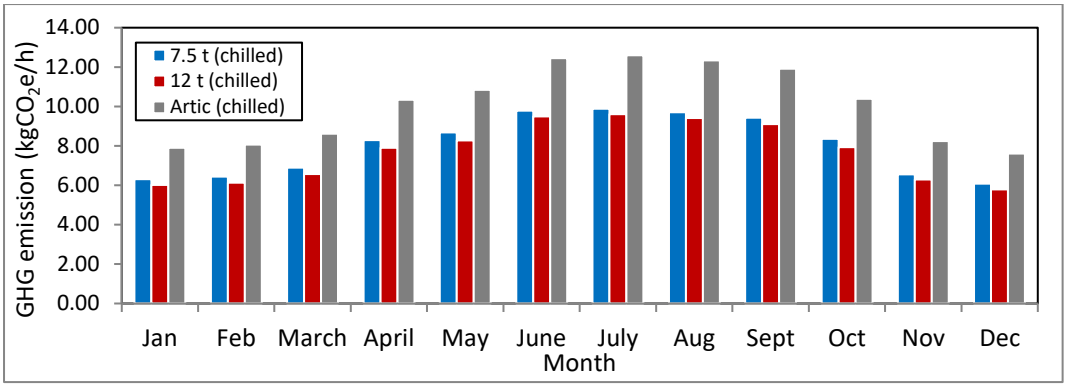

(b)

Figure 3.12: CO_2e emission from different vehicle categories for (a) chilled operation (b) frozen operation.

As can be observed in the figures, the auxTRUs can be responsible for significant amount of GHG emissions. For chilled operation, the CO_2e emission of 7.5 t and 12 t varies between 2.68 $kgCO_2e/h$ to 6.83 $kgCO_2e/h$ while for artic varies between 4.03 $kgCO_2e/h$ and 9.37 $kgCO_2e/h$. Meanwhile for frozen operation, the CO_2e emission of 7.5 t and 12 t varies between 5.83 $kgCO_2e/h$ and 9.69 $kgCO_2e/h$ while for artic between 7.62 $kgCO_2e/h$ to 12.60 $kgCO_2e/h$.

The warmer months of the year account for higher GHG emissions due to higher fuel consumption during the period. In comparison, the colder months of the year account for less environmental impact.

As discussed earlier, every litre of diesel is responsible for 2.6762 kg of CO_2e (a combination of 99% of CO_2, 0.00024% of CH_4 and 0.0078 of N_2O). Provided the fuel consumption of auxTRU can vary anywhere between 0.66 l and 5.10 l per operating hour, the overall environmental impact of auxTRU can be quite substantial presenting high risk to human health.

3.4.3.1 GHG emissions for 50% less door opening time

Figure 3.13 presents the GHG emissions for 50% less door opening time.

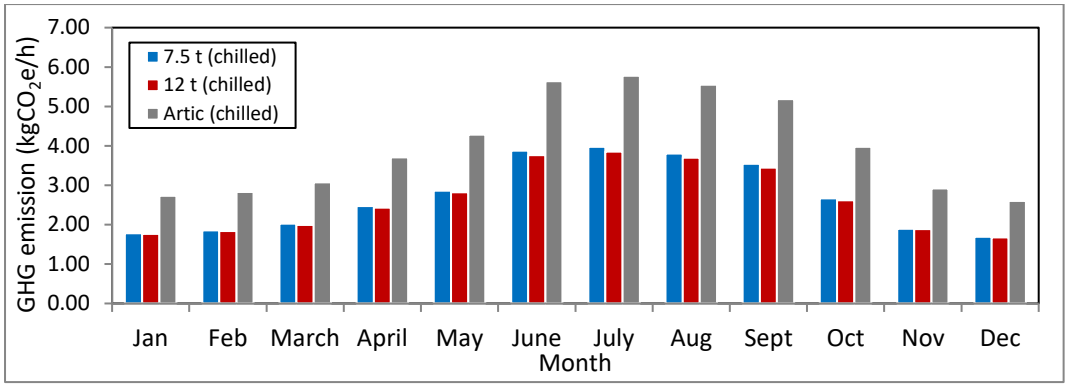

(a)

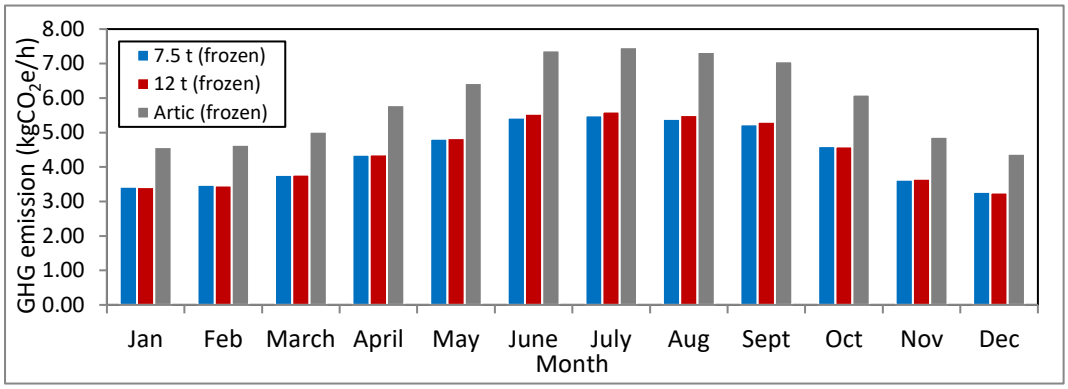

(b)

Figure 3.13: CO_2e emission from different vehicle categories for 50% of the door opening time (a) chilled operation (b) frozen operation.

As can be seen in Figure 3.13, provided the door opening time can be reduced, the overall environmental impact can be reduced as well. For chilled operation, the CO_2e emission of 7.5 t and 12 t varies between 1.68 $kgCO_2e/h$ to 3.85 $kgCO_2e/h$ while for artic varies between 2.60 $kgCO_2e/h$ and 5.77 $kgCO_2e/h$. Meanwhile for frozen operation, the CO_2e emission of 7.5 t and 12 t varies between 3.26 $kgCO_2e/h$ and 5.61 $kgCO_2e/h$ while for artic between 4.38 $kgCO_2e/h$ to 7.47 $kgCO_2e/h$.

3.4.4 Direct environmental impact-refrigerant leakage

Survey conducted by Cenex estimated the refrigerant charge of vehicle category 3.5 - 7.5 t to be 5 kg, 7.5 -12 t to be 6 kg and 12 -18 t to be 6 kg too [10]. The annual refrigerant leakage rate was estimated to be around 5% per year. However, some manufacturers even claim the annual leakage rate to be up to 20% per year for smaller units and some static refrigeration units recorded to have 25% annual leakage rates.

Figure 3.14 presents the GHG emission of working fluid R404A for different refrigerant leakage rates.

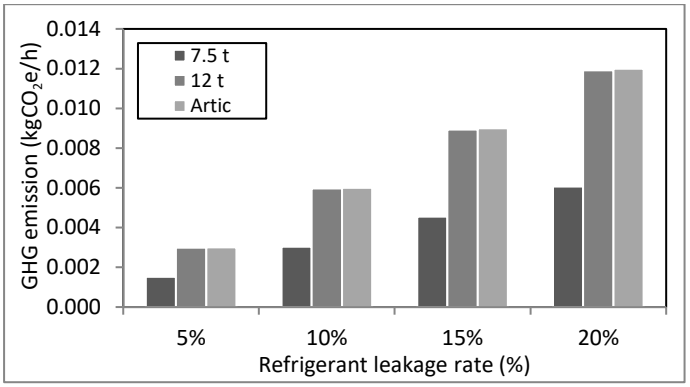

Figure 3.14: GHG emission from refrigerant leakage for different leakage rates ($kgCO_2e/h$).

For all vehicle categories, 7.5 t accounts for least refrigerant related GHG emissions. The GHG emissions for vehicle category 12 t and artic is same which is mainly due to the same refrigerant charge values for both the vehicle categories.

As expected, higher refrigerant leakage rate is responsible for more GHG emissions. Though the direct GHG emissions from refrigerant are much less in comparison to the indirect GHG emission from fuel combustion, it is still significant and need to be addressed.

3.5 Model validation- Investigation work at Kuenhne and Nagel (K&N) distribution centre

In order to validate and improve the model, an internal investigation was conducted with logistics company, Kuenhne and Nagel International AG, at a distribution centre located in Feltham. The investigation work was conducted on an 18 tonne distribution truck. Several sensors were positioned inside the truck to record data in regards to temperature variations. The fuel consumption data was manually collected by the driver and route operation data recorded using a microlise tracking system inside the truck. The distribution data and parameters were then used in the model to estimate the average fuel consumption. These model estimated results were then compared with the fuel consumption provided by the depot to assess the accuracy of the model.

The model takes into account several parameters collected during the investigation, which includes;

- The internal and external dimension of the body.
- The layout and properties of insulation (material type, thermal conductivity, density, specific heat capacity, thickness etc.).
- The ambient temperature and the temperature settings (refrigeration type) inside cargo space.
- The infiltration rate based on the specific heat of air and approximate air density.
- Hours of operation (for each delivery) per day.
- The duration and frequency of door openings.
- Cooling capacity of the refrigeration units and fuel consumption rate of the auxiliary engine.

3.5.1 Overview of the investigation (20/05/2017-22/05/2017)

The test recordings were performed between 20/05/2017 to 22/05/2017 on a traditional 18 tonne rigid truck (8.68 m × 2.6 m × 2.35 m) (l × w × h). The refrigeration unit is run using diesel auxiliary engine in this truck.

Figure 3.15: External and internal view of the refrigerated vehicle.

3.5.2 Measurement equipment and sensors

3.5.2.1 Temperature measurement

Thirteen HOBO pendant digital temperature loggers with data recording time interval of 30 s were installed at different positions inside the refrigerated chamber, as illustrated in Figure 3.16, to measure the temperature at different locations of the refrigerated chamber.

Figure 3.16: External and internal view of the refrigerated vehicle.

3.5.2.2 Door opening duration measurement

A HOBO UX90-001M State/Pulse/Event/Runtime Data Logger (512K), as illustrated in Figure 3.17, was installed in the vehicle to record the frequency and duration of door openings with recording time interval of 30 s. There are two parts of the sensor, the receiver and the magnetic strip. The receiver was attached at the edge (stable) of door and the magnetic strip on the edge of roll-up door, such that when the door was closed the parts came in contact.

Figure 3.17: HOBO UX90-001M state/pulse/event/runtime data logger

However, due to vibrations around the door, the door sensor failed to record reliable measurements. The frequency and number of door openings for this case were hence determined using variations in internal temperature.

3.5.2.3 Microlise fleet tracking system

A microlise system, as illustrated in Figure 3.18, was used for tracking each delivery. However, since the system required manual entries and was not updated by the depot to latest version, the loading and unloading time were found to be unreliable and this may have introduced errors in the measurements. Fuel consumption records were obtained from driver's manual entries.

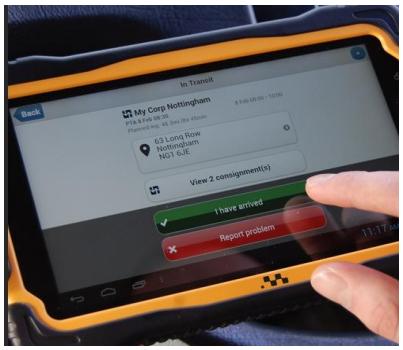

Figure 3.18: Microlise data logger.

3.5.2.4 Distribution data

The distribution data (distance, hours of operation, and number of drops) were recorded using a microlise data recorder. However, the arrival and departure times were manually recorded by the driver.

3.5.3 Recorded data and parameters

3.5.3.1 Sensors installation plan

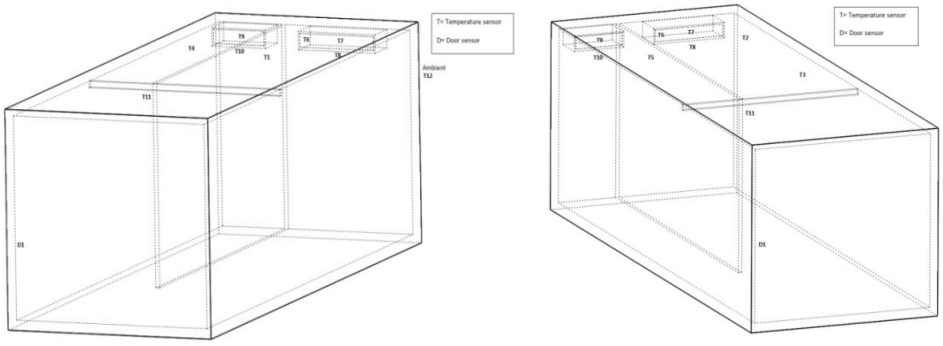

Figure 3.19: Installation of sensors from different views.

3.5.3.2 Microlise recorded data

Table 3.4 presents the delivery data recorded by the microlise system.

Table 3.4: Microlise recorded data for each delivery round to and from depot.

Delivery start date	Delivery end date	Delivery start time	Delivery end time	Duration (h)	km variance
20/05/2017	20/05/2017	07:12:00	11:14:00	04:02:00	267
20/05/2017	21/05/2017	17:03:00	00:56:00	07:53:00	160
21/05/2017	21/05/2017	16:37:00	21:54:00	05:16:00	61
22/05/2017	22/05/2017	06:50:00	10:44:00	03:54:00	303
22/05/2017	22/05/2017	16:01:00	19:40:00	03:39:00	157

3.5.3.3 Sensor recorded data

Table 3.5 presents the mean temperature values recorded by the sensors.

Table 3.5: Mean ambient temperature and mean temperature of each compartment for each delivery.

	20/05 (1st)	20/05 (2nd)	21/05	22/05 (1st)	22/05 (2nd)
Mean ambient temperature (°C)	17.64	13.11	21.29	17.74	25.16
Mean internal temperature (Room 1) (°C)	2.14	10.68	8.71	1.93	9.82
Mean internal temperature (Room 2) (°C)	3.67	9.14	5.78	5.47	8.98
Mean outlet temperature (Unit 1) (°C)	-12.45	6.12	2.31	-20.97	-3.06
Mean outlet temperature (Unit 2) (°C)	3.10	3.32	-2.46	2.97	4.09
Mean temperature of wall with exterior facing (Room 1) (°C)	5.03	11.34	10.02	7.94	12.66
Mean temperature of wall with exterior facing (Room 2) (°C)	2.85	8.32	4.86	4.24	7.70

Mean temperature of wall of central barrier (Room11) (°C)	-3.30	9.48	7.84	-9.71	4.74
Mean temperature of wall of central barrier (Room 2) (°C)	3.50	7.86	4.20	4.61	7.16
Mean ceiling temperature (°C)	4.67	11.23	8.27	7.55	12.07

3.5.3.4 Door opening

As mentioned, due to the unstable door in vehicle 1, no data could be recorded by the door sensor. For this reason, the duration of door opening was analysed using the internal temperature. These data were later compared with the drop off time recorded by the driver. When the cold space inside the trailer encounters infiltration, there is an increase in the mean internal air temperature. Depending on how long the door is open for, the mean internal temperature continues to increase until it reaches the ambient point (infiltration temperature equivalent to ambient). However, the temperature sensors can encounter a slight delay with data recordings, the door openings time may range slightly different to the estimated values (±2 minutes). The figures provided in Table 3.6 for first validation trial were hence rough estimates and not the actual recordings.

Table 3.6: Door opening duration for each distribution.

Delivery date	Total door opening time (h)	Number of door openings
20/05/2017	00:57:00	9
20/05/2017	01:12:00	5
21/05/2017	01:42:00	17
22/05/2017	00:58:00	8
22/05/2017	00:45:00	8

3.6 Comparison of model-based and manual recorded data

Figure 3.20 presents the comparison between the model-based fuel consumption using the data parameters from the investigation and the manual fuel consumption.

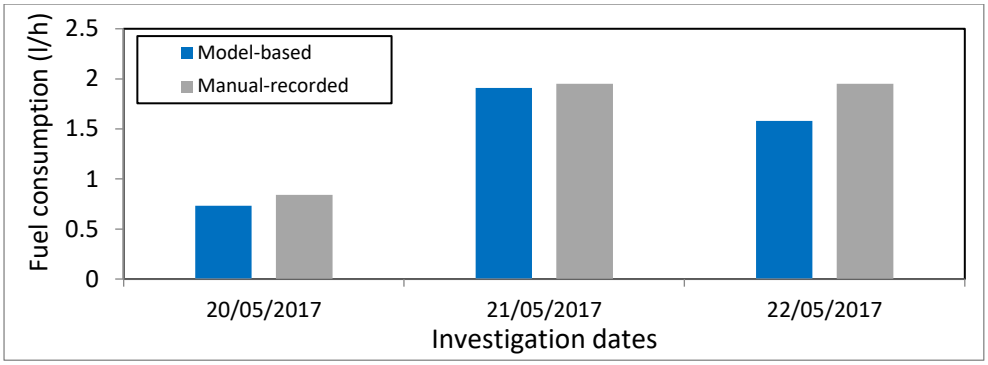

Figure 3.20: Model based fuel consumption vs. fuel consumption from recorded data (l/h).

If we observe Figure 3.20, we can see that the difference between the fuel consumption of model-based estimates and manual recordings are within the range of 2% and 18%.

The parameters for door opening duration used in the model were based on temperature readings rather than the actual door opening sensor (the door sensor failed to record any data due to constant vibration at the door), hence the readings could either be over or under estimated. And since infiltration accounts for the largest share of thermal load, it can greatly affect the overall outcome. The fuel consumption rates of the recorded data were estimated using the refill amount and the hours of operations for the number of deliveries.

Theoretical work can only provide rough estimations. For more robust estimations, more investigations would need to be carried out. However, in order to obtain rough estimates of fuel consumption based on refrigeration load, this model would be sufficient for the purpose.

3.7 Summary

This chapter discussed the theoretical model developed to estimate the refrigeration load and fuel consumption based on normal distribution schedule for different vehicle categories. It was estimated that infiltration during door openings accounted for the highest share of thermal load, more than 50% in cases of frequent delivery drops and longer door opening duration. The fuel consumption varied between 1.5 l/h to 4.71 l/h while the indirect GHG emissions from fuel consumption varied between 2.68 $kgCO_2e/h$ and 9.64 $kgCO_2e/h$ for different vehicle categories for chilled and frozen distribution. The direct GHG emission for refrigerant leakage varied between 0.002

$kgCO_2e/h$ and 0.012 $kgCO_2e/h$. These results are based on the average distributions parameters collected in collaboration with LoCity with Transport for London (TfL). The door opening frequency and distribution period for the collected data were analysed to be higher than the ones collected from the investigation conducted with Kuehne + Nagel International AG (K&N). However, considering the collected data is average parameter, and not every distribution centre operates in similar manner, the difference was found to be within limitation. The model was validated using the investigation data. The deviation between the investigation-based data and model-based results are within reasonable range.

CHAPTER 4

Environmental impact of vapour compression TRU powered using auxiliary engine and cryogenic based TR technologies

Chapter 3 assessed the energy demand and environmental impacts of diesel powered auxTRU engine. Use of diesel to power the 'inadequately-regulated' auxiliary engines can result in significant level of GHG emissions. Currently, there are several alternative transport refrigeration (TR) technologies which can eliminate the use of diesel and even refrigerants. However, many of the claims are based on the energy usage and environmental impacts during operation and do not include production emissions of the working fluids. Chapter 4 investigates the energy consumption and environmental impacts of two cryogenic transport alternatives to vapour compression system, LCO_2 and LN_2 working fluids. In the study, emissions from both production and operation of the cryogenic fluids are considered.

4.1 Properties of stored cryogen

The storage pressure is a function of the thermo-physical properties of the cryogen. LCO_2 is stored at 8.6 bar while LN_2 is stored at 3 bar [60]. The fluids in storage tanks at filling stations are at much higher pressure and lower temperature, LN_2 at 18 bar and -196°C and LCO_2 at around 22 bar and -57°C [78, 79].

Figure 4.1 illustrates the direct and indirect cryogenic transport refrigeration system.

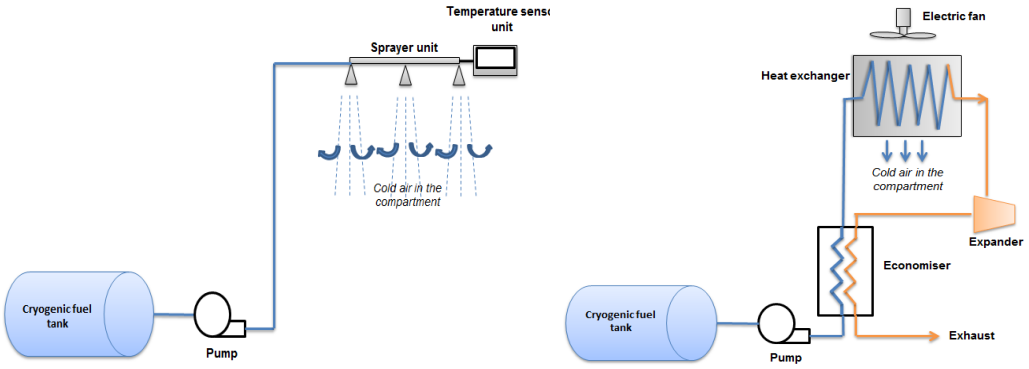

(a) (b)

Figure 4.1: Cryogenic transport refrigeration system (a) direct and (b) indirect.

4.2 Modelling methodology

The analysis in this chapter was carried out using a spreadsheet model developed to determine the energy consumption and GHG emissions of both vapour compression and cryogenic food transport refrigeration systems (please refer to Chapter 3 for details of the model). The energy consumption was estimated as fuel intensity or mass of cryogen required per kg of food item per km of the distance travelled. The GHG emissions were calculated as the mass of CO_2e per functional unit of the product. Only the fuel/ mass intensity required to run the refrigeration system was taken into account and not the fuel consumption from the vehicle's main engine.

The model performs three main calculations:

1. Refrigeration load encountered by the refrigerated vehicle throughout the year for a given distribution schedule.
2. Energy intensity in the form of fuel consumption or quantity of cryogenic fluid used for food distribution.
3. Environmental impact of the fuel/ cryogenic fluid.

4.2.1 Food distribution parameters

The following temperature controlled food distribution parameters and assumptions were considered for the investigation:

- Three different TR systems, (i) diesel powered vapour compression TR system with R452A refrigerant, (ii) LCO_2 cryogenic TR system, and (iii) LN_2 cryogenic TR system.

- Two most commonly used vehicle sizes, an 18 tonne medium rigid vehicle and a 38 tonne articulated vehicle.
- A refrigerant leakage rate of 10% per year for the vapour compression system [80].
- A stamped Euro pallet with dimension of 1.2 m × 0.8 m for arrangement of food products in the chamber. Products are normally stacked to a height of 1.6 m on the pallet.
- A capacity of 6 pallets for the medium rigid vehicle and 17 pallets for the articulated vehicle.
- A selected range of food products, as listed in Table 4.1. All food products were assumed to have been pre-chilled or frozen at the required temperature before loaded on the vehicle.

Table 4.1: Selected range of refrigerated food products.

Food Product	Euro pallet equivalence	Total weight in Euro pallet (kg)
Milk in roll container	726 litres	750
Cheese in cardboard box	36 boxes	1037
Ready meals	1500 packs	750
Fresh meat	500 packs	500
Frozen chips in cardboard box	64 boxes	640
Frozen peas in cardboard boxes	72 boxes	576

- A delivery journey of 10 hours with door opening taking place every other hour.
- For each round trip, the trailer was assumed to be fully loaded and the refrigeration system switched on for the delivery journey. On the return journey, the vehicle was assumed to be empty and the refrigeration system switched off, hence, the return journey does not account for any fuel/mass intensity for refrigeration.
- The driving distance was estimated using the combined drive cycle specified by Common Artemis Driving Cycles (CADC) for HGVs heavier than 12 tonnes.

- Annual ambient temperature of London (please refer Chapter 3, Figure 3.4).

4.2.2 Energy consumption and environmental impact

4.2.2.1 AuxTRU

The method specified in Chapter 3 is used to estimate the energy consumption for the vehicle category for each distribution, which is based on the cooling capacity of the TRU. The fuel consumption per kg of food can be determined using,

$$F_{diesel} = \frac{F}{D \times V_{pallet} \times M_{pallet}} \quad 4.1$$

Where:

F= total fuel consumption for the distribution (l)

D = total distance (km)

V_{pallet} = number of pallets in the chamber

M_{pallet} = total mass of the food products in a pallet (kg)

Using the most recent GHG emission conversion factor for UK, an emission factor of 2.676 kgCO_2e per litre for diesel and 0.462 kgCO_2e per kWh for electricity were used in the model [74]. The production related emission factor was estimated to be around 0.926 kgCO_2e per litre of diesel [81]. The production related GHG emissions of diesel fuel per unit mass of food product per km of delivery can be estimated using;

$$GD_{production} = F_{diesel} \times EFP_{diesel} \quad 4.2$$

Where:

F_{diesel}= fuel consumption (l/km-kg)

EFP_{diesel} = production related emission factor of diesel (kgCO_2e/l)

In the absence of data specifically for the production related emissions of R452A, it was assumed that the production of R452A will have similar emissions to other HFCs. Data for R404A, R410A and R407F published by Casini et al. [32] confirm this to be the case with very little differences between the three refrigerants. Based on this

assumption, the production emission of R452A was estimated to be 0.214 $kgCO_2e$ per kg of refrigerant. The production related GHG emissions of refrigerants can be estimated using;

$$GR_{production} = Amount\ of\ leakage \times EFP_{refrigerant} \quad 4.3$$

Where:

$EFP_{refrigerant}$= production related emission factor of refrigerant ($kgCO_2e/kg$)

The overall GHG emission per kg of food product per km during the operation was determined using;

$$GD_{operation} = Indirect\ emissions + Direct\ emissions \quad 4.4$$

4.2.2.2 Cryogenic TR systems

The thermophysical properties of the two fluids at tank's storage pressure, as presented in Table 4.2, were initially determined using the REFPROP software [82].

Table 4.2: Thermophysical properties of selected fluids.

Properties	LCO_2	LN_2
Vehicle's tank pressure (bar)	8.6	3
Boiling point (°C)	-44.074	-185.24
Latent heat of vapourisation (kJ/kg)	329.65	183.96
Specific heat capacity at constant pressure (kJ/kg·K)	0.9954	0.8841
Liquid density (kg/m^3)	1132.2	755.7

Liquid cryogen when expanded to atmospheric pressure becomes gaseous. The overall mass (m_c) required to overcome the thermal load was determined using the energy transformation equation below;

$$Q_c = m_c(L_v + C_p(T_s - T_v)) \quad 4.5$$

Where:

m_c = mass of cryogenic fluid (kg)

L_v= latent heat of vaporisation (kJ/kg)

C_p= specific heat capacity (kJ/kg-K)

T_s= desired temperature of the chamber (K)

T_v= temperature of vapourisation (K)

Tajima et al. [34] estimated the energy required during separation of CO_2 using clathrate hydrate formation to be 0.853 kWh/kg. ASCO, a CO_2 manufacturer, provided energy consumption values for separation of CO_2 as a function of the plant's capacity: 0.414 kWh/kg for capacity of 70 kg/hr, 0.325 kWh/kg for 160 kg/hr, 0.295 kWh/kg for 285 kg/hr, 0.266 kWh/kg for 500 kg/hr and 0.241 kWh/kg for 1000 kg/hr [83]. Data from Latif et al. [84] and emission factor of 0.462 $kgCO_2e$ per kWh of electricity results in an emission factor of 0.305 $kgCO_2e$ per kg of LCO_2 for the production of LCO_2, which falls between the values given by [85] and [83]. The value of 0.305 was selected for the calculation here.

The European Industrial Gases Association (EIGA) specifies a benchmark for the production of LN_2 to be 0.549 kWh per kg of LN_2, which, assuming an emission factor of electricity as 0.462 $kgCO_2e$/kWh results in an emission factor of 0.254 $kgCO_2e$ per kg of LN_2 [86]. The collected data were used in the model to calculate the GHG emissions of the fluids during the production stage. Provided that both LCO_2 and LN_2 were recovered and then released to the atmosphere after use, their operation related emissions can be neglected. The production related GHG emission of LCO_2 and LN_2 can be estimated using,

$$GLCO_{2_{production}} = F_{fluid}\ of\ LCO_2 \times EFP_{LCO2} \quad 4.6$$

$$GLN_{2_{production}} = F_{fluid}\ of\ LN_2 \times EFP_{LN2} \quad 4.7$$

Where:

EFP_{LCO2} = production related emission factor of LCO_2 ($kgCO_2e$/kg of LCO_2)

EFP_{LN2}= production related emission factor of LN_2 ($kgCO_2e$/kg of LN_2)

4.3 Results

4.3.1 Refrigeration load

Using the same equations and method provided in Chapter 3, the refrigeration load was estimated using the average ambient temperature of each month. Figure 4.2 illustrates the hourly refrigeration load for chilled and frozen distribution for the two vehicle categories.

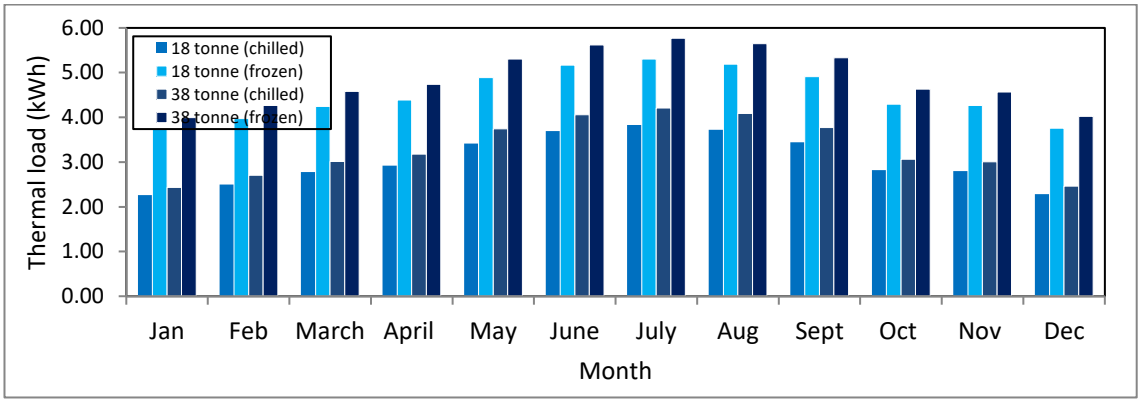

Figure 4.2: Hourly thermal load for chilled and frozen distribution (kWh).

As can be seen in Figure 4.2, that during the warmer months of the year the refrigeration load is higher than that for the colder months. The refrigeration load is at its peak between June and August due to higher ambient temperatures during these months.

As expected, the 38 tonne vehicle has higher thermal load than the 18 tonne vehicle due to 38 tonne having larger volume and surface area. Since the refrigeration load is based on the temperature difference between the ambient and the air in the refrigerated space, frozen distribution accounts for higher thermal load than chilled.

4.3.2 Energy consumption of auxTRU and cryogenic TR systems

Table 4.3 presents the hourly fuel and cryogenic fluid consumption during a chilled and frozen food product distribution journey in the London area for the two vehicle categories. The energy density comparison is provided in Appendix A.

Table 4.3: Total amount of diesel, LCO_2 and LN_2 for the same distribution journey

	Fuel consumption	Fuel consumption	LCO_2 mass consumption	LCO_2 mass consumption	LN_2 mass consumption	LN_2 mass consumption

	of 18 t vehicle (l/h)		of 38 t vehicle (l/h)		of 18 t vehicle (kg/h)		of 38 t vehicle (kg/h)		of 18 t vehicle (kg/h)		of 38 t vehicle (kg/h)	
Month	Chilled	Frozen	Chilled	Frozen	Chilled	Frozen	Chilled	Frozen	Chilled	Frozen	Chilled	Frozen
Jan	1.19	1.96	1.28	2.10	21.81	37.80	23.45	40.45	23.43	40.51	25.19	43.35
Feb	1.31	2.09	1.42	2.24	24.10	40.21	26.05	43.19	25.89	43.09	27.98	46.29
March	1.46	2.23	1.58	2.41	26.75	43.00	29.06	46.35	28.75	46.08	31.22	49.67
April	1.53	2.31	1.67	2.49	28.14	44.45	30.62	47.99	30.22	47.63	32.89	51.44
May	1.79	2.57	1.97	2.79	32.92	49.46	36.05	53.69	35.36	53.02	38.73	57.55
June	1.94	2.71	2.13	2.95	35.60	52.29	39.09	56.88	38.24	56.05	41.99	60.96
July	2.01	2.78	2.21	3.03	36.91	53.66	40.57	58.44	39.65	57.51	43.58	62.63
Aug	1.95	2.73	2.15	2.97	35.85	52.55	39.37	57.18	38.51	56.32	42.30	61.28
Sept	1.81	2.58	1.98	2.80	33.16	49.73	36.33	53.97	35.63	53.29	39.02	57.85
Oct	1.48	2.25	1.61	2.43	27.19	43.45	29.55	46.86	29.20	46.56	31.75	50.22
Nov	1.47	2.24	1.58	2.40	26.95	43.20	28.98	46.26	28.95	46.30	31.14	49.58
Dec	1.20	1.97	1.29	2.11	22.03	38.03	23.73	40.75	23.66	40.75	25.49	43.66

As can be seen in Table 4.3, the fuel consumption of the 18 t vehicle varies between 1.2 l/h and 2.0 l/h for chilled and between 2.0 l/h and 2.8 l/h for frozen distribution respectively. For the 38 t vehicle, the fuel consumption varies between 1.3 l/h and 2.2 l/h for chilled and between 2.1 l/h and 3.0 l/h for frozen distribution respectively.

The mass consumption of LCO_2 for the 18 t vehicle varies between 21.8 kg/h and 36.9 kg/h for chilled and between 37.08 kg/h and 53.7 kg/h for frozen distribution. For the 38 t vehicle the mass consumption of LCO_2 varies between 23.5 kg/h and 40.6 kg/h for chilled and between 40.5 kg/h and 58.44 kg/h for frozen distribution.

The mass consumption of LN_2 for the 18 t vehicle varies between 23.4 kg/h and 39.7 kg/h for chilled and between 40.5 kg/h and 57.5 kg/h for frozen distribution. For the 38 t vehicle, the mass consumption varies between 25.2 kg/h and 43.6 kg/h for chilled and between 43.4 kg/h and 62.6 kg/h for frozen operation.

The mass consumption of the cryogenic fluids is higher than the mass consumption of diesel mainly due to the differences in energy density.

4.3.3 Environmental impacts

Using the fuel and mass consumption of the journey, the environmental impacts of each food product per unit mass of food per km of distance travelled were determined. Both production and operation related environmental impacts were estimated separately and then combined to estimate the overall impact.

4.3.3.1 Production related GHG emissions for distribution of different food items

Figure 4.3 to 4.8 present the production related GHG emissions during distribution of the different food products.

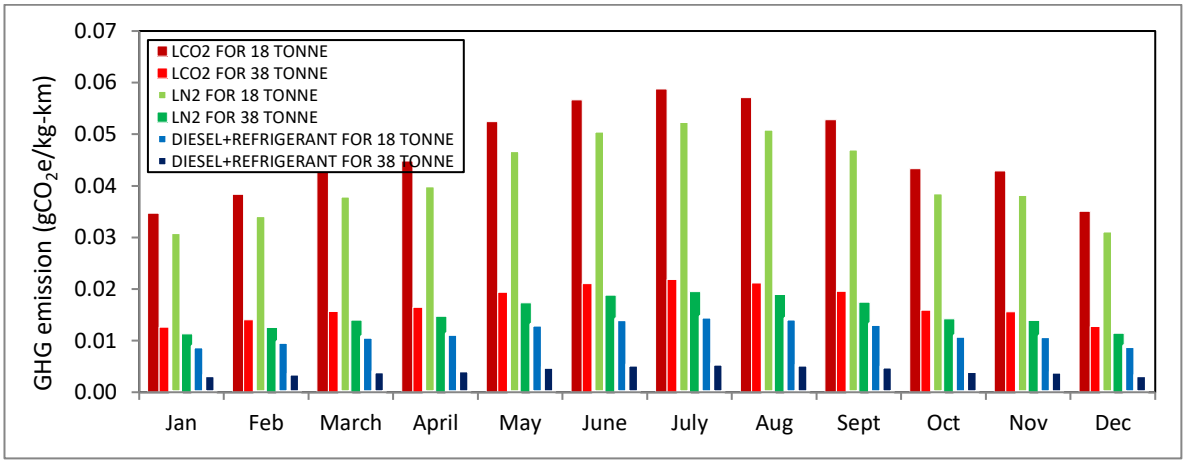

Figure 4.3: Production related GHG emissions during distribution of milk.

Figure 4.3 presents the production related GHG emissions during distribution of milk using an 18 tonne and a 38 tonne truck for three different transport refrigeration units. As can be seen, the production related emissions of the LCO_2 and LN_2 is much higher than that of combined diesel and refrigerant mainly due to the production of cryogen being an energy-intensive process and requirement of more cryogen (mass in kg) to provide same level of cooling.

It can be observed that the GHG emission of the emission of 38 tonne per kg of product is less 18 tonne vehicle category. This is mainly due to 38 tonne vehicle category providing more space capacity than an 18 tonne vehicle. In similar manner, Figure 4.4- 4.8 presents the GHG emissions during distribution of different food products.

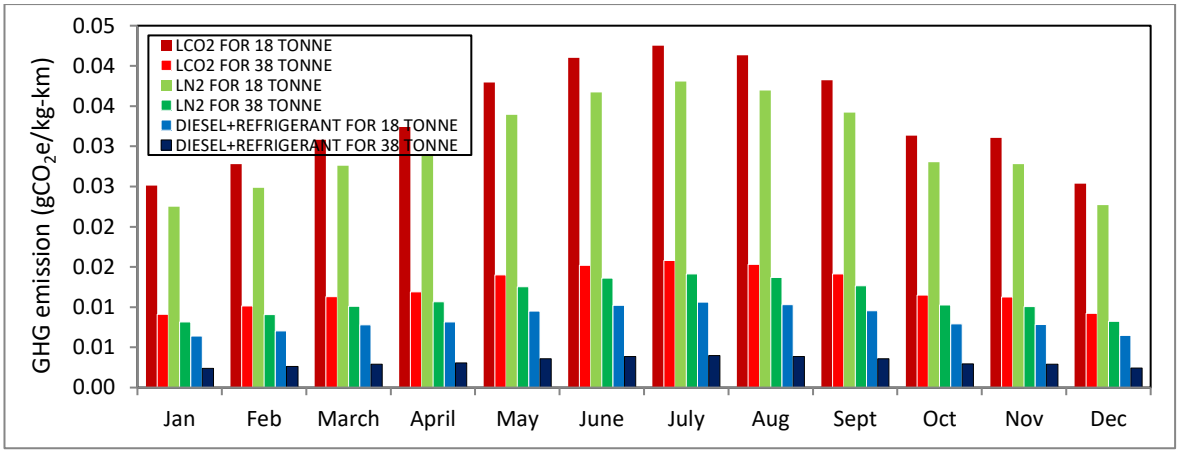

Figure 4.4: Production related GHG emissions during distribution of cheese.

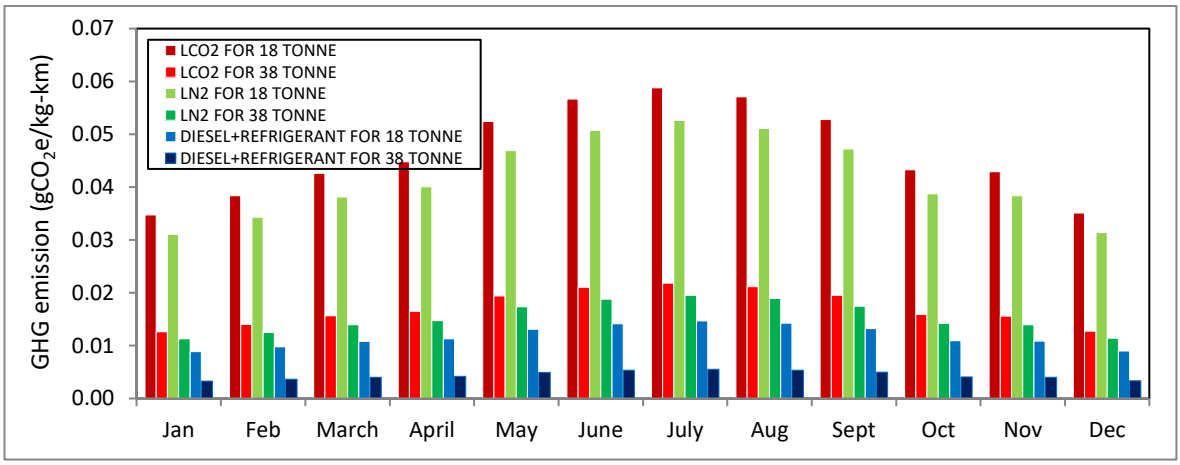

Figure 4.5: Production related GHG emissions during distribution of ready meals.

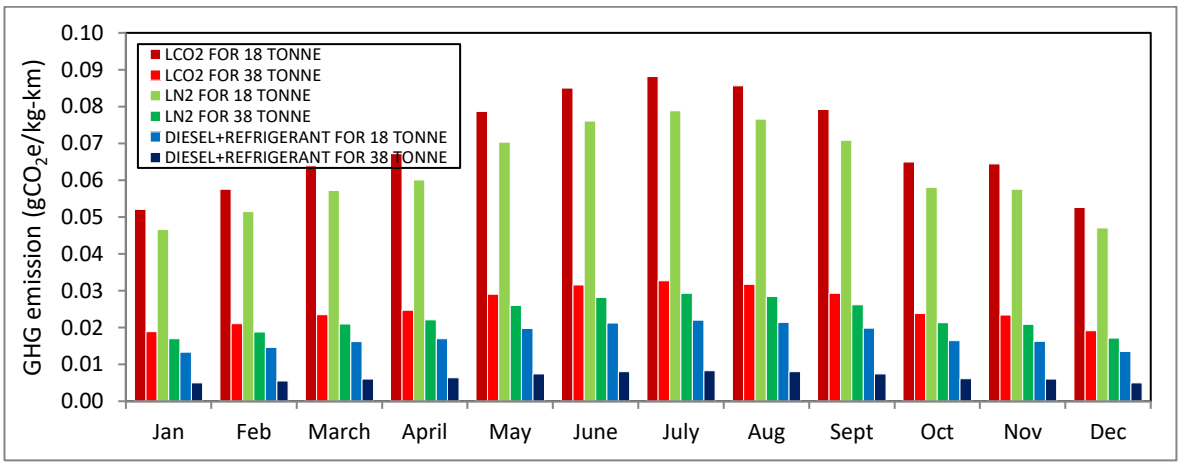

Figure 4.6: Production related GHG emissions during distribution of fresh meat.

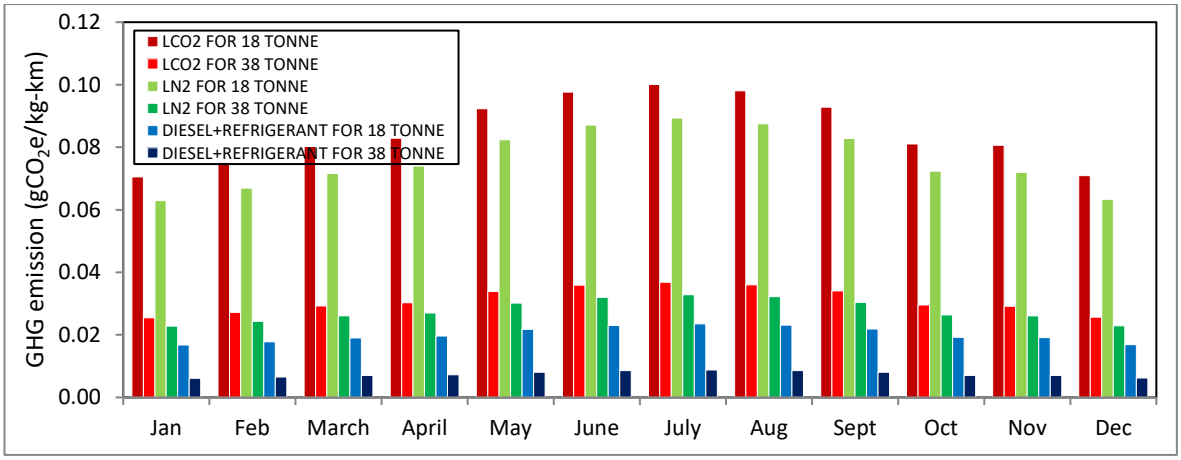

Figure 4.7: Production related GHG emissions during distribution of frozen chips.

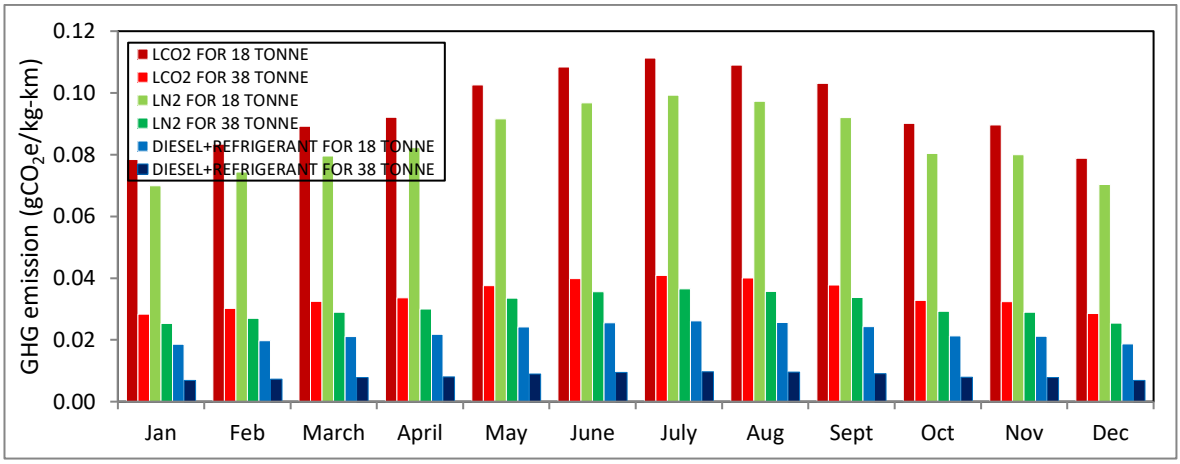

Figure 4.8: Production related GHG emissions during distribution of frozen peas.

The production related emission of diesel and refrigerant combined is almost 66% lower than the production related emissions of the cryogenic fluids.

The higher production related emission of cryogens is mainly due to higher energy needed for their manufacture. Additionally, as can be seen in the figures, the quantity of LCO_2 and LN_2 needed to provide the same level of refrigeration is much higher compared to the quantity of diesel.

The frozen food products are responsible for slightly higher environmental impacts in comparison to the chilled products due to the lower temperature required during distribution. Another contribution factor in the volume of space required in the refrigerated vehicle per unit mass for the transportation of different products.

4.3.3.2 Production and operation related GHG emissions for distribution of different food items

Table 4.4 to 4.5 presents the production and operation related GHG emission during distribution of different food items using an 18 tonne and 38 tonne vehicle. The GHG emissions varies for each month due to the variance in thermal load encountered for each month.

Table 4.4: Total GHG emissions (production and operation) for food distribution with different refrigeration technologies using 18 tonne vehicle.

Food products	Fluid type	Total GHG emissions (gCO_2e/kg-km) for 18 tonne vehicle (production and operation)											
		Jan	Feb	March	April	May	June	July	Aug	Sept	Oct	Nov	Dec
Milk	LCO_2	0.03	0.04	0.04	0.04	0.05	0.06	0.06	0.06	0.05	0.04	0.04	0.04
	LN_2	0.03	0.03	0.04	0.04	0.05	0.05	0.05	0.05	0.05	0.04	0.04	0.03
	Diesel+ Ref	0.03	0.04	0.04	0.04	0.05	0.06	0.06	0.06	0.05	0.04	0.04	0.04
Cheese	LCO_2	0.03	0.03	0.03	0.03	0.04	0.04	0.04	0.04	0.04	0.03	0.03	0.03
	LN_2	0.02	0.02	0.03	0.03	0.03	0.04	0.04	0.04	0.03	0.03	0.03	0.02
	Diesel+ Ref	0.03	0.03	0.03	0.03	0.04	0.04	0.04	0.04	0.04	0.03	0.03	0.03
Ready meals	LCO_2	0.03	0.04	0.04	0.04	0.05	0.06	0.06	0.06	0.05	0.04	0.04	0.04
	LN_2	0.03	0.03	0.04	0.04	0.05	0.05	0.05	0.05	0.05	0.04	0.04	0.03
	Diesel+ Ref	0.03	0.04	0.04	0.04	0.05	0.06	0.06	0.06	0.05	0.04	0.04	0.04
Fresh meat	LCO_2	0.05	0.06	0.06	0.07	0.08	0.09	0.09	0.09	0.08	0.06	0.06	0.06
	LN_2	0.05	0.05	0.06	0.06	0.07	0.08	0.08	0.08	0.07	0.06	0.06	0.05
	Diesel+ Ref	0.05	0.06	0.06	0.07	0.08	0.08	0.09	0.08	0.08	0.06	0.06	0.05

Frozen chips	LCO_2	0.07	0.08	0.08	0.08	0.09	0.10	0.10	0.10	0.09	0.08	0.08	0.07
	LN_2	0.06	0.07	0.07	0.07	0.08	0.09	0.09	0.09	0.08	0.07	0.07	0.06
	Diesel+ Ref	0.07	0.07	0.07	0.08	0.08	0.09	0.10	0.09	0.09	0.07	0.07	0.07
Frozen peas	LCO_2	0.08	0.08	0.09	0.09	0.10	0.11	0.11	0.11	0.10	0.09	0.09	0.08
	LN_2	0.07	0.07	0.08	0.08	0.09	0.10	0.10	0.10	0.10	0.09	0.07	0.07
	Diesel+ Ref	0.07	0.08	0.08	0.09	0.09	0.10	0.10	0.10	0.09	0.08	0.08	0.07

Table 4.5: Total GHG emissions (production and operation) for food distribution with different refrigeration technologies using 38 tonne vehicle.

Food products	Fluid type	Total GHG emissions (gCO_2e/kg-km) for 38 tonne vehicle (production and operation)											
		Jan	Feb	March	April	May	June	July	Aug	Sept	Oct	Nov	Dec
Milk	LCO_2	0.01	0.01	0.02	0.02	0.02	0.02	0.02	0.02	0.02	0.02	0.02	0.01
	LN_2	0.01	0.01	0.01	0.01	0.02	0.02	0.02	0.02	0.02	0.01	0.01	0.01
	Diesel+ Ref	0.01	0.01	0.02	0.02	0.02	0.02	0.02	0.02	0.02	0.02	0.02	0.01
Cheese	LCO_2	0.01	0.01	0.01	0.01	0.01	0.02	0.02	0.02	0.01	0.01	0.01	0.01
	LN_2	0.01	0.01	0.01	0.01	0.01	0.01	0.01	0.01	0.01	0.01	0.01	0.01
	Diesel+ Ref	0.01	0.01	0.01	0.01	0.01	0.02	0.02	0.02	0.01	0.01	0.01	0.01
Ready meals	LCO_2	0.01	0.01	0.02	0.02	0.02	0.02	0.02	0.02	0.02	0.02	0.02	0.01
	LN_2	0.01	0.01	0.01	0.01	0.02	0.02	0.02	0.02	0.02	0.01	0.01	0.01

	Diesel+ Ref	0.01	0.01	0.02	0.02	0.02	0.02	0.02	0.02	0.02	0.02	0.02	0.01
Fresh meat	LCO_2	0.02	0.02	0.02	0.02	0.03	0.03	0.03	0.03	0.03	0.02	0.02	0.02
	LN_2	0.02	0.02	0.02	0.02	0.03	0.03	0.03	0.03	0.03	0.02	0.02	0.02
	Diesel+ Ref	0.02	0.02	0.02	0.02	0.03	0.03	0.03	0.03	0.03	0.02	0.02	0.02
Frozen chips	LCO_2	0.03	0.03	0.03	0.03	0.03	0.04	0.04	0.04	0.03	0.03	0.03	0.03
	LN_2	0.02	0.02	0.03	0.03	0.03	0.03	0.03	0.03	0.03	0.03	0.03	0.02
	Diesel+ Ref	0.02	0.03	0.03	0.03	0.03	0.03	0.03	0.03	0.03	0.03	0.03	0.02
Frozen peas	LCO_2	0.03	0.03	0.03	0.03	0.04	0.04	0.04	0.04	0.04	0.03	0.03	0.03
	LN_2	0.03	0.03	0.03	0.03	0.03	0.04	0.04	0.04	0.03	0.03	0.03	0.03
	Diesel+ Ref	0.03	0.03	0.03	0.03	0.04	0.04	0.04	0.04	0.04	0.03	0.03	0.03

As can be seen from Table 4.4 and Table 4.5, for the products investigated, the production and operation related GHG emissions for the 18 t vehicle vary between 0.03- 0.11 gCO_2e/kg-km, 0.03- 0.10 gCO_2e/kg-km and LCO_2, LN_2 and diesel and refrigerant combined respectively. For the 38 t vehicle, the GHG emissions vary between 0.01- 0.04 gCO_2e/kg-km, 0.01- 0.04 gCO_2e/kg-km and 0.01- 0.04 gCO_2e/kg-km for LCO_2, LN_2 and diesel and refrigerant combined.

As can be seen, the 38 t vehicle has lower GHG emissions compared to the 18 t vehicle per unit mass of product, due to its higher carry load capacity and lower specific energy consumption. It should be noted, however, that the estimates are based on a fully loaded truck. The results can vary depending on the product loading patterns.

During the operation phase, the vapour compression TRU is responsible for emissions due to diesel fuel combustion and refrigerant leakage. For the cryogens, the emissions from the operation of the systems will be almost negligible as discussed earlier. Hence, the GHG emissions of the cryogens are primarily due to the energy consumed at the production phase.

Compared to the vapour compression and LCO_2 technologies, the LN_2 technology exhibits slightly lower emissions for all products and ambient temperatures. The difference is more pronounced for the 18 tonne vehicle TRUs and chilled food distribution. Diesel emissions are slightly higher than the emissions from the cryogenic TRUs for frozen food distribution with the 18 tonne vehicle.

4.4 Economic considerations

The price of diesel in the UK is approximately £1.2 per litre, while the price of the cryogenic fluids is approximately £0.12 per kg of LCO_2 and £0.08 per kg of LN_2 [38, 39]. Using the fuel and mass consumption presented in Table 4.3 for different transport refrigeration technologies, it can be estimated that the running cost of the cryogenic TRUs will be very similar compared to the running costs of diesel driven TRUs.

In terms of capital cost, cryogenic systems at present have higher installed costs at around £22,000 compared to diesel driven TRUs which is estimated at £18,000-£21,000 for a rigid TRU [35]. Moreover, unlike the petroleum fuel infrastructure

already in place, additional investments would be required to achieve the same level of refilling facilities for cryogenic systems, further increasing infrastructure cost.

4.5 Summary

This chapter provided an overall assessment on the suitability of cryogenic transport refrigeration using LN_2 and LCO_2 in comparison to auxTRU powered by diesel, based on current production and operation related GHG emissions. It was estimated that the fuel intensity of diesel powered vapour compression TRUs (1.19 l/h to 3.03 l/h) is much lower than the mass intensity of the LCO_2 and LN_2 cryogenic TRUs (21.81 kg/h to 62.63 kg/h) for the distribution scenarios investigated enabling diesel driven systems to have much greater range of temperature controlled food distribution without tank refilling compared to cryogenic systems. The production emissions of the diesel fuel and refrigerant in auxTRUs are as much as 66% lower than the production emissions of cryogenic fluids as larger quantities of cryogens are required to overcome the same cooling demand compared to diesel in diesel driven vapour compression refrigeration systems.

When the total emissions (production and operation) are considered, the emissions from diesel driven vapour compression and cryogenic systems were found to be similar for the food products and distribution journeys considered. Even though the LN_2 system exhibited slightly lower emissions than the other two systems the differences are too small, and within the context of assumptions made, it is difficult to draw definitive conclusions. Emissions from TRUs in the distribution of temperature controlled food products with larger articulated vehicles are more than 50% lower than emissions from TRUs on smaller rigid vehicles due to the larger carrying capacity of articulated vehicles.

The running costs of cryogenic transport refrigeration systems were found to be at a par with those of conventional driven TRUs but the installed and infrastructure costs are higher reducing their economic attractiveness. This may change if future legislation places restrictions in the use of diesel driven TRUs due to particulate and NOx emissions from diesel engines.

CHAPTER 5

Comparison of Environmental impacts between diesel, all electric and hydrogen fuel cell powered Transport Refrigeration Units

Chapter 4 investigated and compared the environmental impact of transport refrigeration units (TRU) powered using auxiliary diesel engine and cryogenic LCO_2 and LN_2 based transport refrigeration technologies. As discussed in Chapter 2, along with cryogenic based systems there are other alternatives, which unlike the cryogenic systems, only eliminate the use of diesel. The cooling unit still remains the vapour compression system but powered using more sustainable energy source. These alternatives include TRUs powered with hydrogen (H_2) fuel cells and all-electric TRUs powered using battery. Chapter 5 focuses on the production and operation related environmental impacts of these two alternatives and provides a GHG emission comparison with diesel powered auxTRUs for the distribution of different refrigerated food items.

5.1 Overview of fuel cell and battery powered TRU

5.1.1 Fuel cell powered TRU using H_2

In this system, when cooling is required, H_2 is supplied to the fuel cell stack to generate electricity and drive the electric motor, which then drives the compressor of the refrigeration system. The design of this system is very similar to that of auxTRU powered using diesel, however with H_2 as the main energy carrier. The H_2 is stored in a tank (high-pressure vessel) in compressed form at a pressure of approximately 350 bars. The highly pressurised tank normally has capacity of 35 kg H_2. Figure 1 illustrates the system configuration of fuel cell powered TRU.

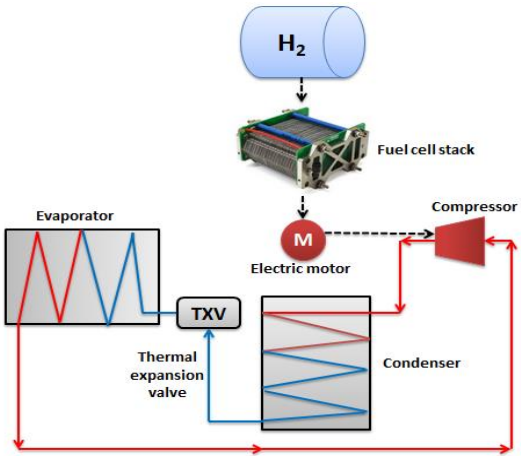

Figure 5.1: Hydrogen fuel cell powered TRU using H_2.

5.2 Battery powered TRU

Similar to auxTRU, this system employs a standard cooling unit driven using an electric motor which is powered electrically using a battery. The battery is charged using grid electricity when the vehicle is stationary at the depot. These advanced batteries are usually constructed using lithium ion (Li-ion). The energy capacity of this vehicle can vary anywhere between 80 kWh and 120 kWh for 7.5 -11 t and between 133 kWh and 290 kWh for 14 -18 t vehicle categories. Figure 5.2 illustrates the system configuration of all-electric TRU powered using a battery.

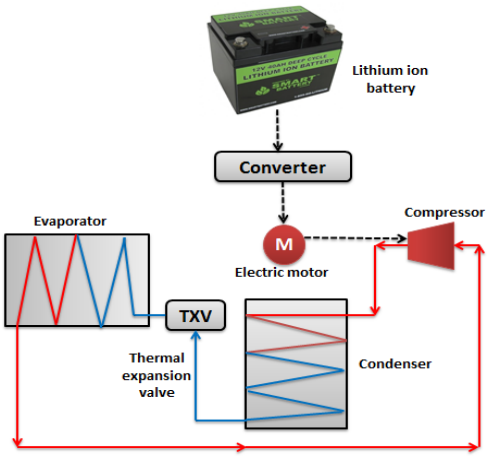

Figure 5.2: Battery powered TRU

5.3 Modelling methodology

The same spreadsheet model, distribution scenario and distribution parameters as presented in Chapter 4, are used for assessment in this chapter so the comparison of

these alternative technologies can be made on a similar basis. The model comprises three main calculations:

1. Average refrigeration load encountered during each month of the year (based on the ambient temperature of London throughout the year).
2. Energy/fuel consumption (in the form of kg for H_2 and kWh for Li-ion battery) during distribution per kg of food product per km of distance travelled.
3. Production and operation related environmental impact in CO_2e during distribution per kg food product per km of distance travelled.

5.3.1 Energy consumption per kg of food product per km of distance travelled

5.3.1.1 AuxTRU

The same method as presented in Chapter 4 is used to estimate the total amount of diesel for the distribution scenario using the estimated refrigeration load.

5.3.1.2 Fuel cell powered TRU

Using parameters from the literature, the fuel cell stacks have an estimated energy production of 15 kWh per kg of H_2 [57]. The electric motor has an efficiency of 92% while the refrigeration unit has an average a COP of 1. As discussed in Chapter 3, similar to diesel engines, almost a third of the energy is used to support other ancillaries leaving two-thirds to be used for cooling purposes. Using these assumptions on losses and energy distribution, the cooling capacity is estimated at 9.25 kWh per kg of H_2 [57].

The mass consumption of H_2 per kg of food product per km of distance travelled is estimated from.

$$M_{H_2} = \left(\frac{Q_{ref}}{C_{H_2} \times D \times V_{pallet} \times M_{pallet}} \right) \quad 5.1$$

Where

Q_{ref} = total hourly refrigeration load (kWh)

C_{H_2} = total cooling capacity per kg of H_2 (kWh /kg-H_2)

D = total distance (km)

V_{pallet} = number of pallets in the chamber

M_{pallet} = total mass of the food products in a pallet (kg)

5.3.1.3 Battery powered TRU

It is difficult to estimate the exact cooling capacity of a battery as the efficiency of batteries can vary. New advanced batteries have a charge/discharge efficiency of 90% [8]. The electric motor is again assumed to have an efficiency of 92%, refrigeration unit a COP of 1. If a third of the grid energy fed to the battery is assumed to be used to power the ancillaries, a cooling capacity of 0.50 kWh per kWh of grid electricity fed to the battery can assumed to be used by the system for cooling [57].

The energy consumption of the battery per kg of food product per km of distance travelled can be estimated using the following equation.

$$P_{battery} = \left(\frac{Q_{ref}}{C_{battery} \times D \times V_{pallet} \times M_{pallet}}\right) \quad 5.2$$

Where

Q_{ref}= total hourly refrigeration load (kWh)

$C_{battery}$= total cooling capacity per kWh of grid electricity fed in the battery (kWh /kWh of grid power)

D = total distance travelled (km)

V_{pallet} = number of pallets in the chamber

M_{pallet} = total mass of the food products in a pallet (kg)

5.3.2 Environmental impact per kg of food product per km

5.3.2.1 AuxTRU

Using the emission factor of 2.676 kgCO_2e per litre of diesel and 0.462 kgCO_2e per kWh for electricity, the production and operation related GHG emissions of diesel were estimated [74]. The production related emission factor was estimated to be around 0.926 kgCO_2e per litre of diesel [81]. The production related GHG emissions

of diesel fuel per unit mass of food product per km of delivery can be estimated using the equations provided in Chapter 4, Eq 4.1- 4.4.

5.3.2.2 Fuel cell powered TRU

Renewables are the most desired sources for hydrogen production. Renewable hydrogen can be produced using electrolysis, biomass conversion and solar energy conversion methods.

Both biomass and solar energy conversion processes have very limited production capacity based on current infrastructure hence, currently, electrolysis is the most favoured process. A 100% efficient electrolysers require as much as 48 kWh of electricity for the production of one kg of H_2 [87].

Using the emission factor in UK to be 0.283 kg CO_2e per kWh of electricity (please note that the emission factor fluctuates every year), the production related emission factor of hydrogen is estimated at 22.176 kgCO_2e per kg of H_2.

$$GHG_{H_2} = M_{H_2} \times EFP_{H_2} \quad 5.3$$

Where:

M_{H_2} = mass of hydrogen (kg)

EFP_{H_2} = production related emission factor of hydrogen (kgCO_2e/ kg-H_2)

5.3.2.3 Battery powered TRU

Most of the UK's electricity is produced by burning fossils fuels, mainly natural gas (42%) and coal (9%). 21% of the electricity comes from nuclear. However, renewables are currently on a massive increase, with sources such as wind, wave, marine, hydro, biomass and solar generating 24.5% of electricity in 2016. In 2017 alone, there was a 15% decrease in the UK electricity CO_2e.

Though Defra has provided emission factors for electric vehicles, the standard only provides emission factor of vehicles upto 3.5 t. Therefore, the emission factor for this particular category is solely based on grid electricity as majority of the all-electric trucks are mainly charged using the plug-in option.

Since the battery is a direct input of grid electricity, the production related emission is estimated to be 0.283 kg CO_2e per kWh of electricity input [88].

The production related emission of the power consumed by battery during distribution can be estimated using;

$$GHG_{battery} = P_{battery} \times EFP_{electricity} \quad 5.4$$

Where:

$P_{battery}$= power consumed by battery (kWh)

$EFP_{electricity}$= production related emission factor of electricity ($kgCO_2e/kWh$)

5.4 Results

For the given distribution parameters, the following results were estimated using the model.

5.4.1 Energy consumption of auxTRU and alternative TRUs

Table 5.1 presents the energy consumption of auxTRU, fuel cell powered TRU and battery powered TRU. The results are estimated on the basis of consumption level per hour.

Table 5.1: Energy usage of diesel auxTRU, fuel cell powered TRU and battery powered TRU

	Diesel 18 t (l/h)		Diesel 38 t (l/h)		H_2 18 t (kg/h)		H_2 38 t (kg/h)		Electric 18 t (kWh)		Electric 38 t (kWh)	
Month	Chilled	Frozen	Chilled	Frozen	Chilled	Frozen	Chilled	Frozen	Chilled	Frozen	Chilled	Frozen
Jan	1.19	1.96	1.28	2.10	0.24	0.40	0.26	0.43	4.52	7.45	4.86	7.98
Feb	1.31	2.09	1.42	2.24	0.27	0.43	0.29	0.46	4.99	7.93	5.39	8.52
March	1.46	2.23	1.58	2.41	0.30	0.46	0.33	0.49	5.54	8.48	6.02	9.14
April	1.53	2.31	1.67	2.49	0.32	0.47	0.34	0.51	5.83	8.76	6.34	9.46
May	1.79	2.57	1.97	2.79	0.37	0.53	0.40	0.57	6.82	9.75	7.47	10.59
June	1.94	2.71	2.13	2.95	0.40	0.56	0.44	0.61	7.37	10.31	8.10	11.22
July	2.01	2.78	2.21	3.03	0.41	0.57	0.46	0.62	7.64	10.58	8.40	11.52
Aug	1.95	2.73	2.15	2.97	0.40	0.56	0.44	0.61	7.43	10.36	8.15	11.27

Sept	1.81	2.58	1.98	2.80	0.37	0.53	0.41	0.58	6.87	9.80	7.52	10.64
Oct	1.48	2.25	1.61	2.43	0.30	0.46	0.33	0.50	5.63	8.57	6.12	9.24
Nov	1.47	2.24	1.58	2.40	0.30	0.46	0.33	0.49	5.58	8.52	6.00	9.12
Dec	1.20	1.97	1.29	2.11	0.25	0.41	0.27	0.44	4.56	7.50	4.91	8.03

As can be seen in the Table, for the 18 t vehicle category, the fuel consumption of auxTRU varied between 1.2 l/h and 2.0 l/h for chilled and between 2.0 l/h and 2.8 l/h for frozen distribution. The mass consumption of H_2 varies between 0.24 kg/h and 0.4 kg/h for chilled and 0.40 kg/h to 0.6 kg/h for frozen distribution. The energy consumption of the all-electric TRU varies between 4.5 kWh and 7.64 kWh for chilled and between 4.5 kWh to 10.6 kWh for frozen distribution.

For the 38 t vehicle category, the fuel consumption of auxTRU varies between 1.3 l/h and 2.2 l/h for chilled and between 2.1 l/h and 3.0 l/h for frozen distribution. For the fuel cell TRU, the mass consumption varies between 0.3 kg/h and 0.5 kg/h for chilled and between 0.4 kg/h and 0.6 kg/h for frozen distribution. For the all-electric TRUs, the energy consumption varies between 4.9 kWh to 8.4 kWh for chilled and between 8.0 kWh and 11.5 kWh for frozen food distribution.

It can be seen from the results that hydrogen has the highest energy density and can thus provide the highest cooling energy per kg compared to the other technologies but it also requires significantly more energy in terms of grid electricity for its production (48 kWh).

5.4.2 Environmental impacts of auxTRU and alternative TRUs

Unlike diesel powered engines fuel cell and battery powered TRUs do not produce emissions from the combustion of fuel at the point of use. The by-products of hydrogen fuel cell TRU water and heat while the by-products of battery powered TRU are just electricity and heat. Hence it can be claimed that both technologies do not produce greenhouse gas emissions during their operation phase but they are responsible for emissions during the production phase if the production of H_2 and electricity is not done using renewable sources.

5.4.2.1 Production related GHG emissions during distribution of different food items

Figures 5.3 – 5.11 illustrate the production related GHG emissions based on the energy usage during distribution of different refrigerated food products.

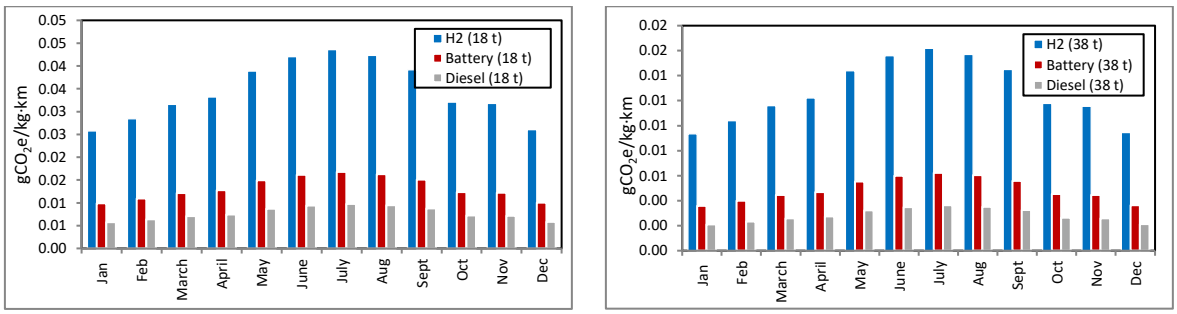

(a) (b)

Figure 5.3: Production related GHG emissions during distribution of milk using (a) 18 t and (b) 38 t vehicle category.

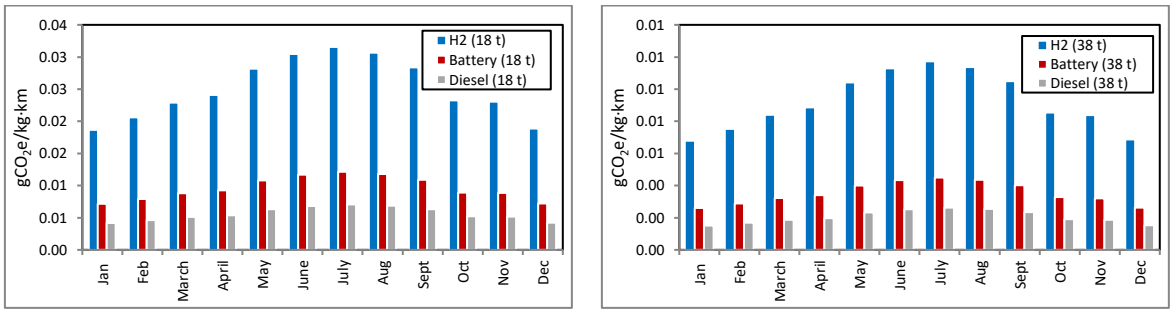

(a) (b)

Figure 5.4: Production related GHG emissions during distribution of cheese using (a) 18 t and (b) 38 t vehicle category.

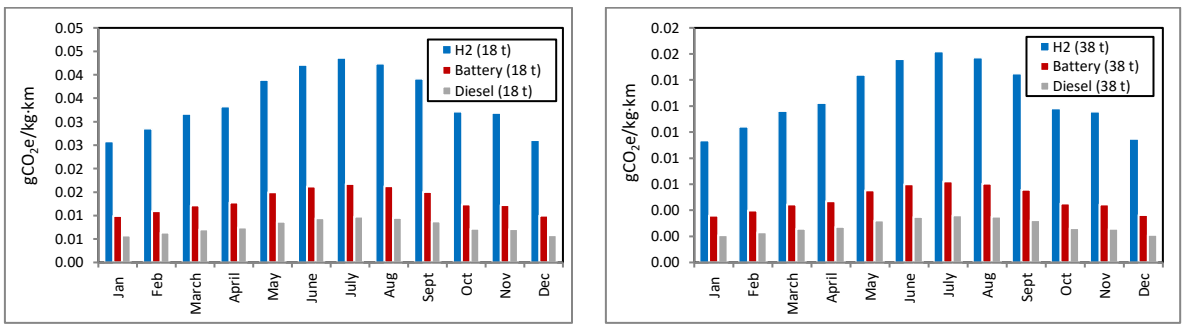

(a) (b)

Figure 5.5: Production related GHG emissions during distribution of ready meals using (a) 18 t and (b) 38 t vehicle category.

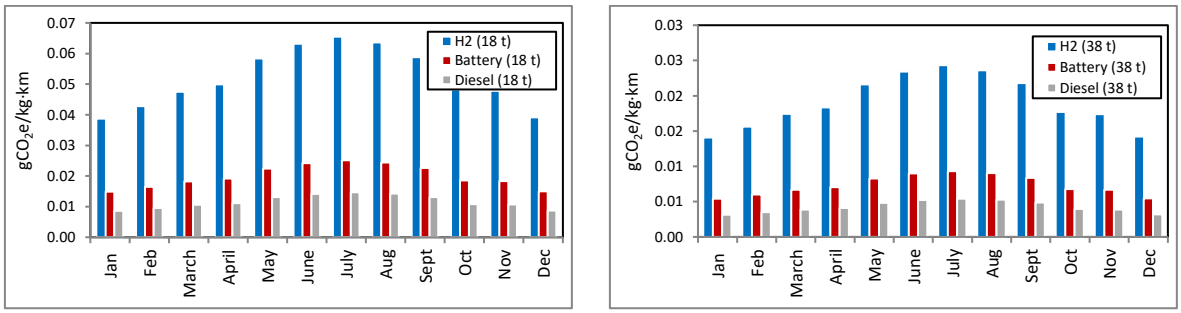

(a) (b)

Figure 5.6: Production related GHG emissions during distribution of fresh meat using (a) 18 t and (b) 38 t vehicle category.

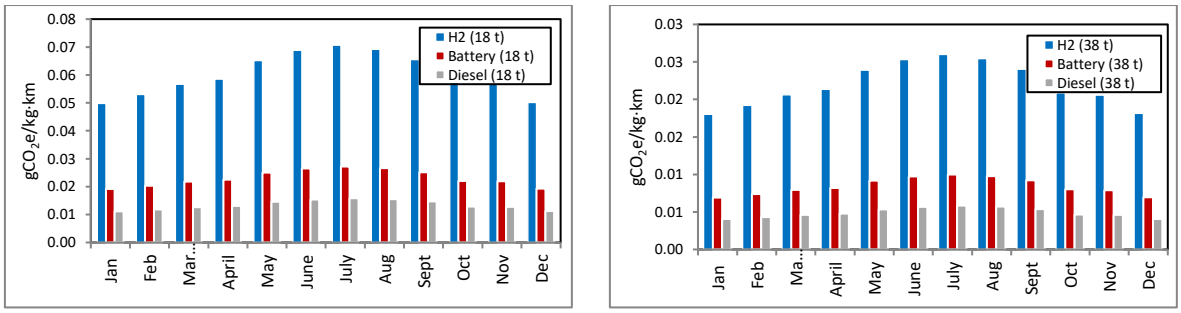

(a) (b)

Figure 5.7: Production related GHG emissions during distribution of frozen chips using (a) 18 t and (b) 38 t vehicle category.

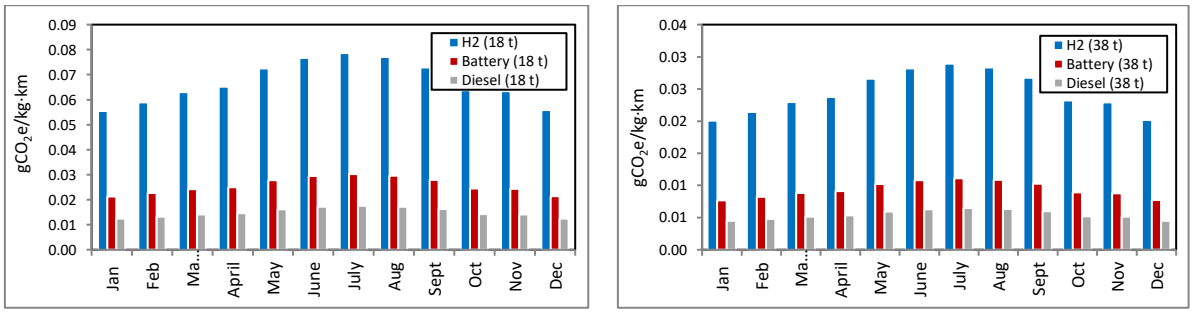

(a) (b)

Figure 5.8: Production related GHG emissions during distribution of frozen peas using (a) 18 t and (b) 38 t vehicle category.

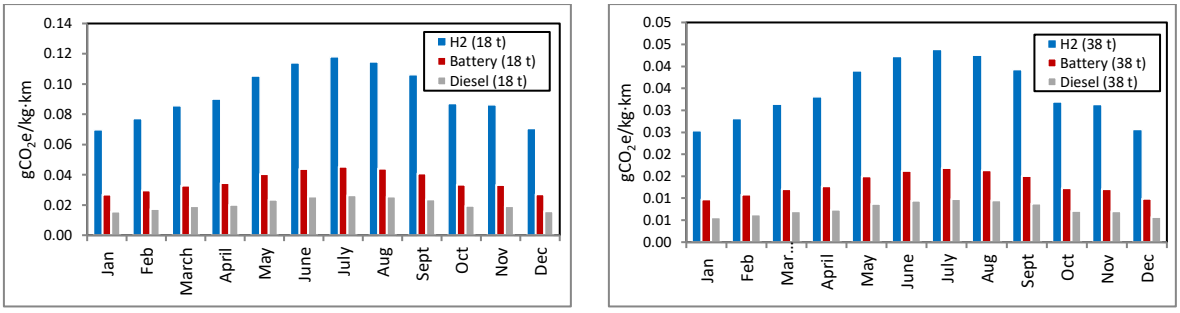

(a) (b)

Figure 5.9: Production related GHG emissions during distribution of strawberries using (a) 18 t and (b) 38 t vehicle category.

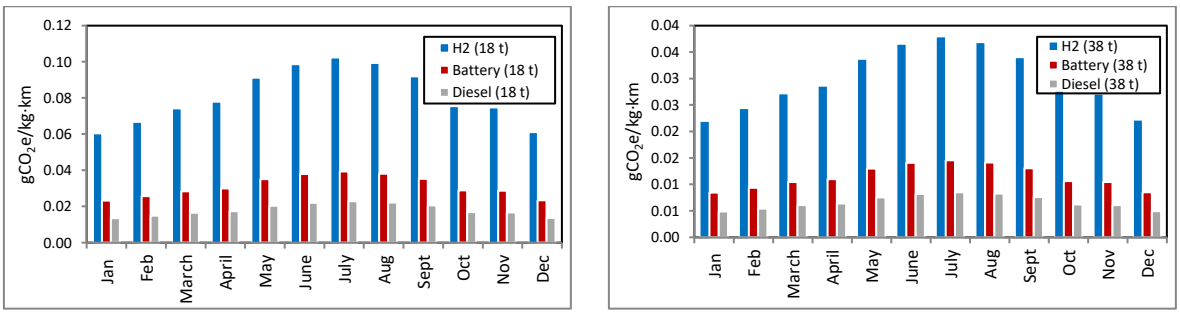

(a) (b)

Figure 5.10: Production related GHG emissions during distribution of apples using (a) 18 t and (b) 38 t vehicle category.

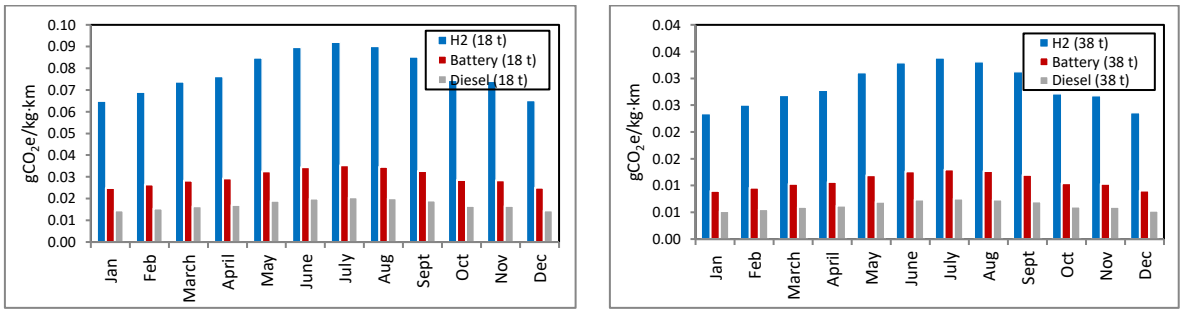

(a) (b)

Figure 5.11: Production related GHG emissions during distribution of ice-cream using (a) 18 t and (b) 38 t vehicle category.

For an 18 t vehicle, the production related GHG emission of selected food items varied between 0.006 and 0.026 gCO_2e/kg-km using auxTRU, 0.0186 and 0.1633 gCO_2e/kg-km using H_2 fuel cell TRU and between 0.007 and 0.045 gCO_2e/kg-km using all-electric TRU.

For a 38 t vehicle, the production related GHG emissions of the food items varied between 0.002 and 0.010 gCO_2e/kg-km using auxTRU, 0.009 and 0.044 gCO_2e/kg-km for H_2 fuel cell TRU and between 0.003 and 0.017 gCO_2e/kg-km using all-electric TRU.

As can be seen, food distribution using H_2 fuel cell accounts for highest GHG emission followed by all-electric and finally diesel. As discussed earlier, the production of hydrogen is an energy-intensive process, producing significant emissions if renewable energy is not used for its production.

Unlike the well-established production of diesel and electricity, current production of H_2 is not as well established in comparison, lacking suitable infrastructure, making the production process more energy intensive.

It can be seen that the GHG emissions during distribution using an 18 t vehicle are higher than those of 38 t vehicle per kg of food. This is mainly due to the larger volume space that a 38 t vehicle provides assumption that the vehicles are fully loaded during distribution. The results can vary significantly, however, based on the utilisation of the vehicle.

As expected, the GHG emissions of frozen food items is higher than chilled food items due to higher temperature difference between the inside of the chamber and outside for frozen in comparison to chilled. However, strawberries, though a chilled food product, still accounts for highest GHG emission due to larger package volume used for the food product and hence less quantity of packages per pallet.

5.4.2.2 Production and operation related GHG emissions during distribution of different food items

Figures 5.12 – 5.20 present the production and operation related GHG emissions based on the energy usage during distribution of different refrigerated food products.

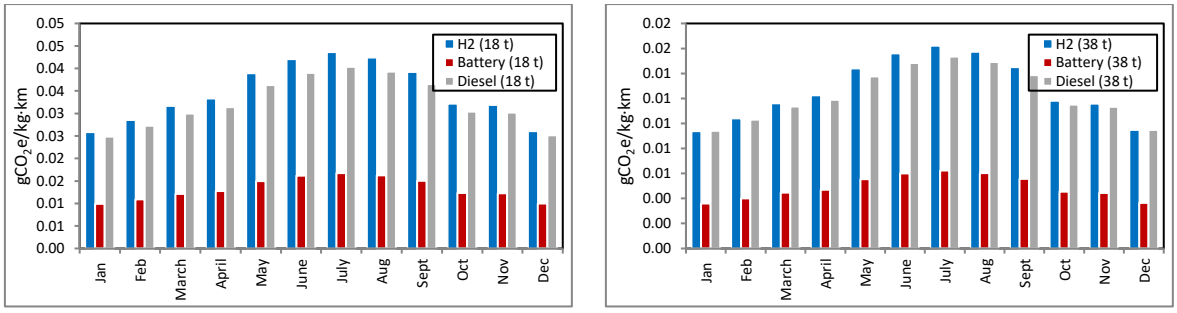

(a) (b)

Figure 5.12: Production and operation related GHG emissions during distribution of milk using (a) 18 t and (b) 38 t vehicle category.

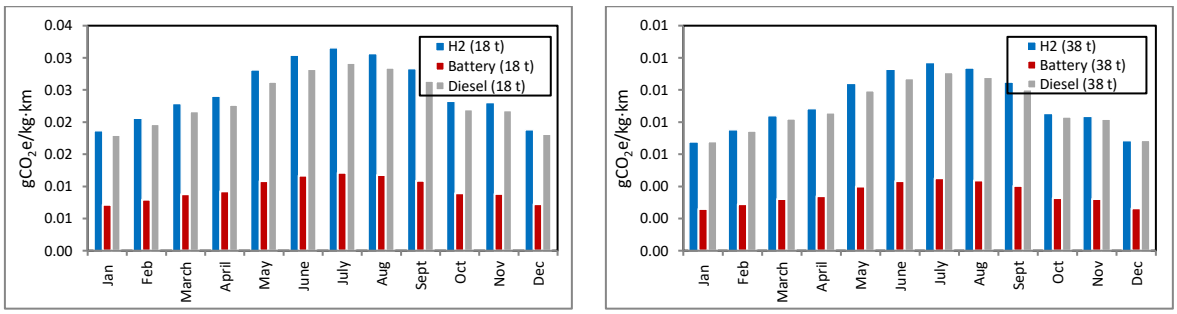

(a) (b)

Figure 5.13: Production and operation related GHG emissions during distribution of cheese using (a) 18 t and (b) 38 t vehicle category.

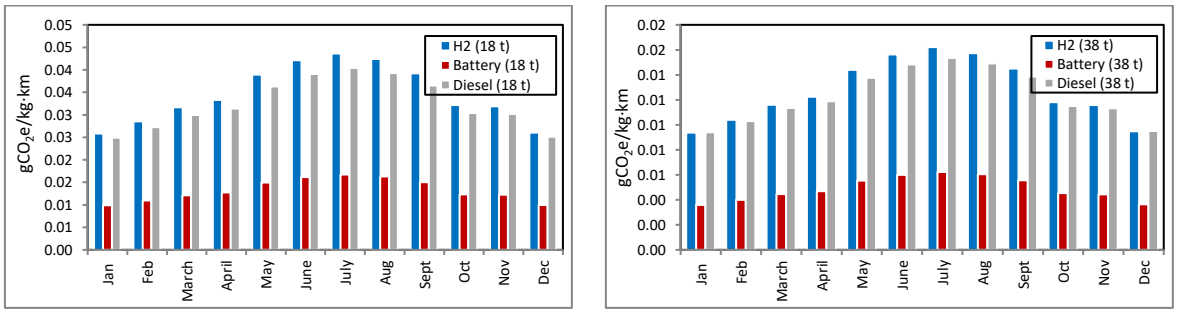

(a) (b)

Figure 5.14: Production and operation related GHG emissions during distribution of ready meals using (a) 18 t and (b) 38 t vehicle category.

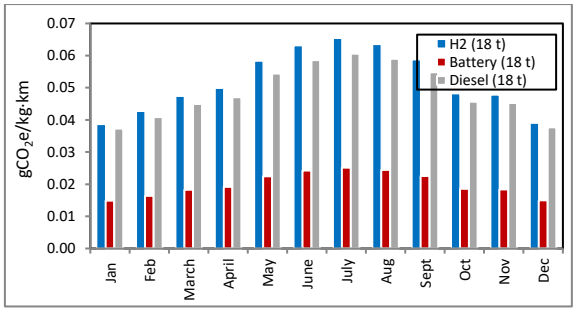

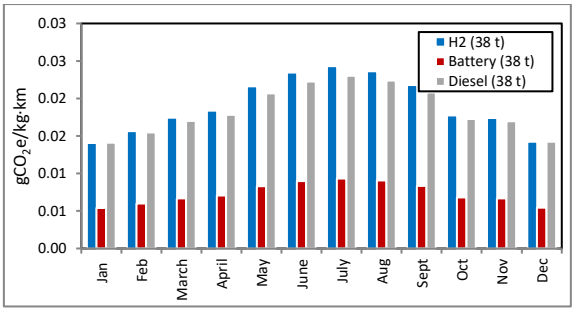

(a) (b)

Figure 5.15: Production and operation related GHG emissions during distribution of fresh meat using (a) 18 t and (b) 38 t vehicle category.

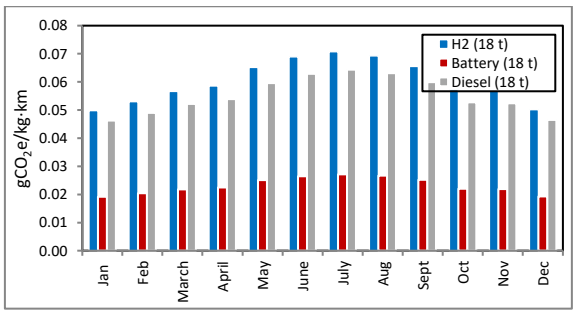

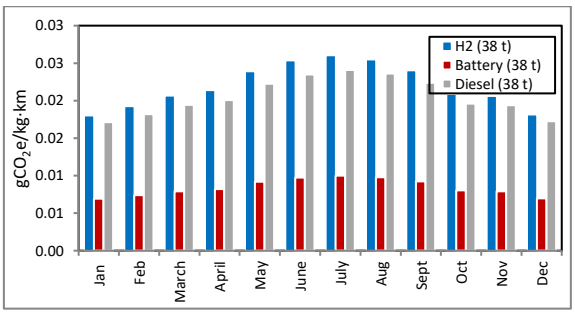

(a) (b)

Figure 5.16: Production and operation related GHG emissions during distribution of frozen chips using (a) 18 t and (b) 38 t vehicle category.

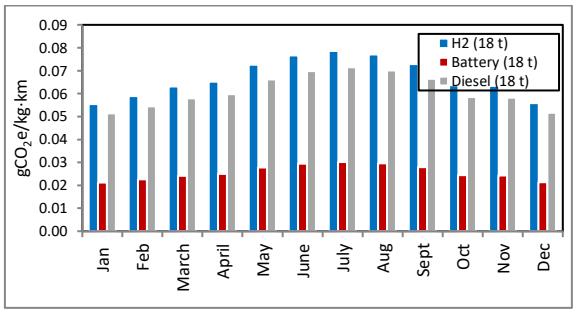

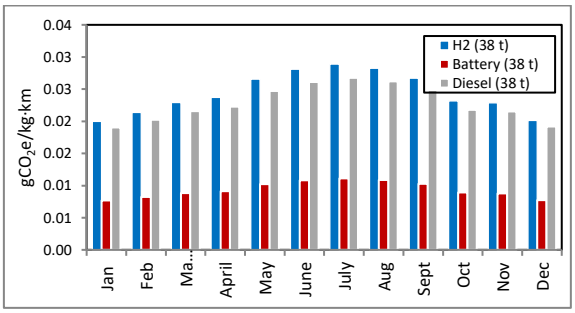

(a) (b)

Figure 5.17: Production and operation related GHG emissions during distribution of frozen peas using (a) 18 t and (b) 38 t vehicle category.

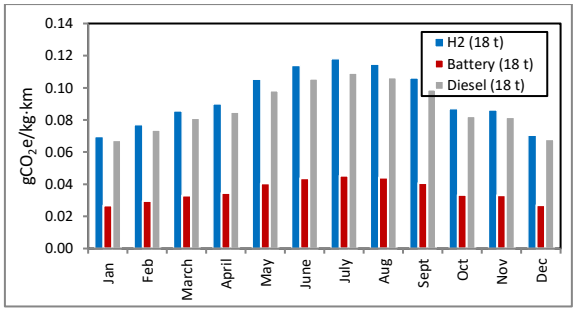

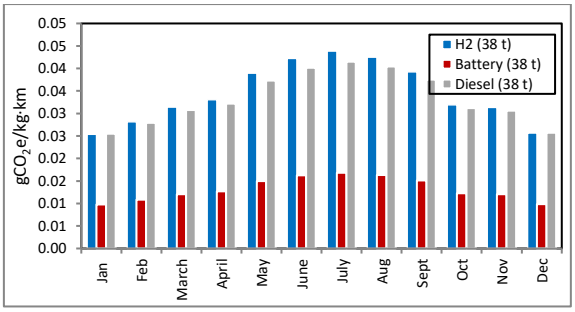

(a) (b)

Figure 5.18: Production and operation related GHG emissions during distribution of strawberries using (a) 18 t and (b) 38 t vehicle category.

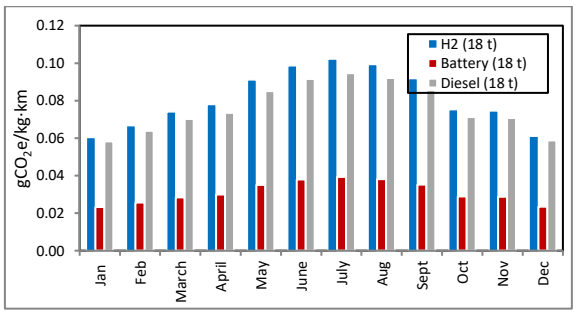

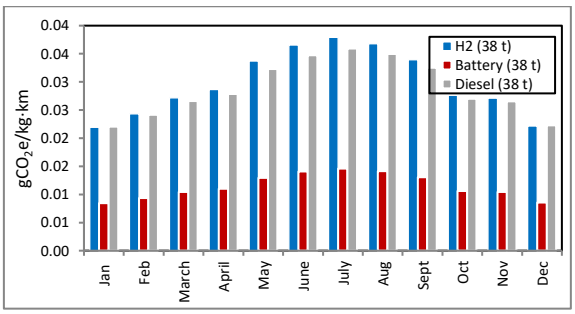

(a) (b)

Figure 5.19: Production and operation related GHG emissions during distribution of apples using (a) 18 t and (b) 38 t vehicle category.

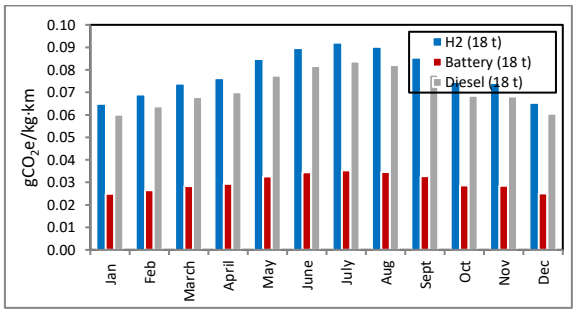

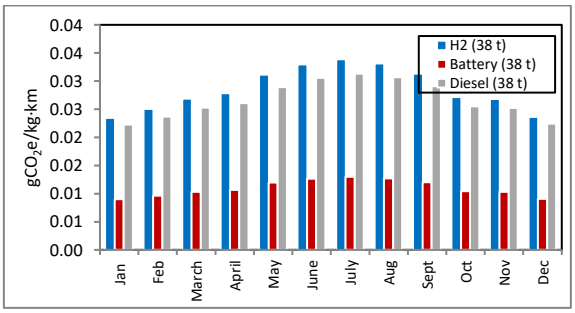

(a) (b)

Figure 5.20: Production and operation related GHG emissions during distribution of ice-cream using (a) 18 t and (b) 38 t vehicle category.

As can be seen, when both the production and operation phases are considered, a different results are obtained compared to the production phase alone. H_2 still accounts for the highest emissions due to the high emissions of the production phase, followed by diesel and finally all-electric.

The diesel powered auxTRU has high emissions during the use phase due to the combustion of fuel in the diesel engine to generate power to drive the refrigeration system. The diesel engine not only produces GHG emissions but also particulate matter (PM) that is released to the atmosphere and can have adverse health impacts.

Similar to H_2, the GHG emissions of all-electric TRUs is mainly due to the production phase only. However, the production related emissions of electricity are much lower than the production of hydrogen (by almost 60%).

As discussed earlier, the electricity generated in the UK is largely from the burning of fossil fuels. Provided more share of electricity can be generated using renewables, significant improvement in the emissions of the alternative technologies can be achieved.

5.4.2.2.1 Li-ion battery for all-electric TRUs

A disadvantage of all electric TRUs powered by Li-ion batteries is the GHG emissions during the manufacturing phase of the batteries. Review work conducted by Hao et al. [89] found the production phase of the battery to have emissions of as much as 109 $kgCO_2e$ per kWh of battery capacity. Considering a battery with a capacity of 34.2 kWh and mass of 300 kg will have a total GHG emission of 53 $kgCO_2e$/kWh [89]. The GHG emissions from the production of the Li-ion battery for the distribution pattern and products considered in thus Chapter are illustrated in Table 5.2.

Table 5.2: Hourly GHG emission for the distribution journey in consideration to the emission from battery production ($kgCO_2e$/h)

	GHG emission related to battery production ($kgCO_2e$/h)			
	18 t-chilled	18 t-frozen	38 t- chilled	38 t- frozen
Jan	2.09	3.44	2.24	3.69
Feb	2.31	3.66	2.49	3.93
March	2.56	3.92	2.78	4.22
April	2.69	4.05	2.93	4.37
May	3.15	4.51	3.45	4.89
June	3.41	4.76	3.74	5.18

July	3.53	4.89	3.88	5.32
Aug	3.43	4.79	3.77	5.21
Sept	3.17	4.53	3.48	4.92
Oct	2.60	3.96	2.83	4.27
Nov	2.58	3.94	2.77	4.21
Dec	2.11	3.46	2.27	3.71

5.5 Economic considerations

In 2015, the H_2 cost was estimated at £7.62 per kg of H_2 with price projected to reduce with increasing demand and 100% utilisation [90]. The average price of electricity was estimated at £0.12 per kWh of electricity while the price of diesel approximately £1.20 per litre [91].

Considering the mass consumption presented in Table 5.1, Table 5.3 presents the rough estimation of hourly operating cost for three different transport refrigeration units using different energy carriers.

Table 5.3: Hourly GHG emission for the distribution journey in consideration to the emission from battery production ($kgCO_2e/h$)

	Diesel 18 t (£)		Diesel 38 t (£)		H_2 18 t (£)		H_2 38 t (£)		Electric 18 t (£)		Electric 18 t (£)	
Month	Chilled	Frozen	Chilled	Frozen	Chilled	Frozen	Chilled	Frozen	Chilled	Frozen	Chilled	Frozen
Jan	1.43	2.35	1.54	2.52	1.83	3.05	1.98	3.28	0.54	0.89	0.58	0.96
Feb	1.57	2.51	1.70	2.69	2.06	3.28	2.21	3.51	0.60	0.95	0.65	1.02
March	1.75	2.68	1.90	2.89	2.29	3.51	2.51	3.73	0.66	1.02	0.72	1.10
April	1.84	2.77	2.00	2.99	2.44	3.58	2.59	3.89	0.70	1.05	0.76	1.14
May	2.15	3.08	2.36	3.35	2.82	4.04	3.05	4.34	0.82	1.17	0.90	1.27
June	2.33	3.25	2.56	3.54	3.05	4.27	3.35	4.65	0.88	1.24	0.97	1.35
July	2.41	3.34	2.65	3.64	3.12	4.34	3.51	4.72	0.92	1.27	1.01	1.38

Aug	2.34	3.28	2.58	3.56	3.05	4.27	3.35	4.65	0.89	1.24	0.98	1.35
Sept	2.17	3.10	2.38	3.36	2.82	4.04	3.12	4.42	0.82	1.18	0.90	1.28
Oct	1.78	2.70	1.93	2.92	2.29	3.51	2.51	3.81	0.68	1.03	0.73	1.11
Nov	1.76	2.69	1.90	2.88	2.29	3.51	2.51	3.73	0.67	1.02	0.72	1.09
Dec	1.44	2.36	1.55	2.53	1.91	3.12	2.06	3.35	0.55	0.90	0.59	0.96

Regardless the lowest mass consumption by H_2 in Table 5.1, when the operation cost of all three technologies are compared, the cost for operating H_2 is the highest followed by diesel powered and finally all-electric.

5.6 Summary

This chapter considered two alternative technologies, H_2 fuel cell and Li-on battery based, to diesel that can be used to power vapour compression transport refrigeration systems based on the GHG emissions during the production and operation phase. The diesel consumption of auxTRU can vary anywhere between 1.9 l/h to 3.03 l/h, the mass consumption of H_2 can vary anywhere between 0.26 kg/h and 0.46 kg/h, the power consumption of all-electric between 4.52 kWh and 11.52 kWh depending on the refrigeration capacity and distribution parameters.

The production related GHG emissions of H_2 is almost five times higher than the production emission of diesel based on the mass consumption required for distribution of different temperature-controlled food products. When both the production and operation related GHG emissions are considered, the all-electric option has the least emissions making it the most suitable choice with regards to the environment.

The lack of refuelling infrastructure for H_2 makes the fuel cell option not very attractive or cost effective at present. Similarly, the all-electric option requires frequent charging at the distribution centre and the lack of charging infrastructure in motorway stations as well as the long charging time, reduces the application of all electric systems to mainly local distribution at present.

CHAPTER 6

Experimental set-up for investigating the performance of an air curtain in refrigerated box and CFD model setup and validation

Chapters 3, 4 and 5 discussed emissions from TRUs powered by auxiliary diesel engines and analysed alternative technologies that have the potential to reduce the environmental impacts of transport refrigeration systems. Regardless of the choice of cooling technology, however, warm air infiltration during door openings has been identified as a major contributor to energy demand in transport refrigeration systems. Attempts to reduce infiltration through the use of plastic strip curtains have not proven successful due to the barrier they provide to the loading and unloading of the vehicle. Air curtains have been recognised as one of the most effective technologies to control air infiltration during door openings in buildings. However, the use of air curtains has not as yet become prevalent in food transport vehicles due to insufficient research and results to demonstrate their effectiveness. This thesis makes a contribution in this area. Chapter 6 presents the experimental setup in the laboratory for the investigation of the performance of air curtain in transport refrigeration systems and results of tests to characterise the performance of an air curtain at different operating conditions. However, since the experimental study is based on a lab-scale sized trailer which is smaller in comparison to the trailer sizes used for food distribution purposes. For this reason, a Computational Fluid Dynamics (CFD) model was developed. This chapter also discusses the CFD model setup of the lab-scale trailer. The CFD model is validated using the temperature results obtained from experiment.

6.1 Introduction

Warm air infiltration during door opening can account for a large percentage of the overall refrigeration load, with its share estimated to be higher for longer door opening durations as discussed in Chapter 2. Many investigations and studies aimed at finding ways to minimise the rate of warm air infiltration in temperature-controlled environments have suggested the use of an air curtain to be one of the most-effective mechanisms [1-5].

The air curtain is a device which draws air either from inside (the cold air inside the chamber) or from outside (the warmer ambient air) and discharges it through the outlet vent to create an air barrier that prevents cold air from escaping out and warm air from entering in.

Though the use of air curtain is more common in warehouses and commercial buildings, the use of the device has not been extensively explored in refrigerated vehicles. There is still a lack of studies that focus on the use of air curtains in refrigerated truck bodies, their efficiency and ways of optimising their performance such that the impact of warm air infiltration can be minimised.

Along with experimental work, numerical simulation using CFD has also proven to be an effective way of studying the airflow behaviour during door openings and the effectiveness of air curtains in reducing infiltration.

As discussed in Chapter 2, a number of investigators have previously used CFD to investigate the performance of air curtains to reduce infiltration in cold rooms and warehouses [1-6]. However, the literature is very limited on the investigation of air curtain performance in transport refrigeration applications.

This chapter discusses the experimental side of work conducted to test the performance of an air curtain.

6.2 Overview of the test facility and test conditions

6.2.1 Refrigerated box (insulated box used for the experiment)

A custom-designed refrigerated box (Figure1) with external dimensions of 3.5 m × 1.9 m × 1.5 m (l × h × w) was used for the test purposes. The size of the box is very similar to that of a home delivery van. The rear side of the box incorporates double door. The door has a dimension of 1.3 m × 1.73 m (w × h).

Figure 6.1: Insulated box used for the experiment.

Table 6.1 represents the thermal properties of the wall provided by the manufacturer.

Table 6.1: Thermal properties of the wall

Properties	
Density (kg/m^3)	45
Thermal conductivity (w/(m.K)	0.027
Temperature limits (°C)	-50/+75

6.2.2 Transport refrigeration unit

A GAH transport refrigeration system, model SR351dsi, was installed on the unit to provide cooling to the box. The cooling unit is charged with R452A. The cooling capacity of the unit is 2260 W at 0°C and 1330 W at -20°C. The cooling unit is powered electrically using a plug-in system.

6.2.3 Air curtain

A custom-designed air curtain, has a length of 1.3 m specifically sized to exactly fit the door opening of the box. The air curtain consists of 15 small 24 V axial fans with a honeycomb at the outlet to smooth discharge flow turbulence. A discharge air velocity of approximately 44.5 m/s could be achieved at maximum voltage. Unlike the heavy air curtains used in cold rooms and warehouses, this device only weighs 10 kg

making it more suitable for distribution trucks. The air curtain was fitted 10 cm away from the door.

6.2.4 Food products

Six 210 litre water tanks with dimensions of 0.93 m × 0.63 m × 0.42 m (h × l × w) and six 65 litre water tanks 0.40 m × 0.40 m × 0.45 m (h × l × w) were used to simulate the product (load) and thermal mass inside the box. These water tanks were ½-¾ filled with water and placed on wooden pallets similar to the way food products are loaded in refrigerated trucks.

6.3 Instrumentation and data logging system

6.3.1 Temperature control system

The box came equipped with a thermostat/control system to control the operation of the cooling unit and the temperature inside the box. The temperature of the unit could be adjusted between -20 °C and 10 °C on the thermostat. The thermostat had a dead band of +/-2 °C, i.e. every time the temperature inside the chamber was 2 °C above the set temperature, the cooling unit would switch on.

The controller also had an automatic defrost function and defrosts every 30 minutes after being switched on and every hour thereafter provide stable temperature was maintained throughout.

6.3.2 Power meter

The power consumption of the unit was measured using Fluke 345 clamp meter for single phase power supply. The power meter was installed in a secure metal box.

For temperature pulldown, the logging time was set to 1 minute. For studying the airflow behaviour during door opening and the performance of air curtain, the logging time was set to 10 s.

6.3.3 Airflow control system

The velocity of the air curtain was controlled using a power supply. The voltage range of the power supply varied between 0 and 30 V.

6.3.4 Temperature measurements

Altogether 68 Type K thermocouples were used in different locations of the box to measure air and product (water temperatures). Out of the 68 thermocouples, 27 were located at the door area. The reading error range of these thermocouples are between 0.5 °C to 1 °C.

All the thermocouples were connected to a C series I/O data logger from National Instruments, NI 9214. The data could be visualised using LabVIEW software.

6.4 Test conditions, airflow characteristics and test methodology

The temperature of the laboratory in which the refrigerated box was placed could be controlled by adjusting the thermostat of the room. The temperature of the lab was set to 21° C while the temperature inside the box and products were set to 4.5 °C. The temperature parameters used for the test were within the range specified by the ATP test standards [6]. The cooling unit was left running for two days in order to pulldown the temperature of the products to the set temperature.

A range of air curtain velocities were tested, 0 – 4 m/s, based on the minimum and maximum capacity of the air curtain. It was found that the outlet velocity along the air curtain honeycomb was not constant. Several tests were initially conducted at three different points at the discharge outlet (right, left, and middle) to determine the correlation between power supply, in the form of voltage, and air curtain velocity, illustrated in Figure 6.2.

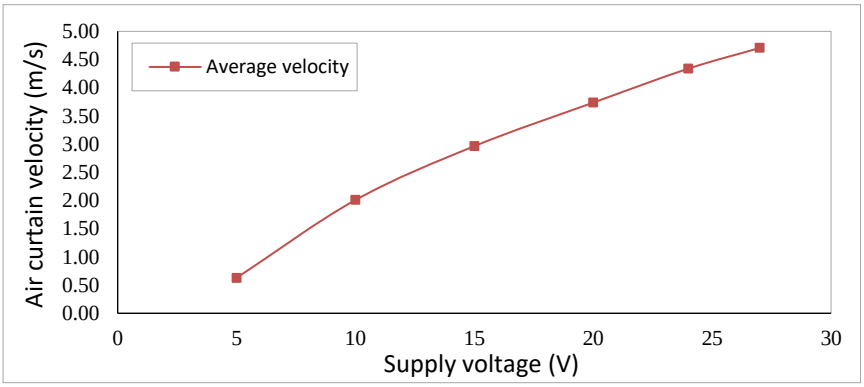

Figure 6.2: Correlation between air curtain velocity and voltage supplied.

Each experiment at each velocity was repeated three times to ensure the consistency of the results.

Based on the survey and average drive cycle discussed in Chapter 3, an average door opening time of 15 minutes was estimated for the distribution trucks. And hence, for each test, the door was opened for 15 minutes.

The cooling unit was initially left running to maintain the internal temperature. Just before conducting the test, all the ventilation fans inside the lab were switched off to minimise the air disturbance around the refrigerated box. The cooling unit was switched off, the air curtain switched on and the door opened for 15 minutes. After the door was shut, the air curtain was switched off and cooling unit switched on. The cooling unit was left running for atleast 16 hours to ensure adequate level of readings for estimating the recovery energy accurately.

6.5 Temperature recordings and analysis

6.5.1 Temperature variations inside the truck during the door opening

Figure 6.2 illustrates the positions of thermocouples inside the refrigerated box.

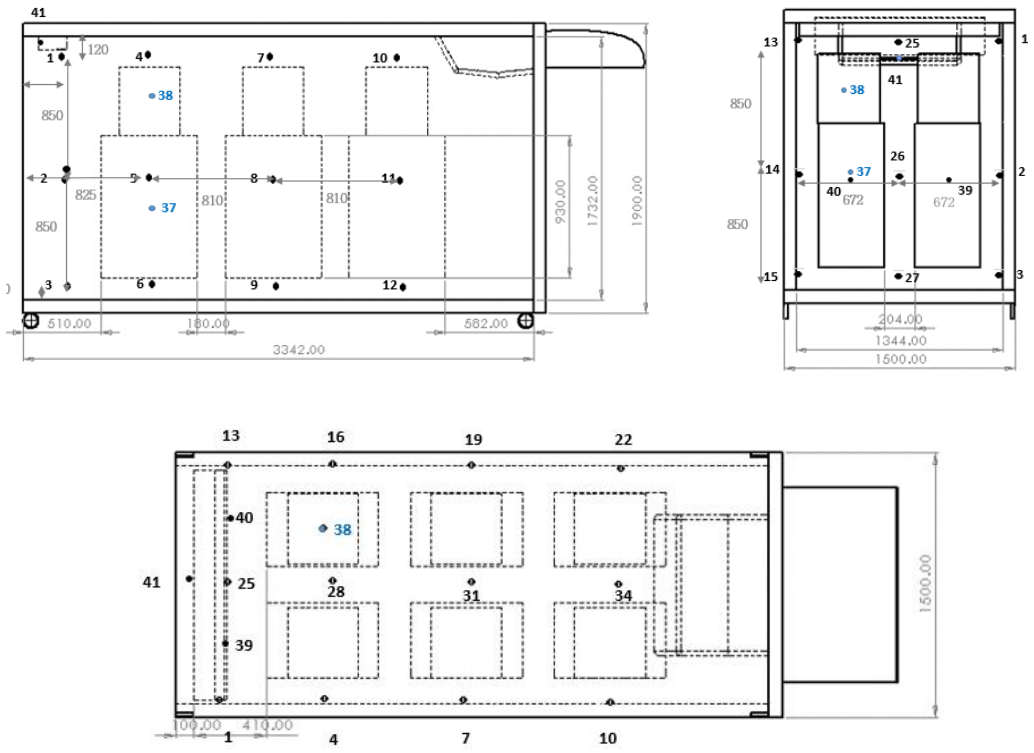

Figure 6.2: Positioning of thermocouples inside the box.

Figure 6.3- Figure 6.7 presents the temperature variations around the door area, inside the box in the middle area and in the innermost area at three different levels, top, middle and low. These temperature variations provide information on the temperature changes in different areas but does not however provide graphical illustration of airflow (this is provided in Chapter 7).

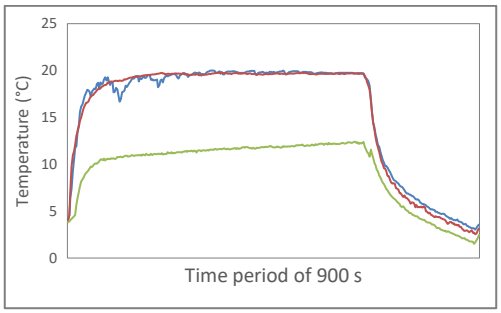

(a)

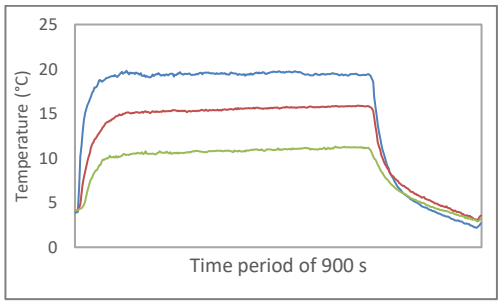

(b)

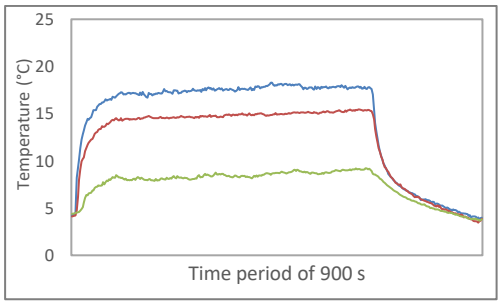

(c)

Figure 6.3: Temperature recordings at the (a) door area, (b) middle area, (c) innermost area without an air curtain (blue=top level, red=middle level, green=low level).

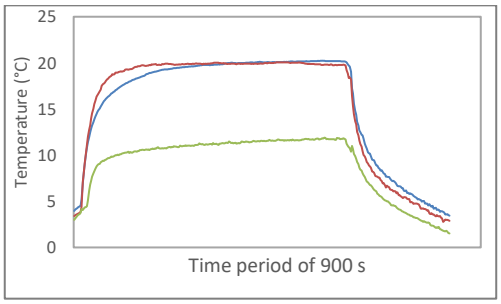

(a)

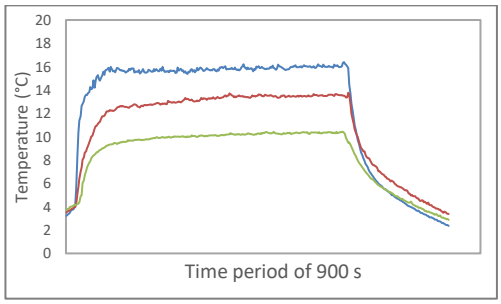

(b)

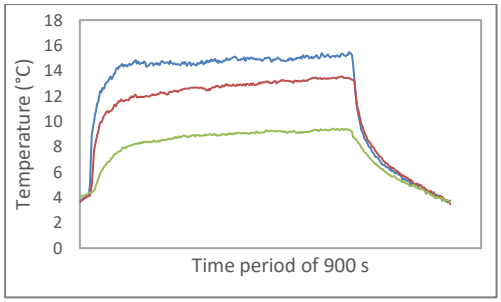

(c)

Figure 6.4: Temperature recordings at the (a) door area, (b) middle area, (c) innermost area at air curtain velocity 1 m/s (blue=top level, red=middle level, green=low level).

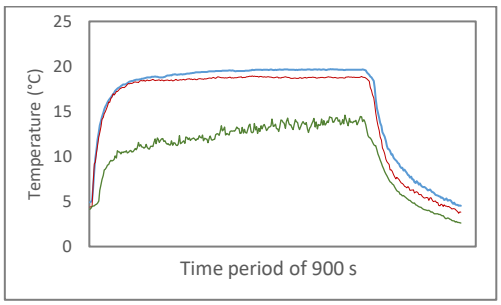

(a)

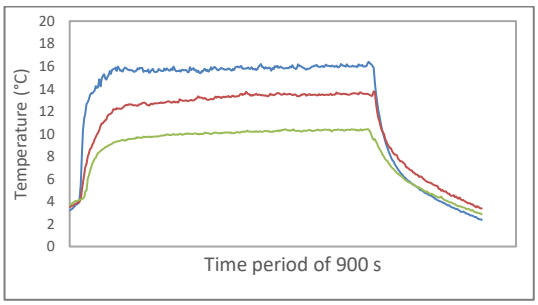

(b)

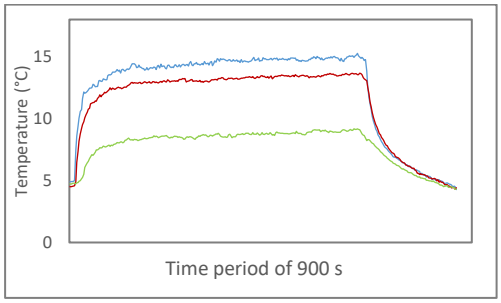

(c)

Figure 6.5: Temperature recordings at the (a) door area, (b) middle area, (c) innermost area at air curtain velocity 2 m/s (blue=top level, red=middle level, green=low level).

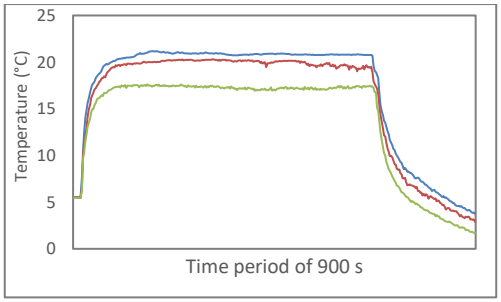

(a)

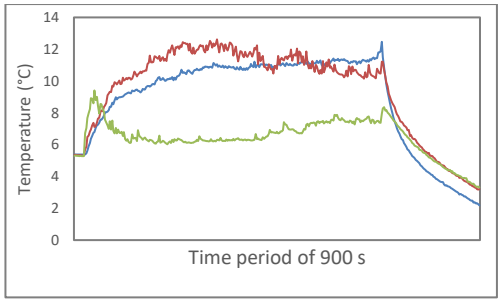

(b)

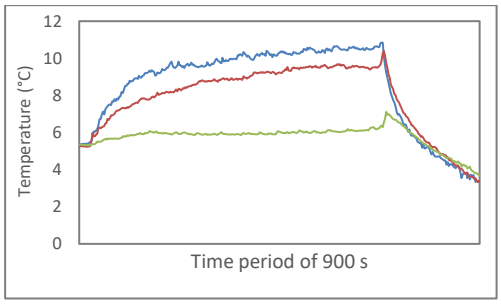

(c)

Figure 6.6: Temperature recordings at the (a) door area, (b) middle area, (c) innermost area at air curtain velocity 3 m/s (blue=top level, red=middle level, green=low level).

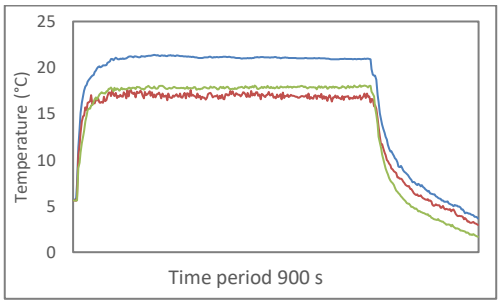

(a)

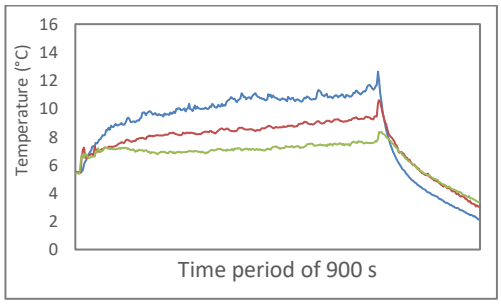

(b)

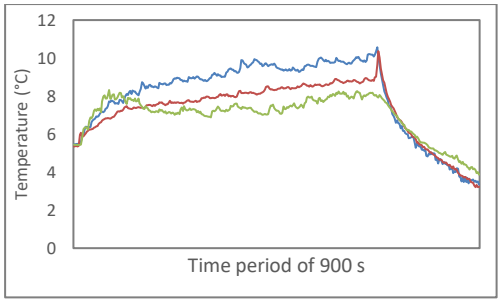

(c)

Figure 6.7: Temperature recordings at the (a) door area, (b) middle area, (c) innermost area at air curtain velocity 4 m/s (blue=top level, red=middle level, green=low level).

In Figure 6.3 (a), the case without an air curtain, the top and the middle levels around the door area have similar high temperature, similar to that of the ambient air while the bottom area stays cold. This illustrates a normal case of warm air infiltration through the upper area of the door and outflow of cold air from the bottom area. For the inner area of the trailer, as expected, it can be seen that the top layer is warmest followed by the middle and bottom area.

When an air curtain is operated at very low discharge velocity, 1 m/s, it can be seen that the temperature variations inside the trailer are very similar to that of the case without an air curtain. This illustrates that at low air curtain discharge velocity, the air curtain is not effective at maintaining the inner temperature of the box.

Similar temperature performance to the 1 m/s can be observed for the 2 m/s around the door area. This shows that even at 2 m/s, the discharge air does not thoroughly impinge on the floor and hence the cold air continues to escape from the lower area. However if we observe the inner area, it can be seen that the overall temperature is lower than for the 1 m/s velocity illustrating reduced loss of cold air.

A much better performance can be observed for air curtain discharge velocities of 3 m/s and 4 m/s, Figure 6.6 and Figure 6.7, indicating the air curtain provides a better sealing of the door area from external air infiltration.

6.6 CFD approach

6.6.1 Physical domain

Initially, a model of the test facility was developed using a commercial 3D CAD tool, 'Solidworks'. Like the actual test rig, the model incorporates all the components in the system- water tanks, air curtain and cooling unit. The trailer model was placed inside a large space of the same dimensions as the lab area and heat gains and air flows in the space were taken into consideration in the CFD modelling.

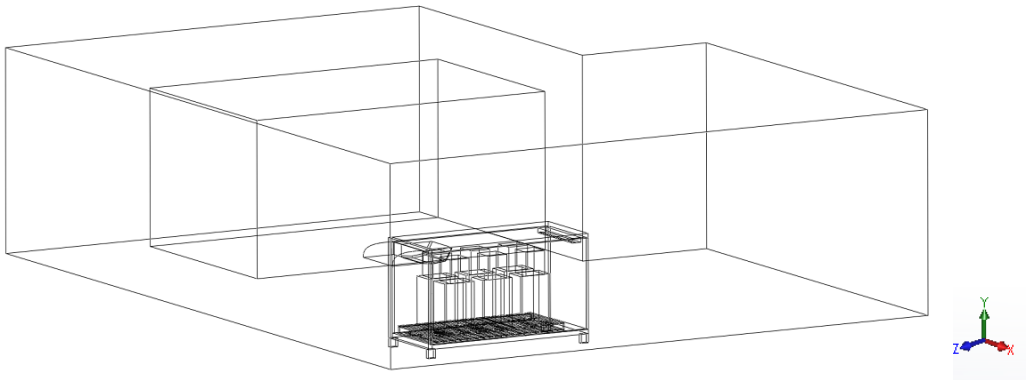

(a)

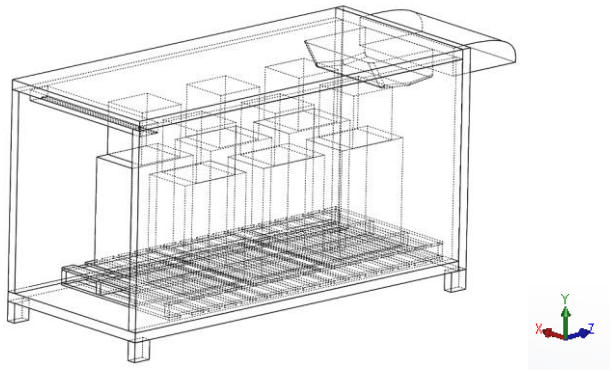

(b)

Figure 6.7: Geometry of the physical domain (a) lab room, (b) box.

6.6.2 Mesh generation

The meshing was developed using the commercial code ANSYS ICEM 14.5. A series of different hexagonal grid sizes (coarse, fine and finer) were adopted for the model to test mesh independence. At a fine mesh of 5.6 million elements, mesh independence was achieved. The model of the surrounding environment consisted of tetrahedral

elements with refined grids at points and edges where more refined output would be required.

6.6.3 Governing equations and models

ANSYS Fluent uses the finite volume method to solve the Navier-Stokes continuity and energy equations.

6.6.3.1 Conservation of mass

For steady flow, the continuity equation in two dimension for an incompressible flow can be expressed in Eq 6.1.

$$\frac{\partial \rho}{\partial t} + \frac{\partial (\rho u)}{\partial x} + \frac{\partial (\rho v)}{\partial y} + \frac{\partial (\rho w)}{\partial z} = 0 \qquad 6.1$$

Where u ,v and w represent the mass average velocities in coordinates x, y and z.

6.6.3.2 Momentum equation

Newton's second law of motion states that the sum of forces acting on the fluid element is equal to the product of its mass and the acceleration of the element. Applying Newton's second law in 3D gives.

$$\rho \frac{Du}{Dt} = \frac{\partial \sigma_{xx}}{\partial x} + \frac{\partial \tau_{yx}}{\partial y} + \frac{\partial \tau_{zx}}{\partial z} + \sum F_x \qquad 6.2$$

$$\rho \frac{Dv}{Dt} = \frac{\partial \tau_{xy}}{\partial x} + \frac{\partial \sigma_{yy}}{\partial y} + \frac{\partial \tau_{zy}}{\partial z} + \sum F_y \qquad 6.3$$

$$\rho \frac{Dw}{Dt} = \frac{\partial \tau_{xz}}{\partial x} + \frac{\partial \tau_{yz}}{\partial y} + \frac{\partial \sigma_{zz}}{\partial_z} + \sum F_z \qquad 6.4$$

The normal stresses σ_{xx}, σ_{xy} and σ_{zz} in Eqs. 6.2- 6.4 are due to the combination of pressure ρ and normal viscous stress componentsτ_{xx}, τ_{yy} and τ_{zz} acting perpendicular to the control volume.

6.6.3.3 The energy equation

The conservation of energy equation is derived from the first law of thermodynamics where the time rate of change of energy is equal to the net rate of heat added and net rate of work done. The equation for the conservation of energy in 2D can be expressed as Eq 6.5.

$$\rho C_p \frac{DT}{Dt} = \frac{\partial}{\partial x}\left[\lambda \frac{\partial T}{\partial x}\right] + \frac{\partial}{\partial y}\left[\lambda \frac{\partial T}{\partial y}\right] + \frac{\partial}{\partial z}\left[\lambda \frac{\partial T}{\partial z}\right] \qquad 6.5$$

Where, T represents the temperature and C_p represents the specific heat at constant pressure.

6.6.3.4 Turbulence model- The k-ε model

Many numerical investigations conducted to study the thermal behaviour of air curtains in cold rooms have used two-equation models to model the turbulence effects, in particular the k- ε model [2, 3, 7, 8]. The k- model is a two-equation semi-empirical eddy-viscosity model in which the Reynolds stresses are assumed to be proportional to the mean velocity gradients, the constant of the proportionality being the turbulent viscosity.

The unsteady flow in this type of cases particularly occurs in three situations: forced convection, natural convection and mixed convection. A comparative study conducted on the accuracy of different turbulence models by Gao et al. [9] indicated the accuracy of RNG k- model to be slightly better than that of standard k- model. However, both the standard and RNG models are equally applicable to model the flow characteristics of forced convection and mixed convection [9]. It has also been reported that the computational effort associated with the RNG k- model is only marginally higher than that for the standard k- model. Due to acceptable level of accuracy and relatively low computational demand based on previous studies, the standard k- model was chosen to be used in this work.

Since the standard k-ε model is a semi-empirical model based on model transport equations for turbulent kinetic energy (k) and its dissipation rate(ε) which can be expressed as,

$$\frac{\partial}{\partial t}(\rho k) + \frac{\partial}{\partial x_i}(\rho k u_i) = \frac{\partial}{\partial x_j}\left[\left(\mu + \frac{\mu_t}{\sigma_k}\right)\frac{\partial k}{\partial x_j}\right] + G_k + G_b - \rho\varepsilon - Y_M \quad 6.6$$

$$\frac{\partial}{\partial t}(\rho\varepsilon) + \frac{\partial}{\partial x_i}(\rho\varepsilon u_i) = \frac{\partial}{\partial x_j}\left[\left(\mu + \frac{\mu_t}{\sigma_\varepsilon}\right)\frac{\partial \varepsilon}{\partial x_j}\right] + C_{1\varepsilon}\frac{\varepsilon}{k}(G_k + C_{3\varepsilon}G_b) - C_{2\varepsilon\rho}\frac{\varepsilon^2}{k} \quad 6.7$$

With the model constants,

$$C_{1\varepsilon} = 1.44,\ C_{2\varepsilon} = 1.92,\ C_\mu = 0.09,\ \sigma_k = 1.0,\ \sigma_\varepsilon = 1.3$$

Where G_k and $G_b$represents the generation of turbulent kinetic energy due to mean velocity gradient and due to buoyancy respectively, and Y_M the fluctuating dilatation in compressible turbulence to the overall dissipation rate.

Near wall treatment

It is crucial to capture the correct thermos-fluid mechanics near the products or the main in the box for accurate representation of the thermal and flow behaviour inside and outside the box. This accuracy is highly dependent on the ability of the grid to resolve solution data from these near-wall regions to the core of the flow field and vice versa. The mean velocity field is affected through the no-slip condition that has to be satisfied at the wall. Accurate representation of the flow in the near-wall region determines successful predictions of wall-bounded turbulent flows.

The near wall region can be further sub-divided into three layers, the viscous sublayer, the fully-turbulent layer and finally buffer layer.

There exists two approaches to modelling the near-wall region. The first approach includes using semi-empirical formulas called “wall functions” to bridge the viscosity-affected region between the wall and the fully turbulent region. Another approach would enable the viscosity-affected region to be resolved with a mesh all the way to the wall including the viscous sublayer also known as “near wall modelling”. For this work, the second approach has been implemented by finely refining the grids along the walls of high viscous regions.

6.6.3.5 Radiation model- Surface-to-surface (S2S) radiation model theory

Heat transfer as a result of radiation is often overlooked in CFD simulations, even in the majority of previous studies in the area of this project. However, for transport refrigeration systems and trailers, it is important to account for the radiation heat transfer load.

For commercial code such as Ansys Fluent, the surface-to-surface radiation model can be used to estimate the radiation exchange in an enclosure. The energy exchange between two surfaces depends on their size, separation distance, and orientation. These parameters are accounted for by a geometric function called a "view factor". The view factor between two finite surfaces and is given by,

$$F_{ij} = \frac{1}{A_i} \iint \frac{Cos\theta_i Cos\theta_j}{\pi r^2} \delta_{ij} dA_i dA_j \qquad 6.8$$

Where A_i and A_j represents the area of surface i and$j$. δ_{ij} is determined by the visibility of dA_j to dA_i . δ_{ij}=1 if dA_j is visible to dA_i and 0 otherwise.

6.6.4 Boundary conditions

For initial condition, the air inside and outside the box is static. The temperature of the lab was set to 21 °C and the temperatures of the box and food products were set to 4 °C, same as the conditions maintained for the experiments.

The model employs a fan using pressure jump across a virtual "fan surface" to control the discharge velocity from the air curtain. In order to obtain the relationship, different pressure difference parameters were assigned for the simulations, one simulation per parameter. Once the simulation was completed, the velocity was measured. Each pressure difference indicated a different velocity.

The inlet of the air curtain is facing outwards and intakes air from outside and discharges it from the outlet. The air curtain is located 10 cm away from the main door as suggested by the guide for the air curtain.

The varying density of the air is based on the ideal gas law and a gravitational acceleration of 9.8 m/s^2 is assigned in the negative y-direction.

The thickness of insulation is 0.079 m for sidewalls and 0.084 m for the roof and floor.

A door opening duration of 15 minutes was used for every door opening simulation.

6.7 Model Validation

A number of simulations were ran at different discharge velocities. The temperature increase after door opening at each discharge velocity was monitored separately and later compared with experimental results to ensure the validity of the model.

Figure 6.15 presents the comparison between the model and experiment-based results. ‘T-sim’ represents the temperature obtained using simulation and ‘T-exp’ represents the temperature recordings from the experiment.

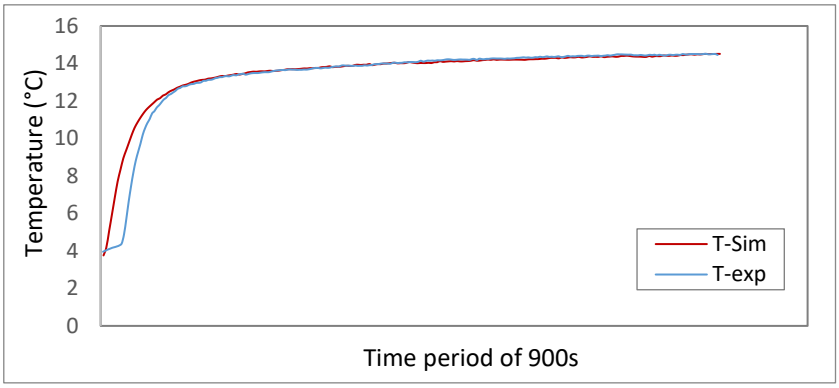

(a)

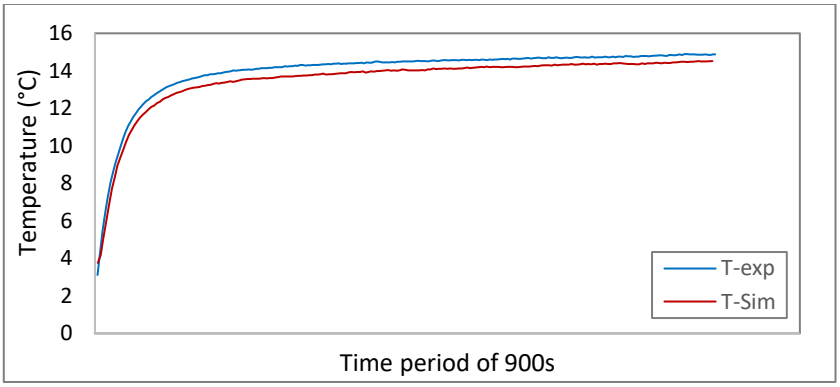

(b)

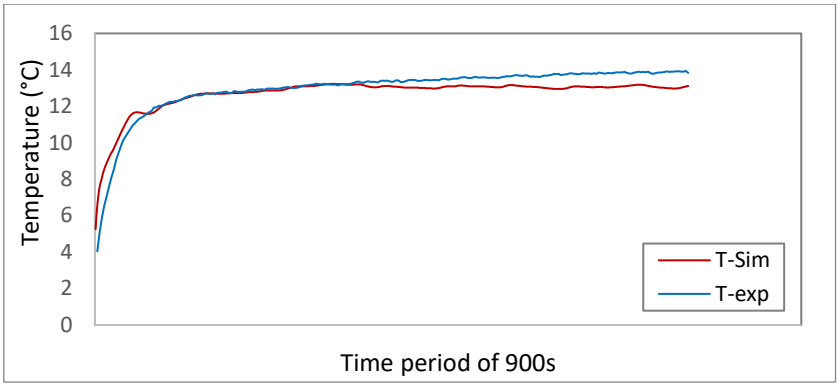

(c)

Figure 6.15: Average internal temperature for door opening period of 900s (a) 0 m/s, (b) 1 m/s and (c) 3m/s.

It can be observed that the difference between the experimental and model-based results is less than 1°C and hence less than 8% deviation which indicates that the model is fairly accurate.

In Figure 6.15 (a), a highest level of accuracy between the model and the experiment can be observed for the door opening case without any air curtain. The slight difference at the beginning could have occurred due to the delay with door opening during the experiment. In the simulation, the door opening is instantaneous unlike the experiment where one has to manually open the door causing a small time delay. This could have caused the slight difference at the beginning.

For Figure 6.15 (b) and (c), though the difference between both the results is less than 1°C, it can be seen that the temperature gain in the tests is higher than that of simulation. This could have been caused due to the inconsistent discharge along the outlet of the air curtain. As mentioned in the overview of the experiment, it was found that the discharge from the air curtain outlet was not consistent, high velocity at one end in comparison to the other end. This may have been caused by the fact the simulation assumes the air velocity of the air curtain is uniform along its entire length. This is not the case with the tests where the velocity varies along the air curtain length due to the positioning of the fans. Due to this, the actual air curtain effectiveness will be lower than that obtained from simulation, allowing more ambient air to infiltrate in the cold box.

Figure 6.16 presents the average product temperature history from the simulation and the tests for 15 minutes of door opening period.

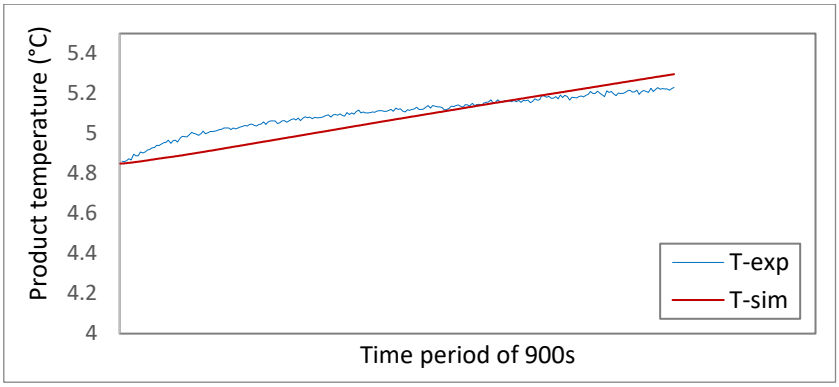

Figure 6.16: Average product temperature increase for door period of 900s with an air curtain.

It can be seen that the model-based product temperature is much more linear than the experimental product temperature though both the temperature histories represents similar range of increase rate between 0.4°C to 0.7°C. Since the food products is denser than other factors affected by warm air infiltration, as predicted, the temperature increase is also very low. The error range of the sensor used for measuring the product during the experiment is in the range of ±0.5°C and since the increase in product temperature itself is no more than 0.7°C, the value obtained from the experiment cannot be considered fit for assessing the energy consumption later.

Due to the uncertainty presented by the sensors during experiment, the simulation value will be considered for further calculations.

Based on internal air temperature, which is also affected by the cold products inside, a minimum level of difference can be observed between the model and simulation results and hence it can be indicated that the model is fairly accurate for conducting further assessments.

6.8 Summary

This chapter discussed the experimental set-up of a test rig to study the performance of an air curtain. The results show that for the experimental set-up considered the air curtain achieved best effectiveness at an air discharge velocity of 3 m/s.

This chapter also discussed the development and validation of a CFD model for use to predict the performance of air curtain in larger vehicles. The results of these simulations are presented in Chapter 7.

CHAPTER 7

Numerical investigation on the performance of an air curtain in distribution trucks at different discharge velocities and angles

Chapter 7 presents a numerical investigation on the performance of an air curtain on larger distribution truck from that considered in Chapter 6 and methods of optimising the energy performance of the air curtain further. The Computational Fluid Dynamics (CFD) model for this particular study was based on the modelling methodology presented in Chapter 6. Alongside an analysis of air curtain performance at different air discharge velocities, the chapter also considers the influence of air curtain positioning and discharge angles on the overall performance of the air curtain in terms of reducing infiltration and improving energy efficiency.

7.1 Introduction

As mentioned in Chapter 2, the majority of previous studies on air curtain performance indicate discharge velocity to be the most important parameter influencing the air curtain effectiveness [30, 40, 42, 43, 47, 48] . Another important design parameter is the discharge angle of the air curtain.

An experimental study conducted by Jaramillo et al. [47] assessed the energy consumption rate for different air curtain discharge angles between two rooms. The results indicated that having an air curtain outlet at a certain angle with respect to the direction of air infiltration can achieve better protection against air infiltration. Similarly, an experimental study conducted by Valkeapaa et al. [43] showed that adjusting the discharge angle can also help achieve improved air-curtain tightness against air leakage.

The above previous studies were focused on applications in cold rooms. Application of air curtains in food distribution trailers offers more challenges due to the limitation of space and weight and variation of external and internal conditions.

7.2 Physical domain

The truck's body is represented using a cuboid box with internal dimension of 8.00 m× 2.50 m× 2.20 m (L × W × H) (Figure 7.1). The insulation thickness is 0.075 m for the sidewalls and ceiling, and 0.1 m for the floor. The dimension of the door is 2.50 m× 2.20 m. The box is fully loaded, with food products placed on pallets with dimensions of 1.20 m× 0.80 m× 1.60 m (L × W × H).

The air curtain, Figure 7.1 (b), has a length of 2.30 m. The suction grille of the air curtain has a height of 0.10 m and is facing outwards, drawing air from the ambient. The discharge nozzle, with a width of 0.05 m is facing downwards and discharges the air drawn in from the ambient at the top of the door vertically downwards towards the floor of the trailer.

The cooling unit is modelled using a parallelepiped solid with dimension of 1.50 m× 0.75 m× 0.20 m (L × W × H), with outlet vent of 0.75 m× 0.20 m.

The truck is placed inside another cuboid solid, which represents the outer atmosphere with dimensions of 25 m× 8 m× 8 m (L × W × H).

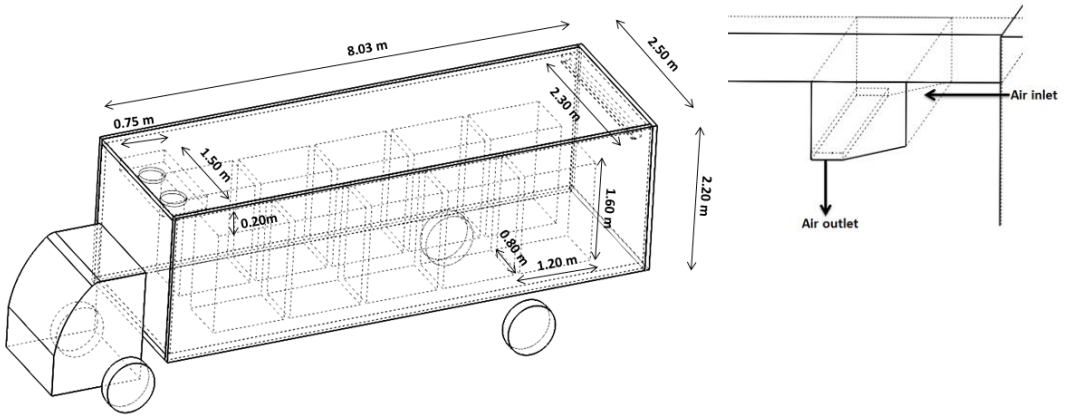

(a)

(b)

Figure 7.1: Physical domain used for the model.

7.2.1 Numerical solution procedure

Hexagonal mesh was adopted for the model using commercial code ANSYS ICEM 14.5. The meshed domain was simulated using ANSYS Fluent 14.5. Turbulence effects were modelled using the standard k-epsilon model for standard wall functions. The surface-to-surface (S2S) radiation model was adopted for the model to take into

consideration the thermal load due to radiation. A total door opening time of 15 minutes was assigned for each case to study the flow pattern for the maximum door opening period.

7.2.1.1 Boundary, initial and test conditions

For initial conditions, the air inside and outside the trailer was assumed to be static. Similar to a realistic situation, the cooling unit was switched on to maintain a consistent internal air and product temperature of 0°C. The ambient temperature is set to 20°C. When the door is opened, the cooling unit is switched off. Table 7.1 summarises the thermal properties of different materials used for the CFD simulation.

Table 7.1: Thermal properties for CFD simulation

	Density (kg/m^3)	Specific heat capacity (J/ kg·K)	Thermal conductivity (W/m·K)
Air	Ideal gas	1006	0.0242
Polyurethane	50	1470	0.022
Food product	300	1000	0.200

Since the cooling unit was switched off when the door was opened, no cooling source was accounted for during door openings. Simulations were performed for air curtain velocities 0 m/s to 5 m/s with 0 m/s representing no air curtain use.

The pressure jump was used to model the operation of the fan and the discharge air velocity.

7.2.1.2 Mesh independence

A structured hexagonal mesh was adopted for the spatial discretisation of the physical domain, ensuring refined elements in the region of higher gradient. Tests were conducted to verify the independence of the mesh, as illustrated in Figure 7.2. At a mesh number of 4.6 million elements, mesh independence was achieved.

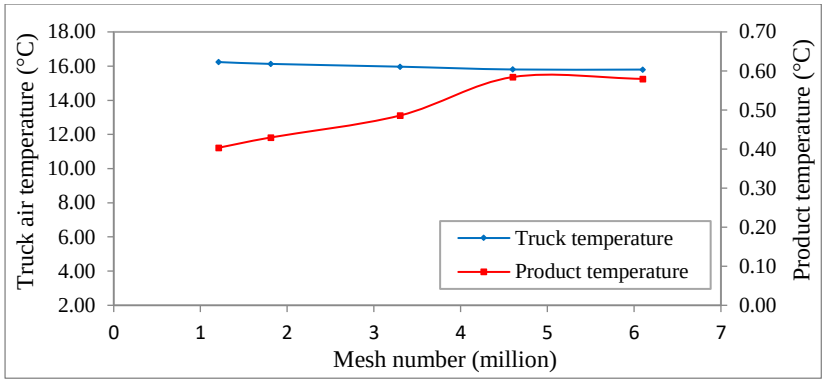

Figure 7.2: Mesh independence test.

7.3 Results and discussion

7.3.1 Natural infiltration mechanisms

Figure 7.3 presents the temperature variations in the truck after 15 minutes of the door opening without any protective mechanisms.

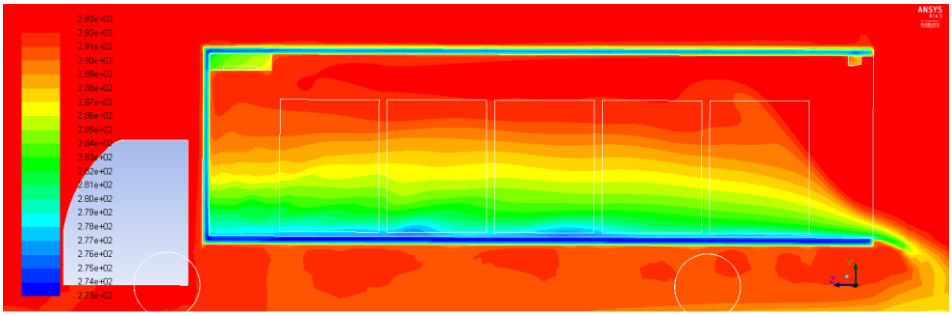

(a)

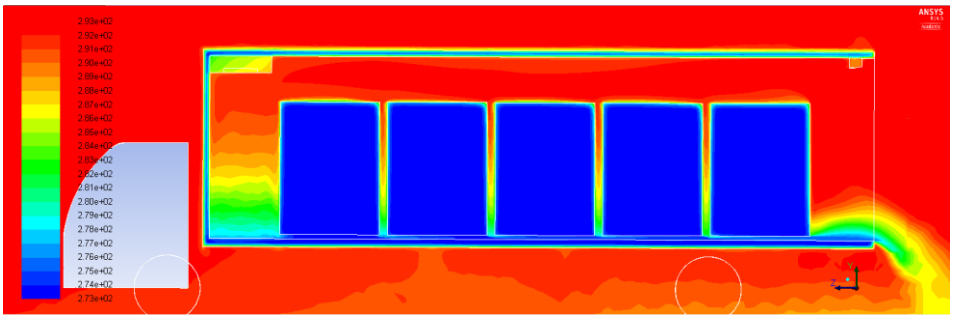

(b)

Figure 7.3: Temperature distribution inside the refrigerated body without an air curtain (a) mid-horizontal plane view, (b) mid-horizontal product view.

It can be seen from Figure 7.3 (a), that when the door of the box is opened the cold air starts flowing out from the lower area while the warm air starts infiltrating the space from the upper area. Since the cold air is denser than the warm air, it stays at the bottom of the truck (due to gravity) and flows out of the truck from the lower part of the opening. The warm air continues to flow into the truck through the upper part of the opening until it dominates the space left by the cold air flowing out.

As illustrated in Figure 7.3 (b), only the outer layer of the food products has higher temperature while the inner part continues to remain cold resulting in minimal increase in the overall product temperature. When the food products come in contact with the warm air during door openings, the outer area of the food products is the first contact point for initial heat transfer. However, since the food products are denser and have higher thermal mass than the internal air, the heat transfer process is not as instant as that of the air. Hence, only a minimal increase in food product temperature can be observed on the outer layer.

With regards to the internal air, it can be seen from the temperature contours that the air temperature in the upper area is almost the same as that of ambient air after door opening time of 15 minutes. The food products, however, also act as cooling source inside the box and hence the lower part continues to remain cold.

The crossflow of cold air flowing out and warm air flowing in (Figure 7.4) is a typical process of natural convection and hence this case is a representation of “natural infiltration”.

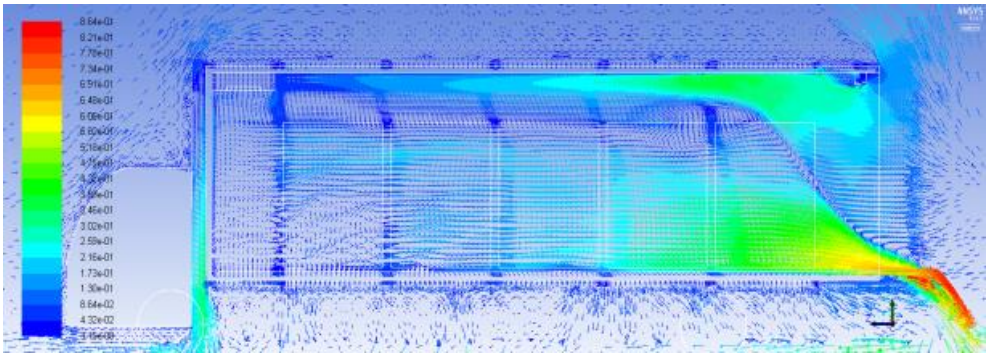

(a)

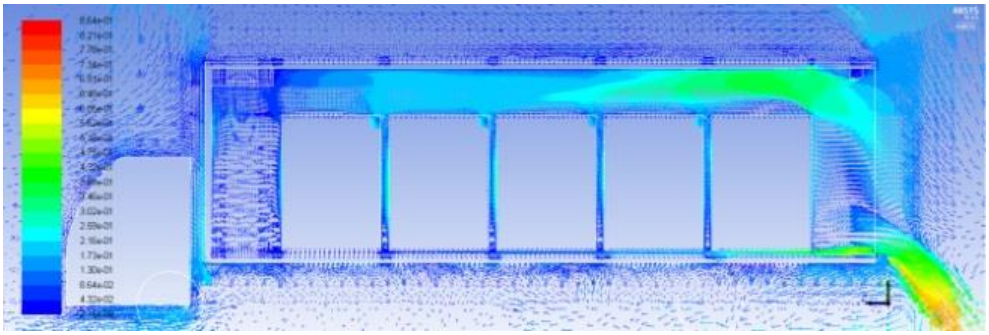

(b)

Figure 7.4: Velocity changes inside the refrigerated truck body without an air curtain (a) mid-horizontal plane view, (b) mid-horizontal product view.

The instantaneous opening of the door allows warm air to suddenly infiltrate the refrigerated space, resulting in high infiltration rate at the beginning. As the natural convective airflow starts building up, the thermal mass of the products starts to work as the cooling sources keeping the internal air temperature lower than the ambient temperature and maintaining natural convection. As the product temperature increases, the air temperature also increases and so will the impacts of natural convection, resulting in overall temperature increase.

7.3.2 Infiltration behaviour with air curtain at different discharge velocities and discharge angles

As mentioned earlier, along with the discharge velocity, the discharge angle has also proven to have an important impact on the performance of an air curtain. Hence, along with different discharge velocities, two different discharge angles, 0° and 10°, have been investigated for this study as illustrated in Figure 7.5. Discharge angle 0° represents straight vertical airflow. Angle 10° is in positive direction towards the opening in the opposite direction to the flow of infiltration air.

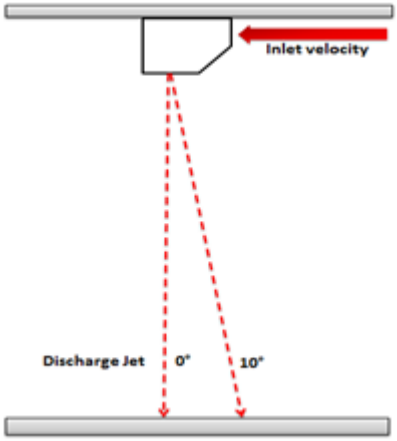

Figure 7.5: Infiltration condition at different discharge angles.

7.3.2.1 Infiltration behaviour at low discharge velocity of 1 m/s

Figure 7.6 presents the temperature contours at discharge velocity 1 m/s at two different discharge angles.

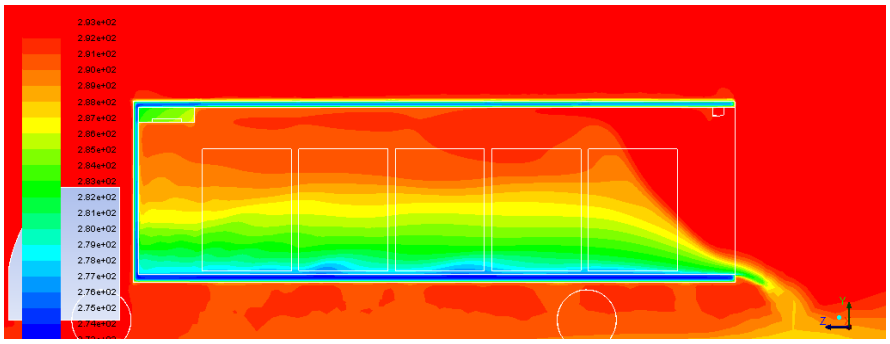

(a)

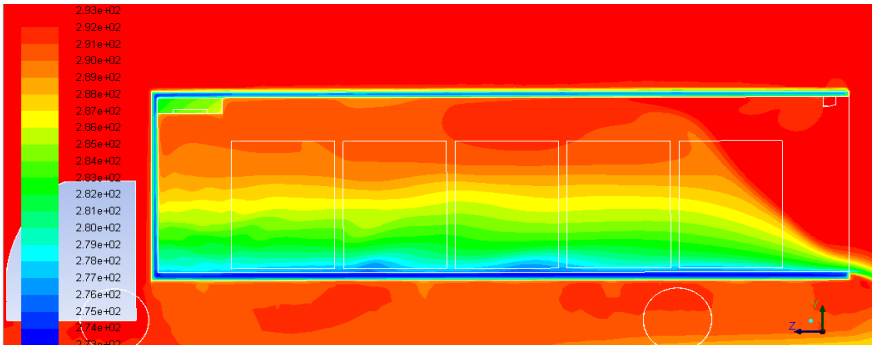

(b)

Figure 7.6: Temperature distribution inside the refrigerated body with an air curtain at mid-horizontal plane view (a) 0° and (b) 10°.

It can be seen that when the discharge velocity is as low as 1 m/s, the discharge from the air curtain outlet is not strong enough to reduce significantly air infiltration and the temperature of the air in the vehicle increases significantly in the upper part of the space. Because of the weak air curtain the air curtain angle, Figure 7.6 (b) has no effect on the air curtain performance.

7.3.2.2 Infiltration behaviour at low discharge velocity of 2 m/s

Figure 7.7 presents the temperature contours at discharge velocity 2 m/s.

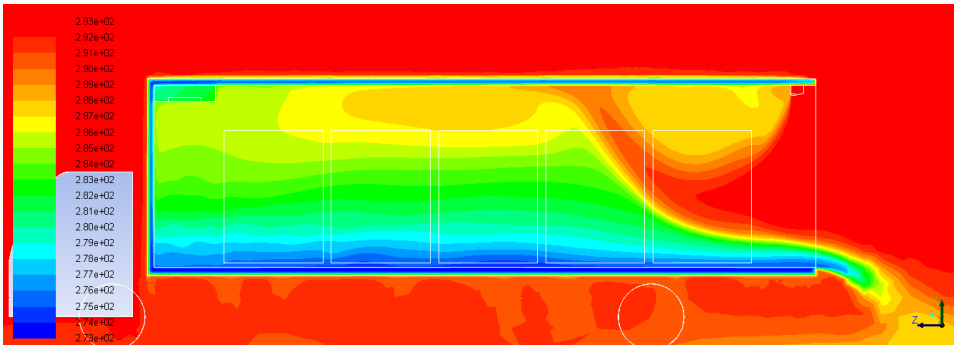

(a)

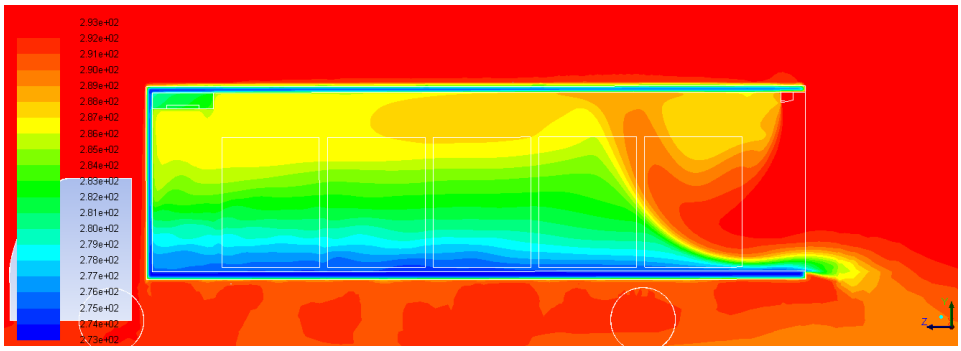

(b)

Figure 7.7: Temperature distribution inside the refrigerated body with an air curtain at mid-horizontal plane view (a) 0° and (b) 10°.

When the air curtain velocity is 2 m/s, the air curtain is effective over wider region and the infiltration is reduced, as presented in Figure 7.7. It can be seen that though the cold temperature is maintained better than the case of 1 m/s, the discharge velocity is still not strong enough to prevent the outflow of the cold air as the flow from the air curtain does not reach the floor.

7.3.2.3 Infiltration behaviour at discharge velocity of 3 m/s

Figure 7.8 presents the temperature contours at discharge angles 0° and 10° at a velocity of 3 m/s.

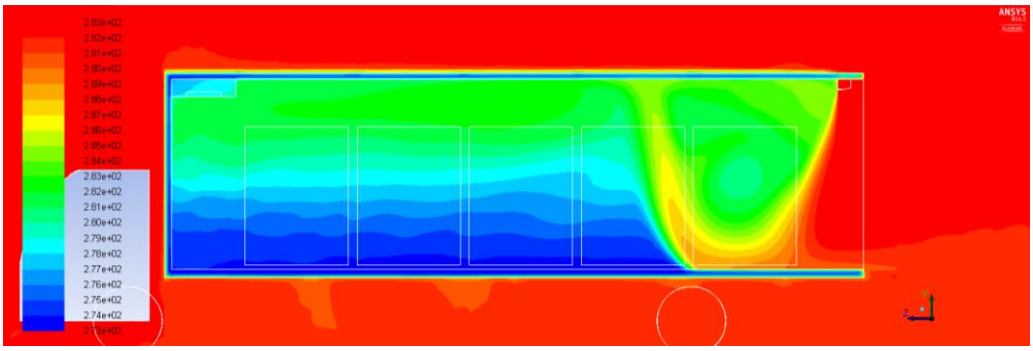

(a)

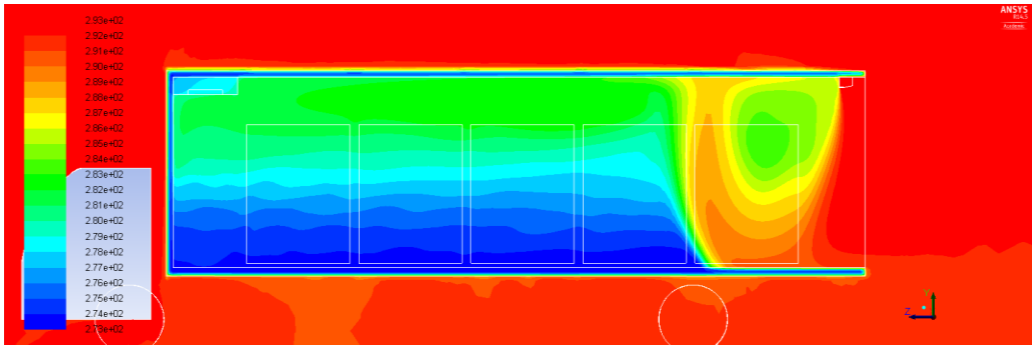

(b)

Figure 7.8: Temperature distribution inside the refrigerated body with an air curtain at mid-horizontal plane view (a) 0° and (b) 10°.

A much better maintenance of temperature can be observed with air curtain at discharge velocity 3 m/s in comparison to the cases of 1 m/s and 2 m/s. It can be seen in Figure 7.8 that in both the cases, the air curtain reaches the floor reducing air infiltration from the outside.

In both the cases, the jet bends into the truck but for the 10° case, resistance to infiltration is better, reducing its effect in the inner areas of the box.

7.3.2.4 Infiltration behaviour at discharge velocity of 4 m/s

Figure 7.9 illustrates the discharge velocity contours near the opening when the air curtain velocity is increased to 4 m/s.

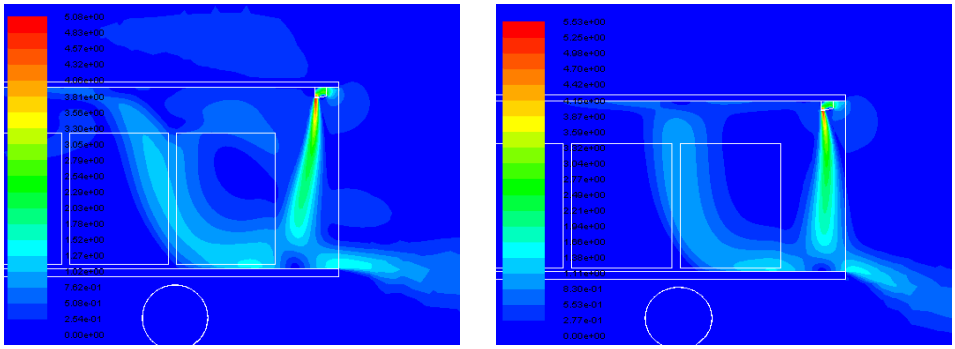

(a) (b)

Figure 7.9: Discharge jet from the air curtain at velocity of 4 m/s and discharge angles of (a) 0° and (b) 10°.

The air curtain velocity at 4 m/s is stronger in comparison to 3 m/s and can reach the floor, unaided by the coanda effect created by the presence of the products close to the door, particularly in the case of the 10°. The resulting temperature distribution at the central plane of the box is shown in Figure 7.11. It can be seen that the temperature close to the floor remains low but the temperature close to the door rises above that for the 3 m/s air velocity shown in Figure 7.8. This is due to the increased turbulence and mixing between the outdoor air and the air curtain air at higher air velocity. Compared to Figure 7.10 (a) and (b) it can be seen that the 10° angle air curtain provides better protection than 0° angle.

Figure 7.10 illustrates the temperature contours at discharge angles 0° and 10° at velocity 4 m/s.

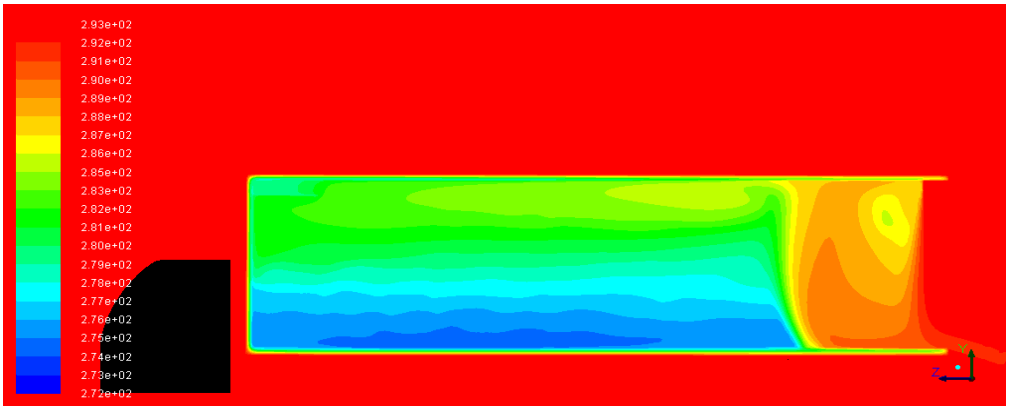

(a)

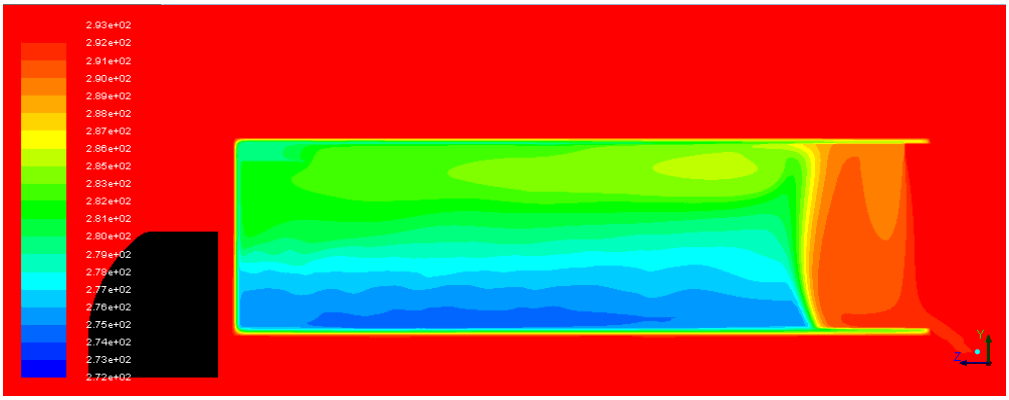

(b)

Figure 7.10: Temperature distribution inside the refrigerated body with an air curtain at mid-horizontal plane view (a) 0° and (b) 10°.

7.3.2.5 Infiltration behaviour at discharge velocity of 5 m/s

Figure 7.11 presents the velocity contours of 0° and 10° at 5 m/s.

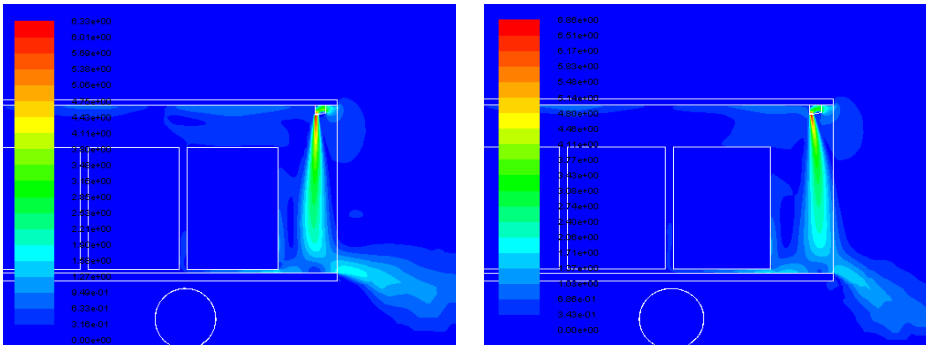

(a) (b)

Figure 7.11: Discharge jet from air curtain outlet at velocity 5 m/s and discharge angles (a) 0° and (b) 10°.

At air curtain velocity 5 m/s, it is observed that the 0° case had a vertical jet, indicating very strong forced convection. For the 10° case, the air curtain flows outwards in the higher part due to its higher momentum and then bends to become near vertical. In both cases the air curtain reaches the floor without the air of the coanda effect but with the penalty of increased turbulence and mixing with the outdoor air. The resulting temperature contours are shown in Figure 7.12.

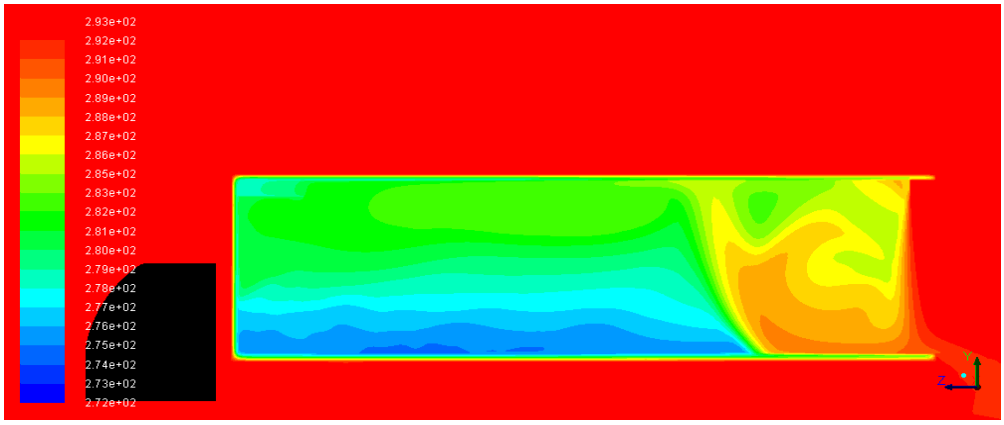

(a)

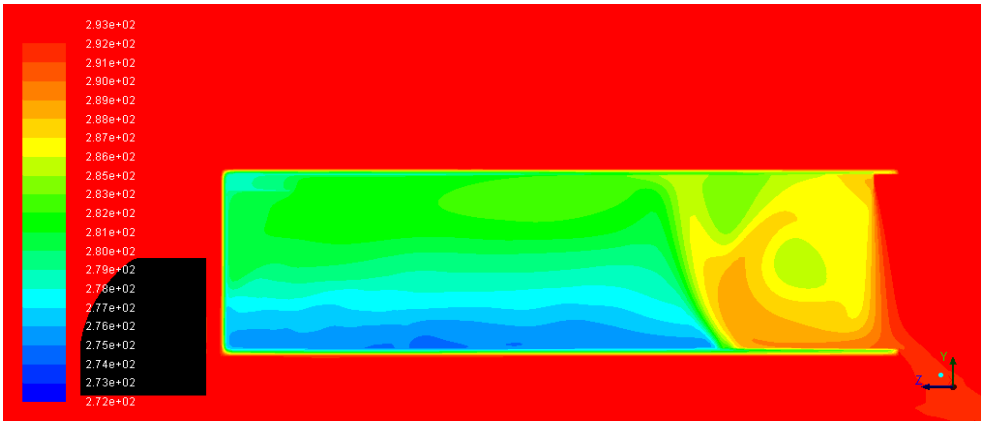

(b)

Figure 7.12: Temperature distribution inside the refrigerated body with an air curtain at mid-horizontal plane view (a) 0° and (b) 10°.

It can be seen that the warm air infiltration affects a larger area close to the door.

7.3.3 Product temperature history at different air curtain velocity without and with air curtain

Figure 7.13 presents the average temperature of the overall food products after 15 minutes of door opening at different discharge velocities and at two different air curtain discharge angles.

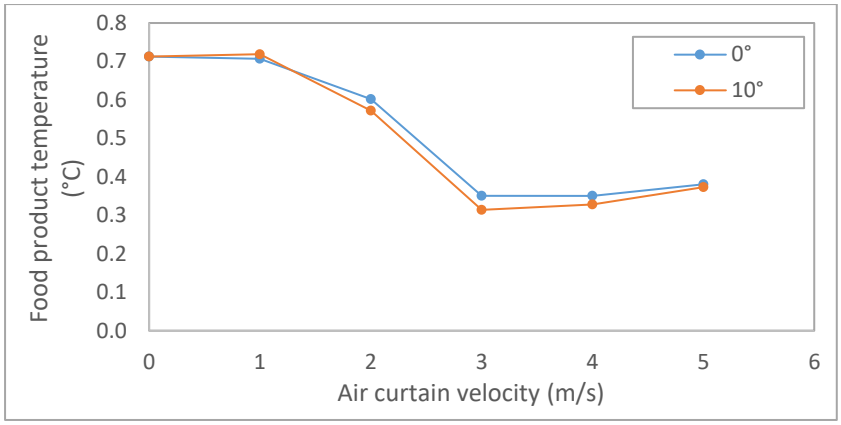

(a)

Figure 7.13: Average food product temperature increase after door opening period of 15 minutes at different air curtain velocities.

It can be seen that at discharge velocity 0 m/s, the temperature increase is highest due to the presence of no protective mechanism. The infiltration of warm air from outside causes the food temperature to rise with the time of door opening.

The air curtain effectiveness increases slightly at a velocity of 2 m/s and reaches maximum effectiveness at 3 m/s. Above this velocity the effectiveness begins to reduce slightly due to the increased turbulence and mixing occurring between the air curtain and the ambient air.

The effectiveness of air curtain angle is a function of the discharge velocity. It increases as the velocity of the air curtain increases to 3 m/s and then decreases as the turbulence and mixing effects become more dominant.

7.3.4 Recovery energy with and without an air curtain

The results for energy consumption in this chapter will be presented in form of recovery energy. Recovery energy can be defined as the energy required to pulldown the overall temperature gain during door opening (internal air, food products and wall) to the initial set temperature. This is assumed to be equal to the energy added to the space and products during door opening. The recovery energy is calculated using Eq 7.1.

$$E_r = \left(M_{air} Cp_{air} \left(T_{fa} - T_{ia}\right)\right) + \left(M_{prod} Cp_{prod} \left(T_{fp} - T_{ip}\right)\right) + \left(M_{wall} Cp_{wall} \left(T_{fw} - T_{iw}\right)\right) \quad 7.1$$

Where E_r represents the total recovery energy, Cp_{air} the specific heat capacity of internal air, Cp_{prod} the specific heat capacity of food products, Cp_{wall} the specific heat capacity of wall, M_{air} the mass of internal air, $M_{prod}$the mass of food products, M_{wall} the mass of wall, T_{ia} the initial temperature of internal air, T_{ip} the initial temperature of food products, T_{iw} the initial temperature of wall, $T_{fa}$the final temperature of internal air, $T_{fp}$the final temperature of food products and T_{fw} the final temperature of wall

7.3.3.1 Recovery energy at different discharge velocities

Figure 7.14 presents the recovery energy after 15 minutes of door opening at different air curtain velocities.

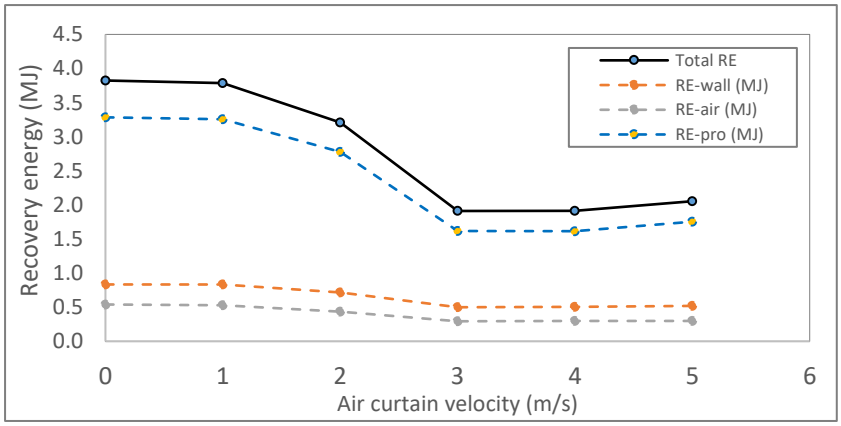

Figure 7.14: Recovery energy at different air curtain velocities.

It can be seen that the recovery energy is at its highest without any air curtain. As the air curtain velocity increases, a drop in recovery energy can be observed with the minimum at the air curtain velocity of 3 m/s when the air curtain effectiveness is at its maximum.

At this velocity the recovery energy is reduced by 50% compared to the case with no air curtain.

Figure 7.14 also shows that the products in the vehicle account for the highest recovery energy compared to the air and the wall due to their much higher thermal mass.

7.3.3.2 Recovery energy at different discharge angles

Figure 7.15 presents the recovery energy after 15 minutes of door opening at the two curtain discharge angles.

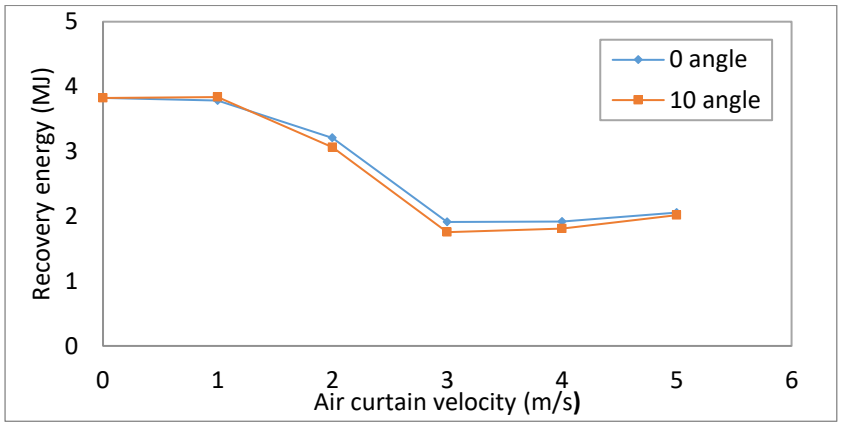

Figure 7.15: Recovery energy at different air curtain angles.

As discussed earlier, the 10° discharge angle is more effective compared to the 0° angle at velocities where the air curtain attains best effectiveness, Maximum improvement in performance is at air curtain discharge velocity of 3 m/s. At this point the 10° angle will lead to a reduction in recovery energy of approximately 9% compared to the 0° angle.

7.5 Summary

Warm air infiltration during door openings in temperature-controlled vehicles can result in significant increase in the refrigeration load and energy consumption.

The experimental and numerical investigations carried out on the performance of air curtains showed that the technology can significantly help reduce the temperature gain during door openings by creating a barrier against outdoor air infiltration. At optimal discharge velocity (air curtain discharge velocity where recovery energy is lowest), for the conditions investigated it was found that the air curtain can reduce the recovery energy by 50% compared to no air curtain. An 18 tonne distribution vehicle does an average of 9 delivery rounds per day with 5 door openings per delivery with average door opening time of 15 minutes (distribution parameters from Chapter 2 based on survey). The average fuel consumption was estimated to be approximately 1.00 l/h to 2.38 l/h and environmental impact 2.82 kgCO_2e/h and 6.70 kgCO_2e/h. Use of air curtain can reduce the overall fuel consumption and GHG emissions by nearly 35%.

However the less the duration of door opening, the less would be the share of thermal load due to infiltration and hence less would be the overall energy savings using an air curtain.

At the optimum velocity it was also found that having an air curtain discharge angle towards the ambient air, can increase the reduction in the recovery energy by an additional 9% compared to a 0° discharge angle.

CHAPTER 8

Conclusions and recommendations for future work

The thesis considered energy demand and environmental impacts of food transport refrigeration systems. The thesis considered and compared current and emerging technologies. It also considered through experimental tests and CFD modelling the potential of air curtains in reducing air infiltration and energy demand through the use of air curtains to reduce air infiltration during door openings. This chapter summarises the findings of the whole thesis and provides suggestions for future work in the area of transport refrigeration.

8.1 Thesis overview

This research makes a contribution to the overall effort of reducing the high energy demand and growing environmental concerns associated with transport refrigeration through the assessment of several prominent energy-reduction technologies. Initially, the energy consumption and environmental impacts of auxTRUs during distribution of different food products was analysed. This was done by conducting an investigation work in collaboration with a leading logistics company Kuehne & Nagel and by developing a theoretical steady-state model to perform all the calculations.

The vast majority of auxTRUs are powered by diesel fuel which contributes to Greenhouse Gas Emissions (GHEs) but also particulate emissions (PMs) most based on these results. The use of diesel particularly in city centre is coming under increasing scrutiny and legislation so the food transport refrigeration industry and retail food organisations are looking for alternative solutions to diesel powered TRUs. For this reason, four alternative technologies were analysed in the thesis to identify their potential in terms of energy efficiency, ease of application and environmental considerations. The four technologies are, cryogenic TRU system using LN_2 or LCO_2, hydrogen fuel cell driven TRU and all-electric powered TRU. These analysis were conducted using the validated model. Both the production and operation related emissions were compared. With regards to the operation phase, all four alternative technologies showed negligible GHG emissions. However, all technologies required energy intensive processes for the production of the cryogenic fluids and hydrogen in

the case of the fuel cell TRU which lead to significant emissions if the energy used is not from low emission sources such as renewable energy.

Considering the current development of the technologies and trends, all electric-powered TRU appears to be the technology with the highest potential for last mile distribution in urban areas using vans or rigid body vehicles where the opportunity exists to charge the batteries at the food distribution centre.

The analysis of auxTRUs, has that infiltration is the highest source of thermal load during multi-drop urban distribution where there are frequent door openings. This is an issue for all temperature controlled distribution vehicles and to reduce infiltration losses this thesis has investigated the effectiveness of air curtains in achieving this.

The investigations involved experimental test on a refrigerated insulated box in the laboratory of dimensions and construction similar to that of home food distribution vehicles and modelling using computational fluid dynamics.

The CFD results were validated against results obtained from the experimental investigations. The model was used to study the performance of air curtains in larger distribution vehicles.

8.2 Main conclusions and contributions to knowledge

The following are the main conclusions of this thesis:

1. AuxTRUs can account for significant energy usage and GHG emissions. The fuel consumption required auxiliary diesel engines to run the TRU for chilled and frozen food distribution can vary between 1.5 l/h and 4.71 l/h and the indirect GHG emissions from 2.68 kgCO_2e/h to 9.64 kgCO_2e/h depending on the vehicle and distribution type. The direct GHG emissions from refrigerant leakage can vary between 0.002 kgCO_2e/h and 0.012 kgCO_2e/h for the different vehicle categories and annual refrigerant leakage rates of between 5% and 20% annually. It should be noted, though, that these results are dependent on the distribution parameters used in the analysis. The results from this analysis have been published in a report by Cenex for Transport for London (TfL) under the project of LoCity.

2. The results outlined above, indicate that TRUs powered with auxiliary diesel engine contribute significantly to greenhouse gas emissions. For this reason, a number of alternative technologies have been analysed. Among these are cryogenic systems using liquid nitrogen (LN_2) or liquid carbon dioxide (LCO_2). The majority of studies conducted on these systems did not include emissions from manufacturing the cryogenic fluids.

   During the operation phase, cryogenic transport refrigeration system using LCO_2 and LN_2 produce minimal GHG emissions. However, the emissions of cryogenic fluids during the production phase were estimated up to 66% higher compared to the production emissions of diesel fuel if renewable energy is not used for their manufacture.

   It was also estimated that the fuel intensity of diesel powered vapour compression TRUs (1.19 l/h to 3.03 l/h) is much lower than the mass intensity of the LCO_2 and LN_2 cryogenic TRUs (21.81 kg/h to 62.63 kg/h) for the distribution scenarios investigated in this study. Diesel driven systems therefore offer much greater range of temperature controlled food distribution without tank refilling compared to cryogenic systems.

   Please note, all the emissions factors used for calculations are subject to changes. Changes in the emission factor will present changes in the results alongside.

3. Alternative technologies considered were the hydrogen fuel cell and all-electric powered TRU systems. In both systems, the main TRU is vapour compression cycle but the energy carriers are H_2 for the fuel cell and electricity for the all-electric system. For the same distribution scenarios, the consumption of diesel in auxTRU was found to vary between 1.19 l/h and 3.03 l/h, the mass consumption of H_2 between 0.26 kg/h and 0.46 kg/h, and electrical consumption of all-electric TRU between 4.52 kWh and 11.52 kWh. The energy density comparison of these technologies is provided in Appendix A.
4. Infiltration during door openings was found to account for the highest share of thermal load, more than 50% in cases of frequent delivery drops and longer door opening duration. This load is independent of the refrigeration technology employed.

The experimental investigations and modelling in this study have shown that the use of air curtains can reduce air infiltration into the vehicle during door openings by almost 30% in small vehicles with door area of 2.3 m^2 and up to 50% in large vehicles with door opening area of 5.5 m^2.

5. There are a number of design and operating parameters that can be used to optimise the performance of air curtains. Among these, a very important parameter is the discharge velocity of the air curtain. Too low a velocity and the air curtain will not reach the floor and thus will not provide full sealing, reducing its effectiveness to reduce infiltration. Too high a velocity will increase turbulence and mixing between external warm air and chilled air in the vehicle, increasing the rate of infiltration. The optimum discharge velocity is a function of the loading of the vehicle and the interaction between the air curtain and the products close to the door.
6. The discharge angle is another important design parameter. A discharge angle towards outside can provide better resistance against infiltration. In the analysis carried out, angle 10° can provide and energy savings upto 10% in addition to the energy saving using optimised discharge velocity. This angle will be a function of the air curtain velocity, the opening height of the door, the temperature difference inside to outside and the outside air velocity and direction. However, the two different angles were only studied to understand the impact of discharge angle on the protective mechanisms. Further studies on different angles will determine more optimum parameter.

8.3 Suggestions for future work

This thesis has considered alternative technologies to auxTRUs and methods to reduce energy requirements during temperature-controlled transportation of food. The analyses were conducted using modelling and experimental methods.

The majority of the work carried out for the first part of the thesis was mainly based on modelling. For this reason, a possible future work would be to analyse these technologies more in-depth using an experimental approach. The experimental data could provide more solid verification of modelling results.

For the numerical investigations, there are many parameters that can be explored in detail for the optimisation of an air curtains in refrigerated food transport vehicles.

Due to time constraints only a few parameters were investigated in this study. However, there are many other parameters that can be investigated such as a twin (double band) air curtain to increase the overall efficiency, and variable speed curtains with the speed adjusted according to the loading of the vehicle to ensure best sealing at all operating conditions at reduced power consumption.

The experimental study of the air curtain was conducted in a lab using a lab-scaled trailer. Future work would be to investigate the performance of air curtains on a larger trailer during actual food distribution. In the laboratory, conditions are much steadier, compared to ambient conditions during actual distribution where the air curtain's performance will be influenced by wind velocity and direction.

Other parameters that are worth of investigation include increasing the thermal resistance of the walls of the refrigerated box through the use of vacuum insulation and the use of solar PV to provide some of the energy required to power the on-board refrigeration system.

REFERENCES

[1] EU: Non-road Engines, Emissions Standard, https://www.dieselnet.com/standards/eu/nonroad.php 2016 (2014).

[2] Dearman, Fridgehub, 'Demand for refrigerated transport could be 'devastating', http://www.dearman.co.uk/#!fridgehub-Demand-for-refrigerated-transport-could-be-devastating/ccrp/5540fdb50cf2731335030f26 2016 (2015) 1.

[3] Global Cold Chain News, , UK temperature controlled-transport market booms (2011).

[4] P. Glouannec, B. Michel, G. Delamarre, Y. Grohens, Experimental and numerical study of heat transfer across insulation wall of a refrigerated integral panel van, Appl. Therm. Eng. 73 (2014) 196-204.

[5] F. Monforti-Ferrario, J. Dallemand, I. Pinedo Pascua, V. Motola, M. Banja, N. Scarlat, N. Scarlat, L. Castellazzi, L. Labanca, P. Bertoldi, D. Pennington, M. Goralczyk, E.M. Schau, E.M. Saouter, S. Sala, B. Notarnicola, G. Tassielli, P. Renzulli, , Energy use in the EU food sector: State of play and opportunities for improvement ISBN 978-92-79-48299-1 (PDF) ISBN 978-92-79-48298-4 (print) (2015) 9.

[6] J. Fichtinger, J.M. Ries, E.H. Grosse, P. Baker, Assessing the environmental impact of integrated inventory and warehouse management, Int J Prod Econ 170, Part C (2015) 717-729.

[7] J. Rodrigue, Chapter 8- Transport, Energy and Environment, in: The Geography of Transport Systems (3rd Edition), Taylor & Francis Group, 2013.

[8] Z. Bengherbi, Liquid Air on the European Highway- The economic and environmental impact of zero-emission transport refrigeration 11 (2015) 3.

[9] J.L. Rodríguez-Muñoz, J.M. Belman-Flores, Review of diffusion–absorption refrigeration technologies, Renewable and Sustainable Energy Reviews 30 (2014) 145-153.

[10] Cenex, Auxiliary temperature reduction units in the Greater London area- Air quality and climate change impacting emissions from temperature controlled transport 5371158 (2018).

[11] Transport for London (TfL), Auxiliary temperature reduction units in the Greater London area- Overview of the study progress to date 5371158 (2018).

[12] ATP, Guide to ATP for Road Hauliers and Manufacturers (03/2017).

[13] DEFRA, , Greenhouse Gas Impacts of Food Retailing SID 5 (2008).

[14] S.A. Tassou, G. De-Lille, Y.T. Ge, Food transport refrigeration – Approaches to reduce energy consumption and environmental impacts of road transport, Appl. Therm. Eng. 29 (2009) 1467-1477.

[15] A. Rai, S.A. Tassou, Energy demand and environmental impacts of alternative food transport refrigeration systems, Energy Procedia 123 (2017) 113-120.

[16] A. Rai, S.A. Tassou, Environmental impacts of vapour compression and cryogenic transport refrigeration technologies for temperature controlled food distribution, Energy Conversion and Management (2017).

[17] UNEP, Lower-GWP Alternatives in Commercial and Transport Refrigeration: An expanded compilation of propane, CO2, ammonia and HFO case studies, Section2: Transport Refrigeration Case Studies DTI/2015/PA (2015).

[18] Global Cold Chain News, Special report: Cryogenic truck refrigeration with nitrogen, Diesel powered fridge alternatives (02/2011) 3.

[19] Fridgehub, Fridgehub, ‘Boris to consider impact of refrigerated trucks on London’s air quality’ 2017 (2015).

[20] P.K. Sarma, S. Das, S. Senapati, U.J. Baruah, U.K. Sah, Refrigeration using waste heat from an engine Bharath University: Chennai 600 073 (2011).

[21] FRIGOBLOCK, Energy Cost Savings with the FRIGOBLOCK Alternator Drive System 2016.

[22] Dearman, , Driving Clean Cold Dearman Zero-Emission- Transport Refrigeration System (Accessed 2016).

[23] Carrier Transicold, Truck/trailer refrigeration unit operation and service manual- Genesis R70, Genesis R90, Genesis TR1000, Multi-Temp 62-02884 Change 05/10 (1997).

[24] Carrier Transicold, Carrier Transicold Presents Latest Innovations for Sustainable Refrigerated Transport at Transport Complete Show (RUEIL-MALMAISON, France - Mar. 14, 2016) 2017 (2016).

[25] Cambridge Refrigeration Technology, Thermal Insulation, http://www.crtech.co.uk/pages/consultancy/insulation.asp 2016 1.

[26] A. Lawton, R. Marshall, , Developments in refrigerated transport insulation since the phase out of CFC and HCFC refrigerants International Congress of Refrigeration,Beijing (2007).

[27] M. Alam, H. Singh, S. Suresh, D.A.G. Redpath, Energy and economic analysis of Vacuum Insulation Panels (VIPs) used in non-domestic buildings, Applied Energy 188 (2017) 1-8.

[28] F. Isaia, S. Fantucci, A. Capozzoli, M. Perino, Vacuum Insulation Panels: Thermal Bridging Effects and Energy Performance in Real Building Applications, Energy Procedia 83 (2015) 269-278.

[29] S.E. Kalnæs, B.P. Jelle, Vacuum insulation panel products: A state-of-the-art review and future research pathways, Applied Energy 116 (2014) 355-375.

[30] A. Hadawey, S.A. Tassou, REDUCING THE ENVIRONMENTAL IMPACT OF REFRIGERATED TRANSPORT VEHICLES USING VACUUM INSULATION PANELS (VIPs) Internal Report (04/2009).

[31] O. Adekomaya, T. Jamiru, R. Sadiku, Z. Huan, Minimizing energy consumption in refrigerated vehicles through alternative external wall, Renewable and Sustainable Energy Reviews 67 (2017) 89-93.

[32] A. Rai, S.A. Tassou, Environmental Impacts of Temperature Controlled Food Distribution, SusTEM2017 Energy Research Centre of the Netherlands (ECN) 4th (2017).

[33] S.A. Tassou, Energy Savings in Refrigerated Transport, http://www.grimsby.ac.uk/documents/defra/08jun10_transport.pdf 8th June 2010 (2010).

[34] S.A. Tassou, M. Kolokotroni, B. Gowreesunker, V. Stojceska, A. Azapagic, P. Fryer, S. Bakalis, Energy demand and reduction opportunities in the UK food chain, Proceedings of the Institution of Civil Engineers - Energy 167 (2014) 162-170.

[35] Air Resource Board, Technology Assessment: Transport Refrigerators (2015).

[36] T. Lafaye de Micheaux, M. Ducoulombier, J. Moureh, V. Sartre, J. Bonjour, Experimental and numerical investigation of the infiltration heat load during the opening of a refrigerated truck body, International Journal of Refrigeration 54 (2015) 170-189.

[37] ASHRAE, Chapter 12- Refrigeration Load, in: 2002 ASHRAE Handbook, 2002.

[38] M. Liu, W. Saman, F. Bruno, Computer simulation with TRNSYS for a mobile refrigeration system incorporating a phase change thermal storage unit, Applied Energy 132 (2014) 226-235.

[39] C.P. Tso, S.C.M. Yu, H.J. Poh, P.G. Jolly, Experimental study on the heat and mass transfer characteristics in a refrigerated truck, International Journal of Refrigeration 25 (2002) 340-350.

[40] A.M. Foster, M.J. Swain, R. Barrett, P. D'Agaro, S.J. James, Effectiveness and optimum jet velocity for a plane jet air curtain used to restrict cold room infiltration, International Journal of Refrigeration 29 (2006) 692-699.

[41] A. Azzouz, J. Gosse, M. Duminil, Experimental determination of cold loss caused by opening industrial cold-room doors, International Journal of Refrigeration 16 (1992) 57-66.

[42] A.M. Foster, M.J. Swain, R. Barrett, P. D'Agaro, L.P. Ketteringham, S.J. James, Three-dimensional effects of an air curtain used to restrict cold room infiltration, Applied Mathematical Modelling 31 (2007) 1109-1123.

[43] A. Valkeapaa, K. Siren, I. Raappana, Air Leakage through Horizontal Air Curtains - an Experimental Study- Helsinki University of Technology, Espoo, Finland
, https://www.aiha.org/aihce06/handouts/a2valkeapaa.pdf 2017 9.

[44] S. Goubran, D. Qi, W.F. Saleh, L.(. Wang, R. Zmeureanu, Experimental study on the flow characteristics of air curtains at building entrances, Building and Environment 105 (2016) 225-235.

[45] L.(. Wang, Z. Zhong, An approach to determine infiltration characteristics of building entrance equipped with air curtains, Energy and Buildings 75 (2014) 312-320.

[46] Brightec nl, Blueseal technical specification, http://brightec.nl/wp-content/uploads/2018/01/Spec-sheet-BlueSeal-air-curtain.pdf 2018 2.

[47] J. Jaramillo, A. Oliva, C.D.P. Segarra, C. Oliet, Application of Air Curtains in Refrigerated Chambers, International Refrigeration and Air Conditioning Conference- Purdue University Paper 973 (2008) 2403, Page 1-2403, Page 8.

[48] J.C. Gonçalves, J.J. Costa, A.R. Figueiredo, A.M.G. Lopes, CFD modelling of aerodynamic sealing by vertical and horizontal air curtains, Energy and Buildings 52 (2012) 153-160.

[49] Hubbard, Hubbard Eutectic System – Transport Refrigeration Unit for deep frozen and ice cream applications.

[50] M. Liu, F. Bruno, W. Saman, Thermal performance analysis of a flat slab phase change thermal storage unit with liquid-based heat transfer fluid for cooling applications, Solar Energy 85 (2011) 3017-3027.

[51] T. Hoying, Power Ahead with Commercial Fuel Cells- PlugPower, Plug Power Inc. POWERAhead with Commercial Fuel Cells 2017 (2014).

[52] R. Garde, F. Jiménez, T. Larriba, G. García, M. Aguado, M. Martínez, Development of a Fuel Cell-Based System for Refrigerated Transport, Energy Procedia 29 (2012) 201-207.

[53] A. Bahaj, Photovoltaic power for refrigeration of transported perishable goods, Photovoltaic Specialists Conference, 2000. Conference Record of the Twenty-Eighth IEEE 28 (2000) 1563.

[54] S. Kalbande, S. Deshmukh, Photovoltaic Based Vapour Compression Refrigeration System for Vaccine Preservation, Universal Journal of Engineering Science Vol. 3(2), pp. 17 - 23 3 (2013).

[55] B. Elliston, M. Dennis, M. Dennis, Feasibility of Solar-Assisted Refrigerated Transport in Australia Solar09 (2009).

[56] H. Pedolsky, R. La Bau, International Refrigeration and Air Conditioning Conference, Reintroduction of Cryogenic Refrigeration for Cold Transport Paper 1021 (2010) 2137.

[57] Z. Bengherbi, Liquid Air on the European Highway, Liquid Air on the European Highway: The economic and environmental impact of http://media.wix.com/ugd/96e3a4_c6f6a0901cf943119aa435f6c09b8380.pdf (2015).

[58] Research and Markets, Global Refrigerated Warehousing Market 2014-2018: Key Vendors are AmeriCold, Lineage, Preferred Freezer Services and Swire, http://www.prnewswire.co.uk/news-releases/global-refrigerated-warehousing-market-2014-2018-key-vendors-are-americold-lineage-preferred-freezer-services-and-swire-279148131.html 2016 (2014) 1.

[59] S.A. Tassou, A. Hadewey, Y.T. Ge, B.L.d. Groutte, Carbon Dioxide Cryogenic Transport refrigeration Systems, The Centre for Energy and Built Environment Research 1 (2010).

[60] Dearman, Dearman- A Technical Introduction, Pg. 3, http://dearman.co.uk/wp-content/uploads/2016/05/Dearman-A-Technical-Introduction-For-Web-1.pdf (Accessed 2016).

[61] natureFridge, natureFridge specification brochure, http://naturefridge.com/wp-content/uploads/natureFridge_brochure(EN)small.pdf 2016 18.

[62] R. Saidur, M. Rezaei, W.K. Muzammil, M.H. Hassan, S. Paria, M. Hasanuzzaman, Technologies to recover exhaust heat from internal combustion engines, Renewable and Sustainable Energy Reviews 16 (2012) 5649-5659.

[63] S. Dieter, L. Thomas, G. Jürgen, Waste Heat Recovery for Commercial Vehicles with a Rankine Process (2012).

[64] K.K. Srinivasan, P.J. Mago, S.R. Krishnan, Analysis of exhaust waste heat recovery from a dual fuel low temperature combustion engine using an Organic Rankine Cycle, Energy 35 (2010) 2387-2399.

[65] Y. Zhang, Y. Wu, G. Xia, C. Ma, W. Ji, S. Liu, K. Yang, F. Yang, Development and experimental study on organic Rankine cycle system with single-screw expander for waste heat recovery from exhaust of diesel engine, Energy 77 (2014) 499-508.

[66] Y. Lu, Y. Wang, C. Dong, L. Wang, A.P. Roskilly, Design and assessment on a novel integrated system for power and refrigeration using waste heat from diesel engine, Appl. Therm. Eng. 91 (2015) 591-599.

[67] J. Wang, J. Wu, Investigation of a mixed effect absorption chiller powered by jacket water and exhaust gas waste heat of internal combustion engine, International Journal of Refrigeration 50 (2015) 193-206.

[68] Paneltex, Paneltex Electric Trucks and Zero-Emission Vehicles 2017 (2014).

[69] Mitsubishi, TEJ35A Electric Transport Refrigeration Unit Using Inverter for Light Trucks (June 2014) Mitsubishi Heavy Industries Technical Review Vol. 51 No. 2 (June 2014) (2014).

[70] J. Prynn, Electric van fleet to guarantee food from farms is truly green in London (9 May 2016), Evening Standard (2016).

[71] MAGTEC, Magtec- Electric Refrigerated Vehicles (workshop presentation) (2017).

[72] Global Cold Chain News, Paneltex enters electric truck challenge (Oct 16, 2012) 2017 (2012).

[73] M. Schmied, W. Knorr, Calculating GHG emissions for freight forwarding and logistics services in accordance with EN 16258 (2012).

[74] Defra - Greenhouse Gas Conversion factor 2015, , DCFCarbonFactors_29_1_2016_161748 Version1.2 (2015).

[75] Gogreen, Go green Adam Model APU specification, http://www.gogreenapu.com/ 2019.

[76] Earth data, Atmospheric science data center, https://eosweb.larc.nasa.gov/ 2015.

[77] Hubbard, Keep it Cool, A Guide to Transport Refrigeration (Accessed 2016).

[78] Linde, Cryogenic Standard Tanks LITS 2, Datasheet of cryogneic storage tanks (2016).

[79] ThermoKing, A Matter of Degrees - Thermo King receives first U.S order for cryogenics units, http://thermoking.com/aboutus/tradepubs/matterofdegrees/modfall02.pdf (2002).

[80] D. Cowan, 2016 (The impact of leakage reduction initiatives and the real skills Europe project).

[81] M. Eriksson, S. Ahlgren, LCAs of petrol and diesel- a literature review, http://pub.epsilon.slu.se/10424/17/ahlgren_s_and_eriksson_m_130529.pdf ISSN 1654-9406 (2013).

[82] NIST, Reference Fluid Thermodynamic and Transport Properties Database (REFPROP): Version 9.1 2016.

[83] ASCO Carbon Dioxide ltd, http://www.ascoco2.com/en/products/co2-und-cryogene-tanks/, CO2 and Cryogene Storage Tanks 2016 1.

[84] N. Latif, F. Ani, H. Hamdan, The performance of a bench scale liquefaction of carbon dioxide, Universiti Teknologi Malaysia No. 29, 84-99 (2009).

[85] H. Tajima, A. Yamasaki, F. Kiyono, Energy consumption estimation for greenhouse gas separation processes by clathrate hydrate formation, Energy 29 (2004) 1713-1729.

[86] EIGA, Position Paper, Indirect CO2 emissions compensation: Benchmark proposal for Air Separation Plants PP-33 (2010).

[87] D. Gardner, Hydrogen production from renewables, http://www.renewableenergyfocus.com/view/3157/hydrogen-production-from-renewables/ 2017 (2009) 1.

[88] GOV.UK, Greenhouse gas reporting: conversion factors 2018, https://www.gov.uk/government/publications/greenhouse-gas-reporting-conversion-factors-2018 2018 (2018) 1.

[89] H. Han, M. Zhexuan, J. Shuhua, L. Zongwei, Z. Fuquan, GHG emissions from the production of lithium-ion batteries for electric vehicles in China, State Key Laboratory of Automotive Safety and Energy, Tsinghua University, Beijing 100084, China Sustainability (4 April 2017).

[90] ITM power, Hydrogen cost structure update, http://www.itm-power.com/news-item/hydrogen-cost-structure-update 2015 (2013) 1.

[91] UK Power, Gas & electricity tariff prices per kWh, https://www.ukpower.co.uk/home_energy/tariffs-per-unit-kwh 2019 (2018).

APPENDIX A

Energy content or calorific value is the same as the heat of combustions and can be calculated from thermodynamical values. In order to standardise the units of different energy consumption rates for ease with comparison, the consumption rate will be converted to MJ based on the energy density of each fuel.

Based on the parameters provided by the source, the energy density of hydrogen is estimated to be 142.2 MJ/kg and diesel to be approximately 45.6 MJ/kg.

Table A.1 provides the standardised energy usage of different TRUs using different powering sources.

Table A.1: Hourly energy consumption in MJ.

	Diesel 18 t		Diesel 38 t		H2 18 t		H2 38 t		Electric 18 t		Electric 38 t	
Month	Chilled	Frozen	Chilled	Frozen	Chilled	Frozen	Chilled	Frozen	Chilled	Frozen	Chilled	Frozen
Jan	54.26	89.38	58.37	95.76	34.13	56.88	36.97	61.15	16.27	26.82	17.5	28.73
Feb	59.74	95.3	64.75	102.1	38.39	61.15	41.24	65.41	17.96	28.55	19.4	30.67
March	66.58	101.7	72.05	109.9	42.66	65.41	46.93	69.68	19.94	30.53	21.67	32.9
April	69.77	105.3	76.15	113.5	45.5	66.83	48.35	72.52	20.99	31.54	22.82	34.06
May	81.62	117.2	89.83	127.2	52.61	75.37	56.88	81.05	24.55	35.1	26.89	38.12
June	88.46	123.6	97.13	134.5	56.88	79.63	62.57	86.74	26.53	37.12	29.16	40.39
July	91.66	126.8	100.8	138.2	58.3	81.05	65.41	88.16	27.5	38.09	30.24	41.47
Aug	88.92	124.5	98.04	135.4	56.88	79.63	62.57	86.74	26.75	37.3	29.34	40.57
Sept	82.54	117.6	90.29	127.7	52.61	75.37	58.3	82.48	24.73	35.28	27.07	38.3
Oct	67.49	102.6	73.42	110.8	42.66	65.41	46.93	71.1	20.27	30.85	22.03	33.26
Nov	67.03	102.1	72.05	109.4	42.66	65.41	46.93	69.68	20.09	30.67	21.6	32.83
Dec	54.72	89.83	58.82	96.22	35.55	58.3	38.39	62.57	16.42	27.00	17.68	28.91